

Topical Review

Flexible nanogenerators for intelligent robotics: design, manufacturing, and applications

Hongfa Zhao^{1,5}, Liguang Ruan^{1,5}, Zihan Wang¹, Mingrui Shu¹, Chuqiao Lyu¹, Bulathsinghala Rameesh Lakshan², Dharmasena Ishara², Changsheng Wu³ and Wenbo Ding^{1,4,*} 

¹ Tsinghua-Berkeley Shenzhen Institute, Shenzhen International Graduate School, Tsinghua University, Shenzhen 518055, People's Republic of China

² Wolfson School of Mechanical, Electrical and Manufacturing Engineering, Loughborough University, Loughborough LE11 3TU, United Kingdom

³ Department of Materials Science and Engineering, National University of Singapore, Singapore 117575, Singapore

⁴ RISC-V International Open Source Laboratory, Shenzhen 518055, People's Republic of China

E-mail: dingwenbo@sz.tsinghua.edu.cn

Received 29 June 2024, revised 15 September 2024

Accepted for publication 19 November 2024

Published 18 December 2024



Abstract

The embodied artificial intelligence (EAI) is driving a significant transformation in robotics, enhancing their autonomy, efficiency and evolution ability. In this rapidly evolving technological landscape, robots need numerous sensors to realize high levels of perception, precision, safety, adaptability, and intelligence. Triboelectric and piezoelectric sensors address these needs by providing high sensitivity, flexibility, and the capability of self-powered sensing, leveraging the revolutionary nature of nanogenerators to convert mechanical energy into electrical energy on basis of Maxwell's displacement current. These sensors surpass externally powered passive sensors by offering continuous operation, reduced maintenance, and the capability to function in remote or harsh environments. The integration of EAI with advanced nanogenerators sensors could position robotics to perform autonomously, efficiently, and safely, paving the way for innovative applications in various domains such as industrial automation, environmental monitoring, healthcare, and smart homes. In this paper, the fundamental theories, design, manufacturing, and applications of nanogenerators are comprehensively reviewed as a

⁵ These authors contributed equally.

* Author to whom any correspondence should be addressed.



Original content from this work may be used under the terms of the [Creative Commons Attribution 4.0 licence](#). Any further distribution of this work must maintain attribution to the author(s) and the title of the work, journal citation and DOI.

foundation of the advanced sensors for intelligent robotics in the new era, with three major application fields: sensing (including human–robot interaction, exteroceptive sensing and proprioceptive sensing), computing and actuating. Perspectives are addressed for nanogenerators systems in future development.

Keywords: triboelectric/piezoelectric nanogenerators, robotics, manufacturing

1. Introduction

Intelligent robotics, enhanced by embodied artificial intelligence, are designed to autonomously perform tasks, utilizing sensing, computing, and actuating technologies to perceive the environment, process information, make decisions, and interact with the physical world [1–7]. Sensing enables robots to perceive their surroundings and gather data for decision-making [8–10]. Computing processes this data, enabling complex algorithms and artificial intelligence to function [11–13]. Actuating components execute actions based on computed decisions [14–16]. Together, these technologies create a cohesive system that enhances robotic capabilities and versatility across various applications.

To achieve human-like capabilities, robots need advanced exteroceptive sensing abilities. These include tactile sensors for precise manipulation and safe interaction [17–21], auditory sensors for speech recognition and sound analysis [22–24], olfactory sensors for detecting hazardous gases and assessing product quality [25–27], and gustatory sensors for chemical analysis and quality control [28, 29]. Proprioceptive sensing is also critical, providing robots with an internal sense of their own body position, movement, and orientation, essential for balance, coordination, and accurate control of robotic limbs [30–34]. Machine learning, a cornerstone technology for modern robotics, effectively computes and classifies the abundant data from these sensors [35–38]. These algorithms process vast amounts of sensory data to recognize patterns, understand the environment, and predict outcomes. Considering the extensive sensor requirements, it is crucial for these sensors to be cost-efficient, easy to fabricate, and widely available in terms of materials. This allows for economical deployment, simplified manufacturing, and rapid prototyping [39–42]. Meanwhile, the power consumption of the large number of sensors should be managed carefully, as it may significantly reduce the endurance of robotic systems [43–45].

Triboelectric and piezoelectric nanogenerators (TENGs and PENGs) can efficiently convert ambient mechanical energy into electrical energy, enabling continuous sensing without the need for external power sources or frequent battery replacements [46–51]. They are cost-efficient and easy to fabricate from widely available, inexpensive materials like polymers [52–54], ceramics [55–57], metals [58–60], biomaterials [61–63], and composites [63–65]. Fabrication processes, including flexible electrode screen printing [66–68], electrospinning [69–74], and 3D printing [75–80], are straightforward and scalable, allowing for mass production and widespread adoption in robotic applications. Furthermore, flexible nanogenerators offer unique properties in weight,

thickness, resilience, and durability, enabling seamless installation on non-flat or moveable parts of robots [81–83]. These advantages make nanogenerators a valuable component for enhancing the capabilities and autonomy of advanced robotic systems, paving the way for broader adoption and more sophisticated applications.

This review summarizes the development of nanogenerators for intelligent robotics, covering fundamentals, design, manufacturing, and applications (figure 1). It starts with the basic theory, including charge transfer process of contact electrification (CE), theoretical modeling, and equation derivations for TENGs, and the piezoelectric effect for PENGs. The review then introduces design and manufacturing approaches, highlighting materials such as common triboelectric, bio-inspired, stretchable, and textile materials for TENGs, and inorganic, organic, and composite materials for PENGs. The strategies to enhance the output performance and manufacturing techniques like 3D printing, roll-to-roll (R2R) manufacturing and electrospinning for nanogenerators are also presented. For robotics applications, the review discusses nanogenerator systems for sensing, computing, and actuating. Robotic sensing is categorized into human–robot interaction, exteroceptive sensing, and proprioceptive sensing. Nanogenerator-based systems integrate sensors, signal acquisition, processing units, wireless transmission, and display interfaces to enable computing and decision-making. Additionally, nanogenerator-based actuators are demonstrated, with TENGs providing power for actuators while PENGs serve as actuators. Nanogenerators show great potential for advancing efficient, intelligent robotic systems across various applications.

2. Fundamentals of nanogenerators

2.1. Theories for TENGs

TENGs have demonstrated remarkable capabilities in energy harvesting and self-powered sensing, while TENG theories have set the foundation for their further development [46, 92, 93]. The working principle of TENGs is based on both triboelectrification/CE and electrostatic induction, leading to two categories/steps of TENG theories. The first category involves the analysis of the triboelectrification process between material interfaces, as studied in material science [94–97]. The second category pertains to theoretical modeling and physical/mathematical derivations based on electrostatic methods [98–100].

Although the phenomenon of triboelectrification has been known for thousands of years, its mechanisms still require

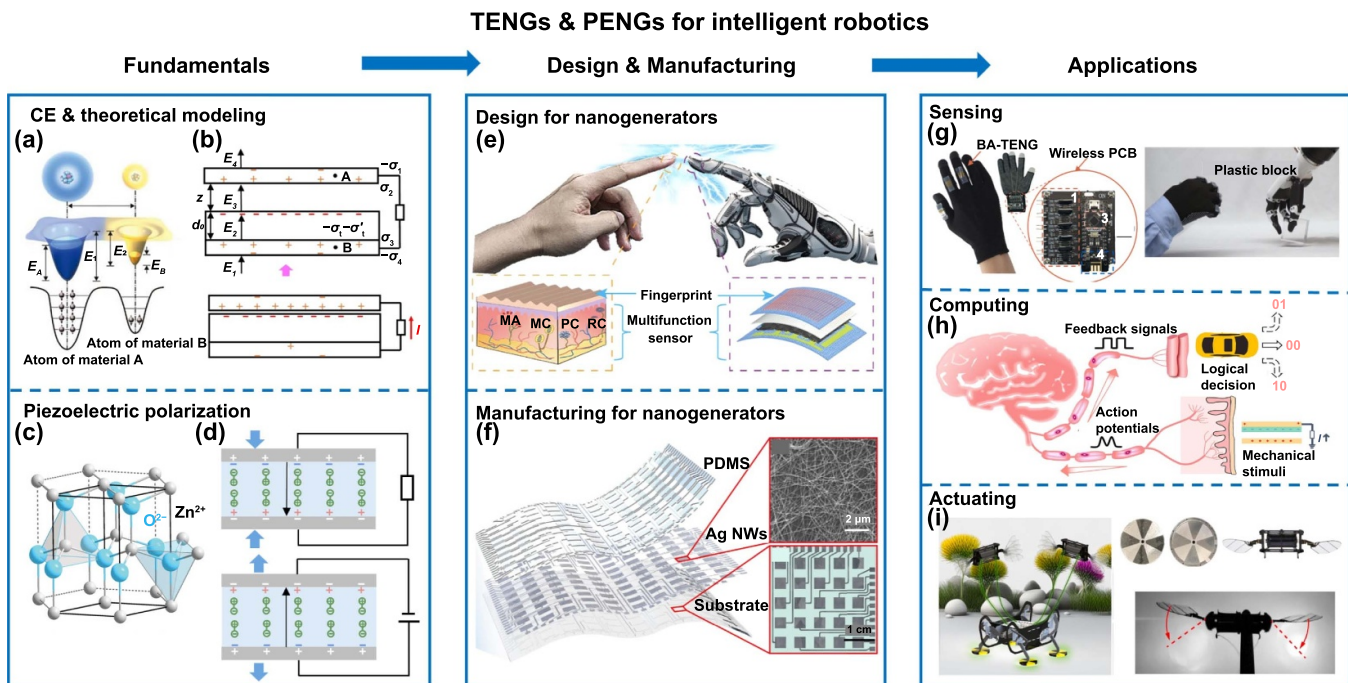


Figure 1. Fundamentals, design, manufacturing and applications for nanogenerators. (a) Schematic diagram for CE theory: reprinted from [84], © 2019 Elsevier Ltd. All rights reserved. (b) Theoretical modeling for TENG: Reproduced from [85] with permission from the Royal Society of Chemistry. (c) Piezoelectric polarization: [86] John Wiley & Sons. © 2016 WILEY-VCH Verlag GmbH & Co. KGaA, Weinheim. (d) Piezoelectric and inverse piezoelectric effect. (e) Design for nanogenerator: reprinted from [87], © 2022 Elsevier Ltd. All rights reserved. (f) Manufacturing for nanogenerator: Reproduced with permission from [88]. © 2022 The Authors. Publishing Services by Elsevier B.V. on behalf of KeAi Communications Co. Ltd. CC BY-NC-ND 4.0 (g) Nanogenerator sensing: Reprinted from [89], © 2021 Elsevier Ltd. All rights reserved. (h) Nanogenerator computing: Reproduced from [90]. CC BY 4.0. (i) Nanogenerator actuating: Reprinted from [91], © 2024 Elsevier Ltd. All rights reserved.

further study. Thanks to TENG technology, this type of energy can be harnessed instead of being harmful to human life. To optimize the design and improve the output performance of the TENG, it is necessary to understand the charge transfer process between the two materials interfaces. Specifically, addressing the intrinsic cause of charge transfer, characteristics of electron donors and acceptors, driving force for charge transfer, the roles played by mechanical forces, and relative parameters for charge transfer amount are essential considerations.

Wu *et al* conducted an analysis of the charge transfer process between two typical materials, polytetrafluoroethylene (PTFE) and aluminum, for fabricating TENGs [101]. The interactions of electrons and atoms were simulated using CASTEP software. Figure 2(a-i) illustrates the calculation of the electrostatic potential for the PTFE molecular chains, Al atoms, and vacuum environment. The fluctuation of the electrostatic potential curve is attributed to the positive electricity of the nucleus and negative electricity of the electrons. The interface barrier to the electrons mainly originates from the confinement of the potential field generated by the nucleus. To transfer from the Al surface to the PTFE surface, electrons need to overcome an average interfacial barrier W ($W = E_b - E_f$), which is significantly lower than their effective work function ϕ_{EF} ($\phi_{WF} = E_v - E_f$). Therefore, it is suggested that interface barrier should be considered as a more fundamental parameter in charge transfer processes instead of focusing solely on work function difference. The electrons in

Al are free electrons in which Fermi level E_f is greater than the internal barrier of Al and form ‘Fermi seas’ from energy band theory (the characteristic of donors). When electron energy exceeds the interface barrier, they are able to transfer from Al to PTFE material (the intrinsic cause of charge transfer).

Another important aspect that needs addressing is related to receptor characteristics. As shown in figure 2(a-ii), it is observed that PTFE has a strong electronegativity due to its electron-deficient structures at C atoms. The low unoccupied molecular orbital (LUMO) serves as a receptor for electrons from Al with its distribution mainly around C atoms, while F atoms play an indirect but significant role in making C atoms electron-deficient and eager to gain electrons from other materials (figure 2(a-iii)). It can be inferred that the friction or the contact–separation process will cause the surface deficiency and facilitate the charge transfer of two materials (the first effect of mechanical forces). In terms of the driving force for charge transfer, it is found that nuclei of C atoms provide attractive forces for incoming electrons while existing electrons within C atoms repel transferred ones (figure 2(a-iv)). Therefore, to achieve charge transfer, the interfaces of the two materials need to be brought into close proximity, which is performed by external mechanical forces (the second effect of mechanical forces).

The research conducted by Prof. Wang has revealed that, during the process of CE, atoms from different materials experience an attractive force region, an equilibrium state point, and a repulsive force region (figure 2(b-i)) [84]. Charge

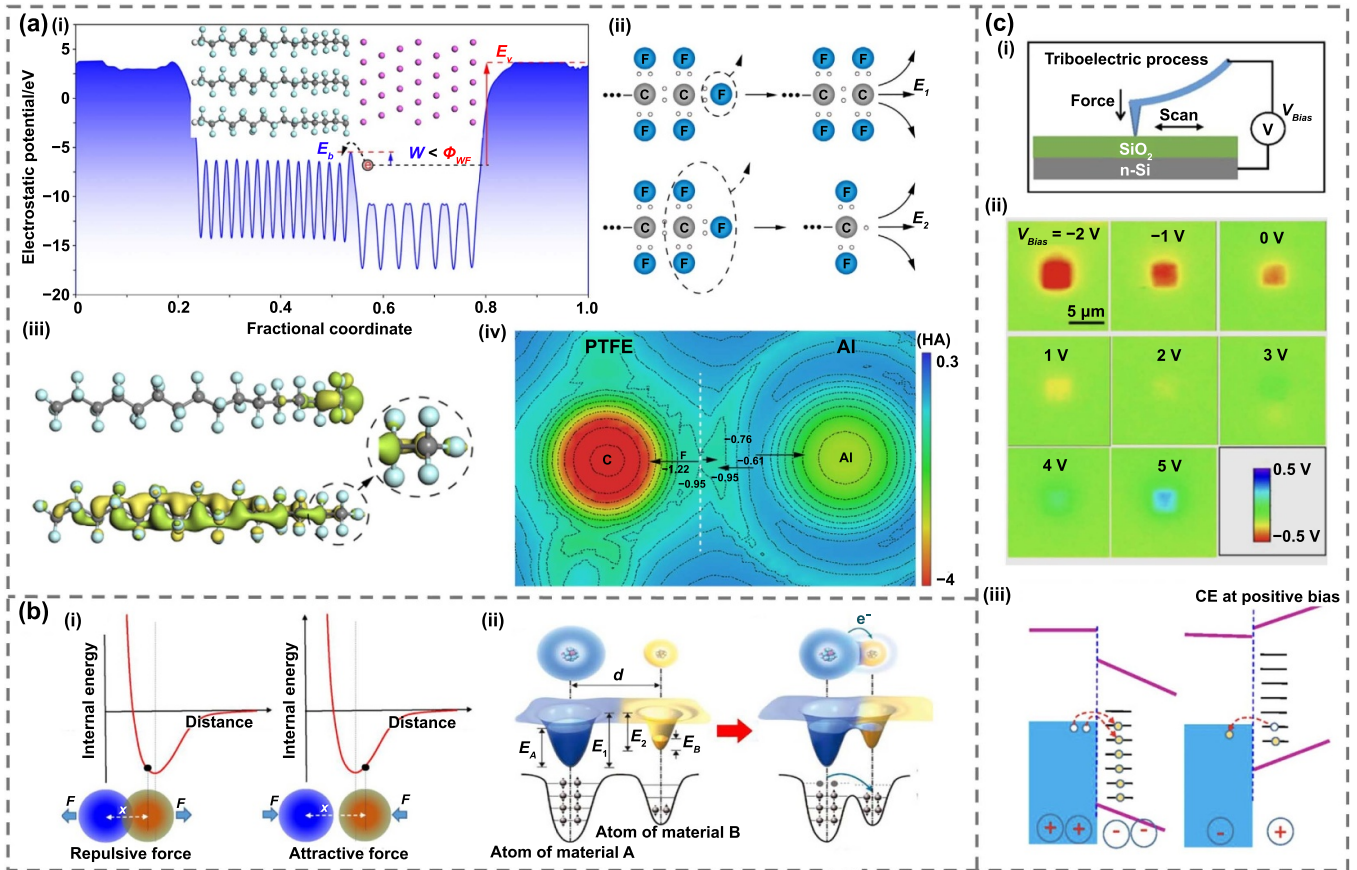


Figure 2. Analysis of charge transfer process between two materials interfaces. (a) Analysis of the charge transfer process between two typical materials (PTFE and Al) to explain the intrinsic cause of charge transfer, characteristics of electron acceptors, and driving force. Reprinted from [101], Copyright (2018), with permission from Elsevier. (b) Analysis of interatomic distances and charge transfer of two materials in a general case. Reprinted from [84], Copyright (2019), with permission from Elsevier. (c) Demonstration of the contact electrification phenomenon based on the SKPM. Reprinted from [84], Copyright (2019), with permission from Elsevier.

transfer only occurs when the atoms are compressed into the repulsive force region, as confirmed by experiments utilizing atomic force microscopy (AFM). In general cases involving two materials (figure 2(b-ii)), when their interfaces are at a large distance, electrons cannot transfer from one material to another due to a high barrier. However, when the two materials come into contact, the electron clouds of their respective atoms overlap. This results in electrons from one material dropping into a deeper potential well of another material, leading to charge transfer. This can be likened to two cups of water with water flowing from one cup to another with lower water level.

The CE phenomenon can be effectively demonstrated through experiments utilizing scanning Kelvin probe force microscopy (SKPM, as shown in figure 2(c)) [102]. When no bias voltage is applied to the Pt AFM tip, the SiO_2 material exhibits a negative surface potential after the CE process, indicating that electrons have been transferred from the metal tip to the SiO_2 material. Applying a negative voltage to the metal tip results in an increased transfer of electrons from the metal to SiO_2 due to a larger surface potential difference.

Conversely, when a positive bias voltage (3–5 V) is applied to the metal tip, it reduces the potential well of the Pt material to a lower level. As a result, there is an electron transfer from SiO_2 to the metal tip, causing a positive potential on the SiO_2 surface. Therefore, in order to enhance charge transfer during CE and improve output performance of designed TENGs, it is essential for two tribo-charge layers to have a significant difference in gaining or losing electrons. Increasing the contact area is also an effective method. And contact pressure should be increased effectively to ensure the atoms from two materials interfaces are compressed into the repulsive region.

When the CE is clear, further step is to establish theoretical models and derive governing equations. Followed by CE and combining with electrostatics, charge distribution (the source, on the right-hand side of Maxwell's equations) is a prerequisite for solving the electric field and charge transfer process (on the left-hand side of Maxwell's equations) for the TENG, so we analyze it from the initial charge distribution [85].

The dielectric materials used to fabricate TENGs usually have a strong electronegativity, and are easy to gain electrons from the environment or other materials. A commonly

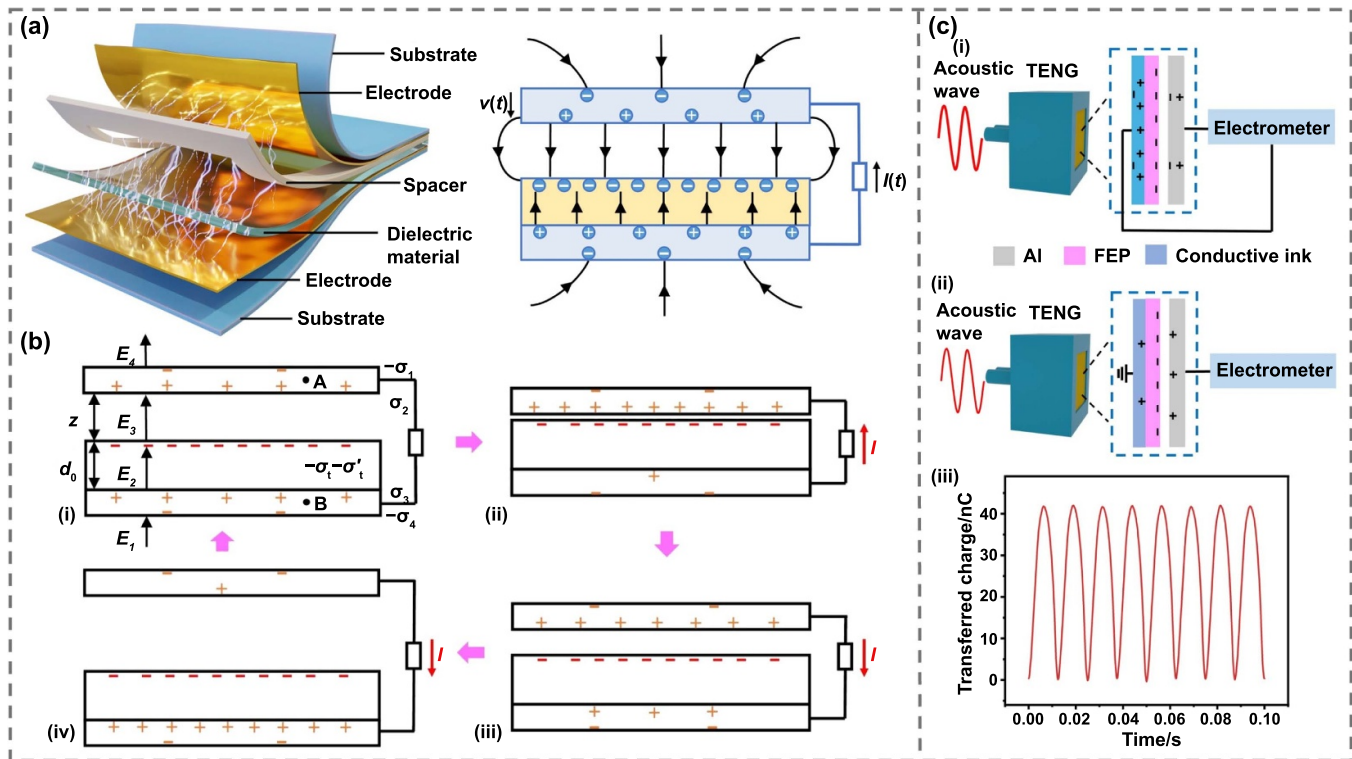


Figure 3. Theoretical modeling and extension analysis for the typical contact–separation mode TENG. (a) Schematic diagram of the contact–separation mode TENG. (b) Theoretical model and working principle of the TENG. (c) Analysis for the characteristic of contact–separation mode TENG transforming into single electrode TENG, for validating the theories. Reproduced from [85] with permission from the Royal Society of Chemistry.

employed method to enhance the output performance of TENGs is to apply plasma spray onto the surface of dielectric materials, resulting in pre-charging charges (σ_t , initial charge). Under the influence of those negative charges, it is easy for the base electrode of the dielectric material to gain positive charges from the environment [103], which are called as compensation charges (σ_c , initial charge). Following fabrication, in a typical contact–separation mode TENG as depicted in figure 3(a), when the independent electrode and dielectric material come into contact and then separate, additional positive and negative triboelectric charges (σ'_t , initial charge) are distributed on their respective surfaces. Furthermore, the electrodes autonomously segregate positive and negative charges to achieve an equilibrium state. It is important to note that for conductors, electrons are always distributed on their outer surfaces. Previous studies have traditionally focused on net charges for demonstrating charge transfer amount intuitively; however, considering all charge distributions are more rigorous and enable practical applications based on physical theory derived from this model.

Taking account of all these factors, the theoretical model is shown in figure 3(b). All charge distributions of the TENG are supposed to be solved at first, as knowledge of charge distribution (the source, on the right-hand side of Maxwell's equations) is a prerequisite for solving the electric field (on the left-hand side of Maxwell's equations). To fulfill charge conservation, electrostatic equilibrium, and equipotentiality of the electrodes, a set of equations can be derived as equation (1):

$$\begin{cases} -\sigma_1 + \sigma_2 + \sigma_3 - \sigma_4 = \sigma'_t + \sigma_c \\ -\frac{\sigma_t + \sigma'_t}{2\varepsilon_0} + \frac{\sigma_1}{2\varepsilon_0} + \frac{\sigma_2}{2\varepsilon_0} + \frac{\sigma_3}{2\varepsilon_0} - \frac{\sigma_4}{2\varepsilon_0} = 0 \\ \frac{\sigma_t + \sigma'_t}{2\varepsilon_0} + \frac{\sigma_1}{2\varepsilon_0} - \frac{\sigma_2}{2\varepsilon_0} - \frac{\sigma_3}{2\varepsilon_0} - \frac{\sigma_4}{2\varepsilon_0} = 0 \\ V_t - \left(-\frac{\sigma_t + \sigma'_t}{2\varepsilon_0} + \frac{\sigma_1}{2\varepsilon_0} - \frac{\sigma_2}{2\varepsilon_0} + \frac{\sigma_3}{2\varepsilon_0} - \frac{\sigma_4}{2\varepsilon_0} \right) z_0 \\ = V_t + \left(\frac{\sigma_t + \sigma'_t}{2\varepsilon_0\varepsilon_r} + \frac{\sigma_1}{2\varepsilon_0\varepsilon_r} - \frac{\sigma_2}{2\varepsilon_0\varepsilon_r} + \frac{\sigma_3}{2\varepsilon_0\varepsilon_r} - \frac{\sigma_4}{2\varepsilon_0\varepsilon_r} \right) d_0 \end{cases} \quad (1)$$

where $\sigma_1, \sigma_2, \sigma_3, \sigma_4$ are charge density on the four surfaces of the two electrodes, respectively, z_0 represents the distance between the two materials, d_0 is the thickness of the dielectric material, ε_0 denotes the vacuum permittivity, ε_r stands for the relative permittivity, and V_t is a defined reference potential at the upper surface of the dielectric material. The corresponding solutions are as equation (2):

$$\begin{cases} \sigma_1 = \frac{\sigma_t - \sigma_c}{2} \\ \sigma_2 = \frac{(\sigma_t + \sigma'_t)d_0}{z_0\varepsilon_r + d_0} \\ \sigma_3 = \frac{(\sigma_t + \sigma'_t)z_0\varepsilon_r}{z_0\varepsilon_r + d_0} \\ \sigma_4 = \frac{\sigma_t - \sigma_c}{2} \end{cases} \quad (2)$$

If the internal distance changes by dz , there will be a charge transfer of dq between the two electrodes. The relationship

between them can be solved as equation (3):

$$\frac{dQ}{dz} = \frac{1}{2} \frac{q(z + dz) - q(z)}{dz} = \frac{1}{2} \frac{dq}{dz} = \frac{(\sigma_t + \sigma'_t) \varepsilon_r S d_0}{(z \varepsilon_r + d_0)^2}. \quad (3)$$

Then the transferred charge Q and the current I can be solved as equations (4) and (5):

$$Q = \int_{z_1}^{z_2} dQ = \int_{z_1}^{z_2} \frac{(\sigma_t + \sigma'_t) \varepsilon_r S d_0}{(z \varepsilon_r + d_0)^2} dz \\ = \frac{(\sigma_t + \sigma'_t) \varepsilon_r S d_0 (z_2 - z_1)}{(z_1 \varepsilon_r + d_0)(z_2 \varepsilon_r + d_0)}, \quad (4)$$

$$I(t) = \frac{dQ}{dt} = \frac{dQ}{dz} v = \frac{(\sigma_t + \sigma'_t) \varepsilon_r S d_0 v}{(z \varepsilon_r + d_0)^2} \quad (5)$$

where v is the movement velocity of the TENG. And the voltage of the open-circuit model provided in the reference is equation (6):

$$V = \frac{(\sigma_t + \sigma_c) d_0 + (\sigma_t - \sigma_c + 2\sigma'_t) \varepsilon_r z_0}{2\varepsilon_0 \varepsilon_r}. \quad (6)$$

Additionally, the displacement current density can be derived as equation (7):

$$\frac{\partial D}{\partial t} = \varepsilon_0 \frac{\partial E_3}{\partial t} = \varepsilon_0 \frac{\partial E_b}{\partial z} \frac{\partial z}{\partial t} = \frac{(\sigma_t + \sigma'_t) d_0 \varepsilon_r v}{(z \varepsilon_r + d_0)^2} \quad (7)$$

where D is the electric flux density, so the displacement current inside the TENG is as equation (8):

$$I_d = \int_S \frac{\partial D}{\partial t} dS = \frac{(\sigma_t + \sigma'_t) d_0 \varepsilon_r S v}{(z \varepsilon_r + d_0)^2}. \quad (8)$$

Comparing equation (5) with equation (7) reveals that the displacement current inside the TENG equals the conduction current in the external circuit.

The study also analyzed different characteristics and applications of the TENG. Previous studies usually compare the voltage, the current and the transferred charge predictions from a theoretical model with the experimental data, as well as with the predictions from other theoretical models. Those are meaningful but not completely accurate, as estimated values (rather than true values) are adopted in those predictions. Therefore, an approach of ‘predicted characteristics correlating’ is proposed in the study, which compares the non-intuitive characteristics of the TENG with the theoretical predictions. If the predictions match the characteristics (phenomena) in practice, the proposed theoretical model is validated. This includes contact–separation mode TENG transforming into single electrode TENG [104] (schematic diagram shown in figure 3(c)), trend of V - Q curve, and figure of merit [105] expressed by basic parameters. The extension analysis for applications includes the effect of the pre-charging charges in experiments [67], output performance of the TENG with working frequencies [106], and TENG-based communications [107], providing a solid and practical theoretical foundation for TENG development.

2.2. Theories for PENGs

Natural quartz was the first piezoelectric material discovered by French physicists Jacques and Pierre Curie in 1880. When a piezoelectric crystal is subjected to external forces, it becomes deformed, causing the positive and negative charge centers within the crystal to be displaced relative to each other. This displacement results in polarization and generates the piezoelectric effect. As a result, the crystal produces bound charges of opposite signs in a specific direction, with the charge density being directly proportional to the magnitude of the external force. Conversely, when a piezoelectric crystal is exposed to an external electric field, the positive and negative charge centers within the crystal move relative to each other due to polarization induced by the electric field. This movement causes the crystal to deform in a particular direction. This phenomenon is known as the inverse piezoelectric effect.

The piezoelectric properties of a dielectric material depend on its crystal structure, specifically the presence of a center of symmetry. Materials with these properties lack a center of symmetry in their crystal structure, such as ZnO with hexagonal wurtzite (figures 4(a) and (b)) [86, 108]. Crystals with piezoelectric properties can be categorized into two types. The first type does not have spontaneous polarization, but an external force can induce crystal polarization, thus exhibiting piezoelectric properties. The second type is a crystal with spontaneous polarization, which exhibits piezoelectric behavior when subjected to an external force, and the strength of this behavior changes. These materials are known as ferroelectrics. The constitutive equation for the piezoelectric effect incorporates both mechanical and electrical parameters. When a piezoelectric material is in a short circuit and not subjected to clamping, the piezoelectric equation is equation (9):

$$D = dT + \varepsilon^T E, \quad (9)$$

where D represents the electric displacement vector, d is the piezoelectric coefficient, T denotes external stress, ε^T is the dielectric constant at a constant stress, and E stands for electric field intensity. When the external electric field E is zero, the surface charge density of the material is directly proportional to the applied stress, and the piezoelectric equation can be expressed as equation (10):

$$\begin{pmatrix} D_1 \\ D_2 \\ D_3 \end{pmatrix} = \begin{pmatrix} d_{11} & d_{12} & d_{13} & d_{14} & d_{15} & d_{16} \\ d_{21} & d_{22} & d_{23} & d_{24} & d_{25} & d_{26} \\ d_{31} & d_{32} & d_{33} & d_{34} & d_{35} & d_{36} \end{pmatrix} \begin{pmatrix} T_1 \\ T_2 \\ T_3 \\ T_4 \\ T_5 \\ T_6 \end{pmatrix}. \quad (10)$$

PENGs utilize piezoelectric materials to convert mechanical energy from the environment into electrical energy. The concept of PENG based on zinc oxide nanowires was first introduced in 2006 (figure 4(c)). In this study, an atomic force microscope probe was utilized to agitate zinc oxide nanowires. When the probe made contact with the compressed surface of ZnO, the Schottky junction was in a connected state, allowing

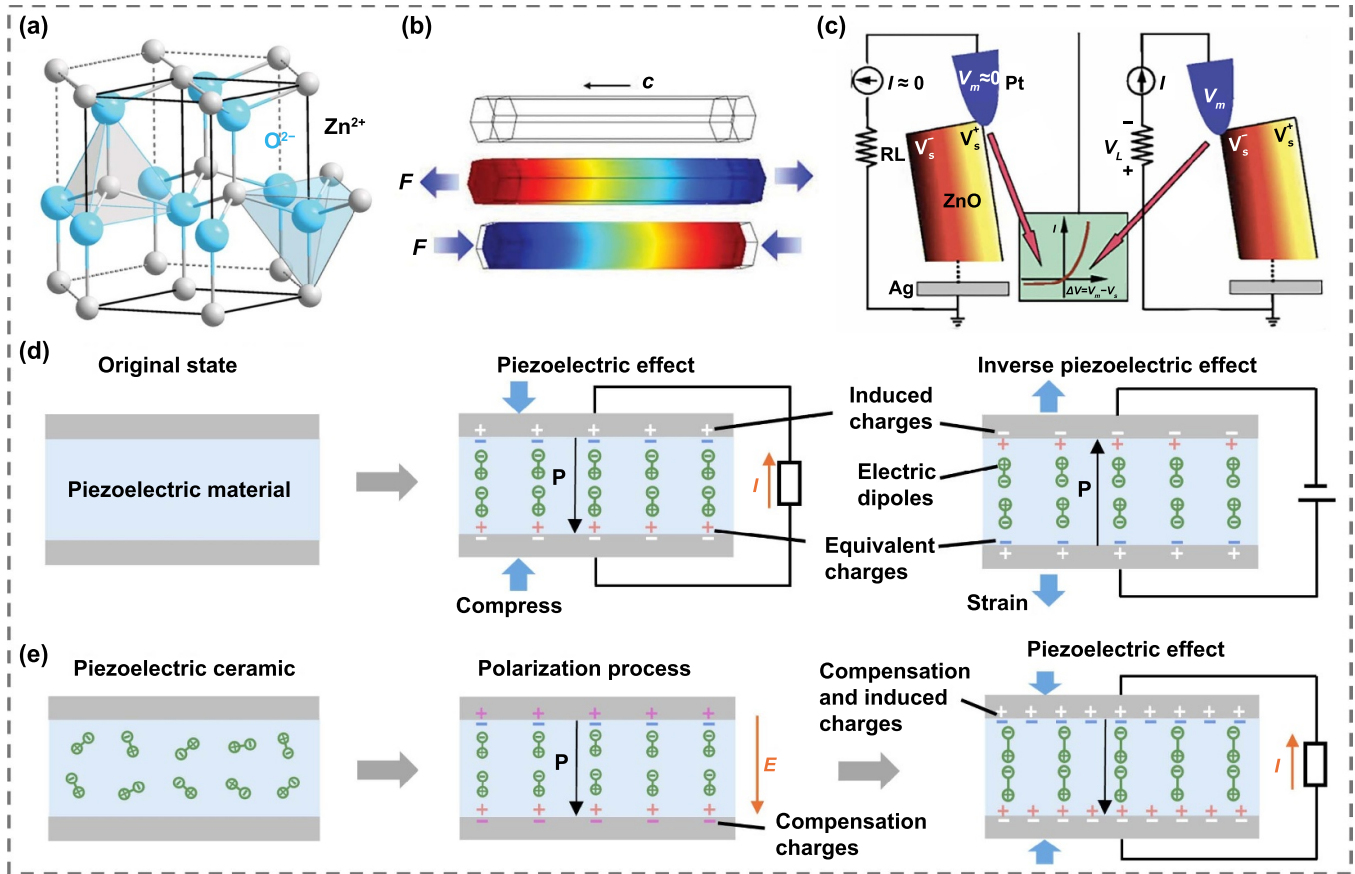


Figure 4. Theoretical analysis of the PENG. (a) Schematic diagram of a piezoelectric material cell. [86] John Wiley & Sons. © 2016 WILEY-VCH Verlag GmbH & Co. KGaA, Weinheim. (b) Simulation of piezoelectric potential distribution for a ZnO nanowire. Reprinted from [108], with the permission of AIP Publishing. (c) Schematic diagram of the PENG based on the ZnO nanowire. From [109]. Reprinted with permission from AAAS. (d) Working principle of the PENG with piezoelectric effect and inverse piezoelectric effect. (e) Working principle of the piezoelectric ceramic based PENG.

the accumulated negative charge on the compressed surface to flow through the probe and into the external circuit. This resulted in a detectable weak output voltage on the external load. These findings laid a solid foundation for the rapid development of PENG technology.

In order to achieve higher energy harvesting efficiency, materials with high piezoelectric coefficients are typically selected for the design and preparation of PENG. When the PENG is subjected to an external force, the centers of positive and negative charges within the material's cells shift. This results in a change in its polarization state and a corresponding change in the accumulated charge (equivalent) on its surface (figure 4(d)). Consequently, electrons are transferred between the two electrodes, generating a current in the external circuit. After removing the external force, the material's polarization state is restored, causing electrons to flow back with a reverse direction. When an alternative voltage is applied on the electrodes of the PENG, vibration will be generated due to the inverse piezoelectric effect. For the piezoelectric ceramic material, an external electric field should be applied first to align the electric domains with different directions (figure 4(e)). Under the influence of the electric field generated by the dipoles inside the material, there will be compensation

charge on the electrodes, similar to that of the TENG. And when the internal polarization electric field changes with the deformation caused by an external force, charges transfer between two electrodes, thus the PENG works.

2.3. Comparison of TENGs and PENGs

We analyze the advantages and disadvantages of TENGs and PENGs from their basic principles. The equation (4) highlights two key factors influencing charge transfer in a TENG: the initial charge and the movement state. The fundamental principle of the TENG lies in the movement of static charges, which alters the electric field and potential, resulting in charge flow until equilibrium is achieved in both the field and potential. Therefore, in the modeling process, the primary focus is on charge distribution, while the solution process considers the conditions of the electric field and potential. Since the motion in a TENG is much slower than the speed of electron transfer, we can assume that the TENG operates in a quasi-static state at any given moment during its movement. As a result, the output performance of a TENG is not inherently limited by frequency. Optimization for TENGs may focus on how to design the movement of the charged materials to meet specific

performance requirements. The broad selection of charged materials, where almost any two materials can exhibit a CE effect, is a major advantage of TENGs. Moreover, because charge transfer is determined by the relative positions during motion, TENGs can operate across a wide frequency range. The main challenge, however, lies in designing a mechanical structure that enables the desired movement for optimal TENG operation.

The piezoelectric effect arises from charge separation in a crystal when mechanical stress is applied to the material. According to equation (10), when piezoelectric materials experience a unidirectional external force, the optimization of the piezoelectric coefficient matrix depends on both the direction of the applied force and the desired piezoelectric response direction. To achieve optimal piezoelectric performance, it is generally beneficial to align the crystal orientation with the direction of the applied force, thereby maximizing critical components of the piezoelectric coefficient. For instance, when mechanical stress is applied along the 3-axis, the longitudinal piezoelectric effect is the dominant response, making the d_{33} piezoelectric coefficient particularly important. To maximize piezoelectric performance, the crystal structure should be oriented to enhance the d_{33} coefficient. Consequently, material selection for PENGs is more restricted compared to TENGs, and the fabrication process is more intricate. The performance of piezoelectric materials is highly dependent on the symmetry and orientation of their crystal structures, often requiring precise alignment to achieve optimal results. The preparation of high-quality single-crystal or polycrystalline piezoelectric materials demands meticulous process control.

In general, TENGs and PENGs each have distinct advantages and limitations, making them suitable for different applications. TENGs are well-suited for capturing energy from low-frequency and irregular mechanical movements. Their wide range of material options, including polymers, metals, and rubbers, makes them flexible, cost-effective, and easy to manufacture. TENGs generate high voltages, making them ideal for applications requiring high voltage but low power. However, they usually produce small currents, and their reliance on surface contact and separation leads to material wear, impacting their durability and lifespan. Additionally, TENGs are sensitive to environmental factors such as humidity, which can diminish their triboelectric performance.

In contrast, PENGs have excellent working performance in high frequencies. PENGs generate stable current outputs under mechanical stress, making it ideal for precision monitoring and energy harvesting applications, such as vibration energy harvesters, structural health monitoring, and microsensors. PENGs are highly sensitive to small mechanical stresses, making it suitable for high-precision sensing. However, PENGs have a more limited material selection, typically relying on specific piezoelectric materials like lead zirconate titanate (PZT) and barium titanate (BaTiO_3), which are costly to produce and involve complex manufacturing processes. Additionally, some piezoelectric materials contain harmful elements like lead, raising environmental and health concerns. Depending on the specific application requirements, TENGs and PENGs can be used in different fields of energy harvesting

and sensing, optimizing performance and energy efficiency when appropriately applied.

3. Design and manufacturing of nanogenerators for intelligent robotics

3.1. Materials for TENGs and strategies to enhance the outputs

The theoretical analysis for TENGs indicates that a significant transfer of charges occurs between two materials interfaces when the two tribo-charge layers have a large difference in their ability to gain or lose electrons. Therefore, the triboelectric series provides valuable guidance for practical TENG design [110–112]. Commonly used materials with strong electronegativity include PTFE, fluorinated ethylene propylene (FEP), polydimethylsiloxane (PDMS), polyvinyl chloride, polyimide (PI), etc. Conversely, commonly used materials with strong electropositivity include aluminum, copper, indium tin oxide (ITO), nylon, paper, and so on. Additionally, other factors such as weight, thickness, flexibility, transparency, stretchability, waterproofness, and biocompatibility should be taken into consideration when designing TENGs for specific application scenarios.

Based on the principles of the triboelectric series, Qu *et al* developed a tactile perception smart finger for material identification as shown in figure 5(a) [113]. The smart sensor integrated a triboelectric sensor array containing several discrete sensors. Each sensor utilized representative materials from the triboelectric series such as polyamide (PA66), polyethylene terephthalate (PET), polystyrene, and PTFE as the tribocharge layer. Due to differences in these materials' abilities to gain or lose electrons, each sensor outputted a distinct signal when it touched different objects. This allowed for accurate material recognition through machine learning with an impressive accuracy rate of 96.8%.

The use of bioinspired structures is an effective strategy for designing high-output performance TENGs. Yao *et al* drew inspiration from the surface morphology of natural plants and developed a TENG-based electronic skin (e-skin) for robotic tactile sensing (figure 5(b)) [114]. By incorporating interlocking microstructures and forming PTFE tiny burrs on the tribo-layers, they were able to increase the pressure measurement sensitivity by 14 times. This TENG-based e-skin was integrated onto a robotic hand to detect pressure distribution and bend angles during handshaking with humans. It can also be used for robotic hands to detect the surface roughness and hardness of touched objects.

For both robotic e-skins and human body wearable e-skins, stretchability is an important factor that should be considered in the design process due to large deformation in joint positions such as fingers, wrists, arms, legs, etc. Bu *et al* developed a stretchable triboelectric–photonic smart skin for tactile and gesture sensing in a robotic hand (figure 5(c)) [115]. With a grating-structured metal film as the bioinspired skin stripe, this smart skin exhibited tunable aggregation-induced emission within a lateral tensile range of 0%–160%. The pressure sensing characteristics remained stable at different

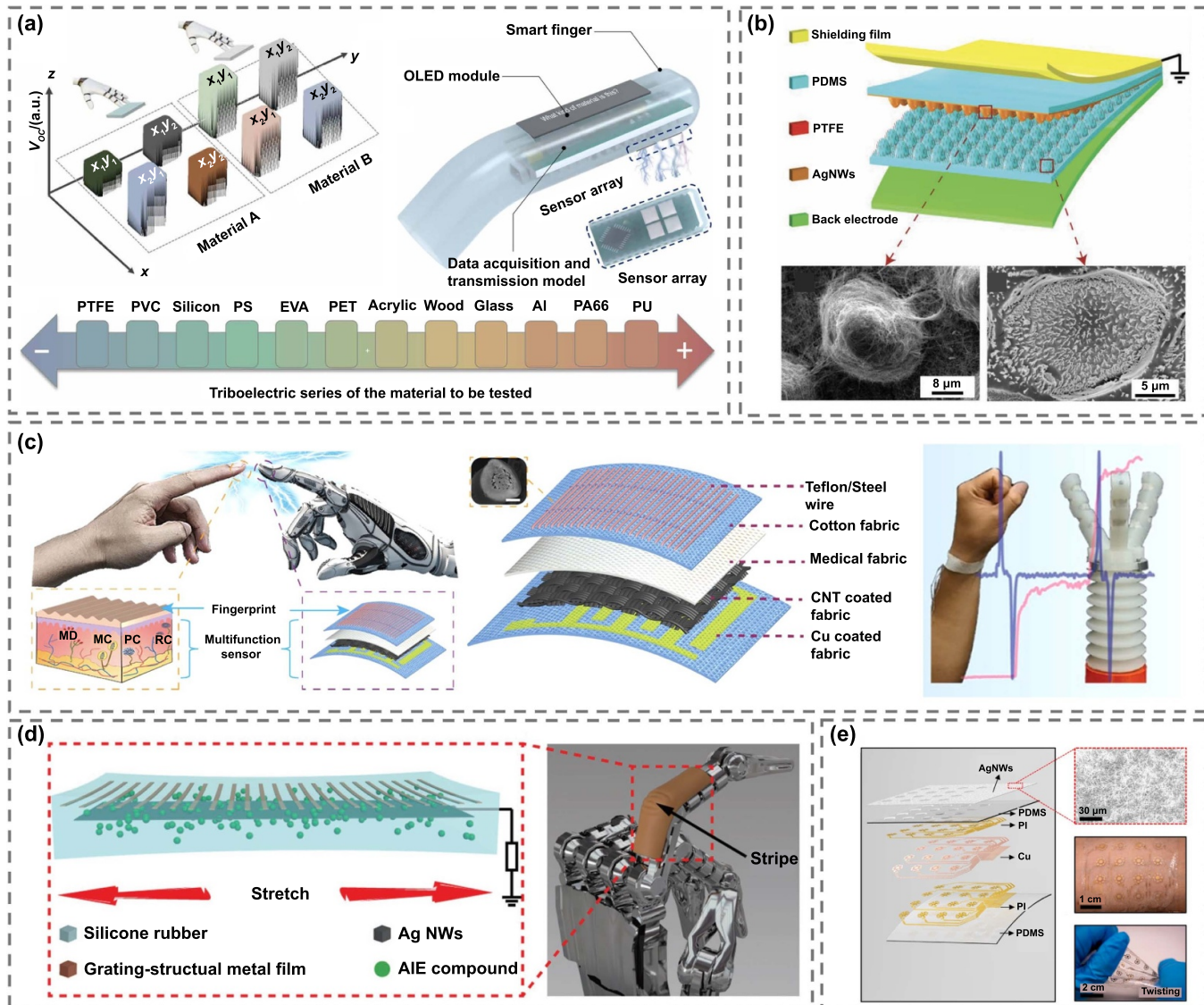


Figure 5. Design of TENGs for robotics. (a) The tactile perception smart finger for material identification. Reproduced with permission from [113]. CC BY-NC 4.0. (b) Natural plants inspired TENG e-skin for robotic tactile sensing. [114] John Wiley & Sons. © 2019 WILEY-VCH Verlag GmbH & Co. KGaA, Weinheim. (c) Stretchable triboelectric-photonic smart skin for tactile and gesture sensing. [115] John Wiley & Sons. © 2018 WILEY-VCH Verlag GmbH & Co. KGaA, Weinheim. (d) TENG sensor array for tactile perception. Reprinted from [116], Copyright (2021), with permission from Elsevier. (e) Textile triboelectric sensor for health monitoring, soft robotic tactile sensing, and human–robot interaction. Reprinted from [87], Copyright (2022), with permission from Elsevier.

stretching levels, demonstrating synchronous and independent sensing properties for external stimuli with great durability. When integrated onto a robotic hand as conformal covering, this smart skin demonstrated multidimensional mechanical sensing abilities for external touch and different gestures with joint bending. In addition to stretchability considerations, it is also necessary to develop sensor arrays for TENG e-skins in order to achieve high-resolution sensing capability in space. He *et al* proposed a type of thin, soft, stretchable, skin-integrated and crosstalk-free tactile sensing array (figure 5(d)) [116]. The 2D trampoline-inspired mechanics design allowed the TENG-based e-skin to have stable tactile sensing ability with unchanged signal outputs under strain up to ~40%. Transparent silver nanowires (AgNWs) networks were employed as a shielding layer via direct spray-coating,

which significantly reduces electrical crosstalk in TENG-based tactile sensor arrays. As a result, the tactile sensor array can be integrated onto various curved surfaces to recognize the shapes of objects that come into contact with it and provide high-resolution tactile pressure mapping.

Recently, textile TENGs have received significant attention due to their flexibility, comfort, portability and energy efficiency, making them highly suitable for wearable technology and smart textiles. Pang *et al* developed a textile triboelectric sensor for health monitoring, soft robotic tactile sensing, and human–robot interaction (figure 5(e)) [87]. Inspired by the skin of the fingertip, the sensor consisted of a triboelectric layer for instantaneous force sensing and a piezoresistive layer for sustained force sensing. Fabricated using cotton fabrics, the tactile sensor could fit comfortably on different body

parts for monitoring sound, physiological signals and joint movement. It could also be easily installed in soft robots that combine machine learning to recognize textures and materials on the touched objects. Additionally, the tactile sensor could serve as a human–machine interface to assist robot control in managing movement and grasping of the soft robot. With significant advantages in terms of cost efficiency, fabrication easiness, and material availability, various robotic sensors have been developed based on TENGs. In addition to the above-mentioned fabrications, other newly developed materials such as high-performance hydrogel, degradable materials, and implantable materials also demonstrate great potential for robotic applications.

TENGs have shown numerous advantages, while enhancing their output performance remains a critical area of research to make them more efficient and practical for applications. One effective approach to achieve this enhancement is surface modification [117, 118], which involves altering the surface properties of the materials used in TENGs to maximize their ability to generate and retain electrical charges. This can be accomplished through various techniques, such as physical micro/nano structuring [119–121], chemical treatments [122–124], biological modification [125], and the application of functional coatings [126, 127]. The primary objectives of surface modification are to increase the contact surface area [120, 128], improve charge density [129–131], and optimize the dielectric properties of the materials [132, 133]. By addressing these factors, surface modification can significantly boost the output voltage and current of TENGs, making them more efficient in converting mechanical energy into electrical energy.

Here we introduce four typical methods. To create microstructures on tribo-charge layers is an effective method to enhance the output performance of TENGs. Fan *et al* reported a transparent flexible nanogenerator as a pressure sensor (figure 6(a)) [134], achieving three types of regular and uniform PDMS patterned arrays (line, cube, and pyramid) at the micrometer scale (5–10 μm) through a common and scalable approach. The process involved fabricating Si wafer molds using traditional photolithography methods, followed by dry or wet etching to create different recessed features. The liquid PDMS elastomer and cross-linker were then mixed, degassed, and uniformly spin-coated onto the surface of the master. After thermal curing, a uniform PDMS layer was peeled off containing the inverse of the original pattern features on the mold's surface. This design significantly improves the output efficiency of the TENG by increasing the contact area and triboelectric change. For a typical TENG with pyramid-featured PDMS pattern, electrical output is increased fourfold compared to TENGs fabricated using flat polymer sheets. As the entire structure of FTNG was fabricated using transparent polymer materials and electrodes, film-featured devices exhibited approximately 75% transparency, resulting in a transparent flexible nanogenerator.

Further developed from microstructuring, nanostructuring has demonstrated even higher efficiency. Park *et al* reported a robust and facile method for the large-scale synthesis of vertically aligned cyclo-diphenylalanine dipeptide nanowires

(figure 6(b)) [135]. They employed a direct thermal evaporation process to densely grow self-assembled dipeptide nanowires on various substrates over a large area. The length of the nanowires could be easily modulated by adjusting the deposition time. The as-grown nanowires exhibited remarkable stability under ambient conditions due to their hydrophobic nature, making them suitable as a positive triboelectric material in high-performance TENGs. Experimental results demonstrated that this approach significantly boosted the electrical output by 150 times.

The theoretical analysis indicates that TENGs exhibit three types of initial charge distribution: triboelectric charge, pre-charging charge, and compensation charge. Micro and nano structuring methods for TENGs serve to enhance the triboelectric charge when the tribo-charge layers come into contact and separate. Another method, in accordance with theory, involves improving the pre-charging charge for TENGs by injecting plasma onto dielectric material surfaces. Wang *et al* reported a method utilizing an air ionization gun to inject ions onto the surface of the FEP film (figure 6(c)) [103]. This type of charge could remain stable for at least several months and enhanced the output performance of the TENG by 25 times. It is important to note that during the ion injection process, the base electrode of the FEP material was grounded. This allowed more ions to be injected onto the FEP material surface as a result of counteracting electric fields generated by positive compensation charges on the electrode against negative pre-charging charges. The output of the TENG increased gradually over five injection processes; however, after fifth injection, there was no significant change in output due to saturated charges on the FEP material surface.

For a typical chemical surface modification approach, Liu *et al* presented a method for enhancing the performance of TENGs by chemically tailoring the molecular surface of cellulose nanofibrils (CNFs) to control their triboelectric charge density figure (6(d)) [136]. They used silane coupling agents with different terminal functional groups, such as $-\text{NH}_2$, $-\text{SH}$, $-\text{CN}$, and $-\text{CF}_2\text{CF}_3$, to modify the surface of CNFs, influencing their electron-donating or electron-withdrawing properties. This chemical modification resulted in a significant improvement in the charge density and output voltage of TENGs, with charge densities reaching up to $13.2 \mu\text{C}\cdot\text{m}^{-2}$ and output voltages as high as 76 V for $-\text{NH}_2$ -treated CNFs. The study also proposed a mechanism using an electron-cloud model to explain how functional groups impact CE. The tailored CNFs demonstrated superior energy harvesting capabilities compared to untreated materials, offering a flexible and efficient approach to improving the performance of TENGs for applications in energy harvesting and self-powered sensing systems.

3.2. Materials for PENGs and strategies to enhance the outputs

Piezoelectric materials play a crucial role in the conversion of mechanical energy into electrical energy and vice versa. They are utilized in various fields, including sensors [137–140], actuators [141, 142], energy harvesting devices

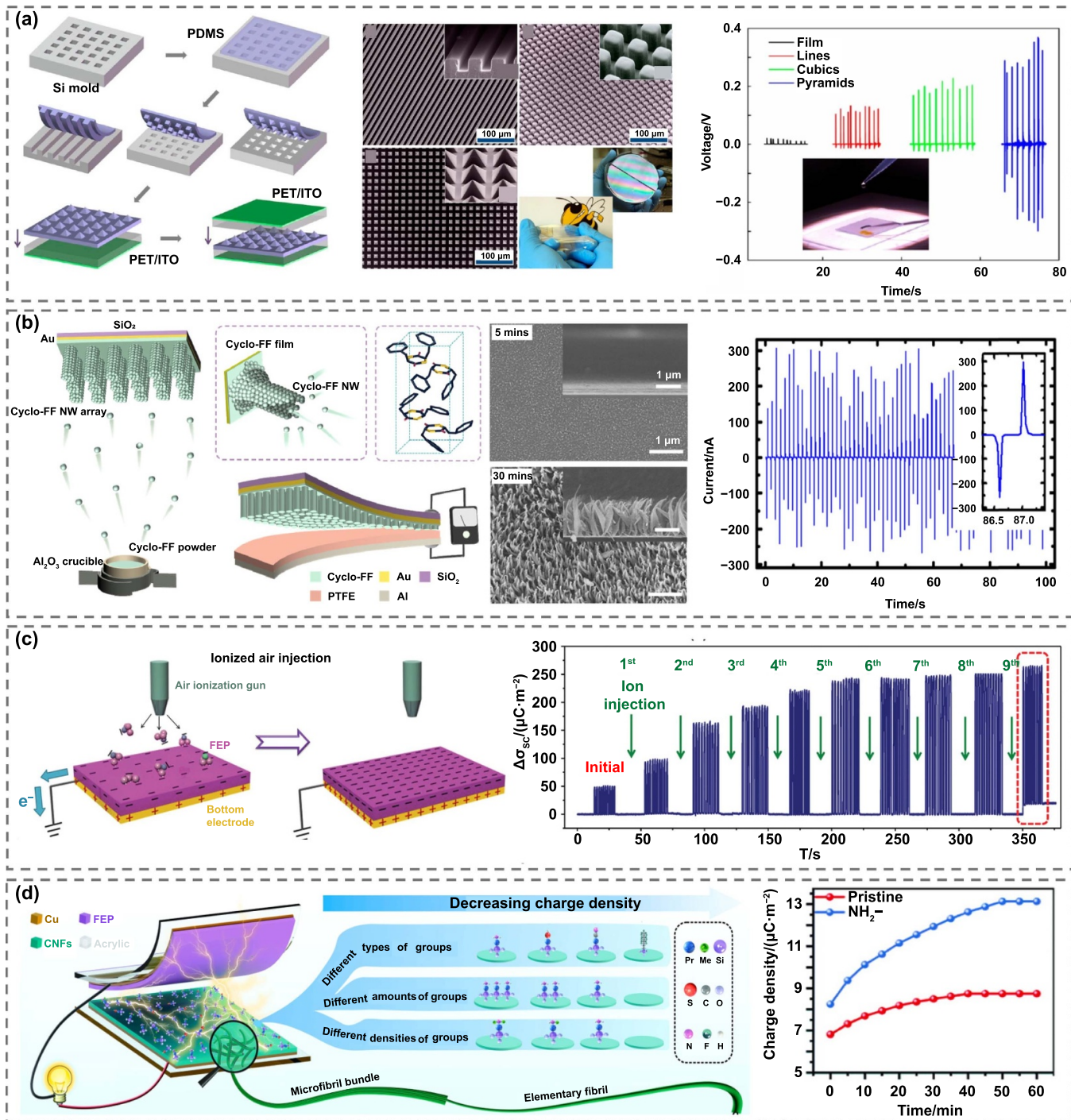


Figure 6. Strategies of surface modification to enhance output performance of TENGs. (a) Microstructuring. Reprinted with permission from [134]. Copyright (2012) American Chemical Society. (b) Nanostructuring. Reprinted from [135], Copyright (2019), with permission from Elsevier. (c) Ion injection on dielectric materials surfaces. [103] John Wiley & Sons. © 2014 WILEY-VCH Verlag GmbH & Co. KGaA, Weinheim. (d) Chemical surface modification to enhance output performance of TENGs. Reprinted from [136], Copyright (2021), with permission from Elsevier.

[143–145], and medical devices [146, 147]. These materials can be broadly categorized into three main groups: inorganic piezoelectric materials, organic piezoelectric materials, and composite piezoelectric materials. Each category possesses unique properties and applications that make them suitable for different technological needs.

Inorganic piezoelectric materials typically consist of ceramics or single crystals known for their high piezoelectric coefficients and stability. They are widely used due to their robust performance across various applications. Typical examples of inorganic piezoelectric materials include PZT, BaTiO_3 , quartz, lithium niobate (LiNbO_3)

and lithium tantalate (LiTaO_3). Park *et al* reported the development of a highly efficient and flexible nanogenerator by depositing PZT thin films onto plastic substrates (figure 7(a)) [148]. This approach combined the high piezoelectric response of PZT with the flexibility and lightweight properties of plastic. The fabrication method involved a sophisticated sol–gel process followed by spin-coating and annealing to ensure uniformity and optimal crystallinity of the PZT films. The resulting device was capable of generating electrical output from mechanical deformations such as bending and stretching, thus enabling the integration of high-performance piezoelectric materials into flexible and wearable electronics.

Organic piezoelectric materials are primarily polymers that exhibit piezoelectric properties. They are highly valued for their flexibility, lightweight nature, and ease of processing, making them suitable for applications where mechanical flexibility is crucial. Typical organic piezoelectric materials include polyvinylidene fluoride (PVDF), poly(vinylidene fluoride-trifluoroethylene) (PVDF-TrFE), and poly(lactic acid) (PLA). Sekine *et al* developed a stretchable acceleration sensor for a robotic machine interface by utilizing a combination of functional soft polymeric materials (figure 7(b)) [149]. The sensor consisted of two fully screen-printed stretchable e-skin layers, with the sensitive layer comprising a nanocomposite material containing a crystalline polymer of P(VDF-TrFE) and a paraelectric polymer PMMA-PBA. This sensor possessed the same tensile strength as human skin (~50%) and demonstrated greater sensitivity to velocity and acceleration. It exhibited excellent adaptability to robot hands and soft robot grippers, successfully functioning as an e-skin while detecting real-time tactile data during handling.

Composite piezoelectric materials combine the properties of both inorganic and organic materials, resulting in materials that offer high piezoelectric performance along with mechanical flexibility and processability. Examples include ceramic-polymer composites, fiber composites, and nanocomposites. Kim *et al* designed a boron nitride nanotube (BNNT) based CE-assisted PENG (figure 7(c)) [150]. This device consisted of two electrode layers with an intermediate BNNT–carbon nanotube (CNT)–PDMS composite layer. The BNNTs in the composite were primarily responsible for the piezoelectric response, while the CNTs facilitate effective electrical connectivity between the BNNTs, enhancing the overall output of the generator. The PENG was employed on a robotic finger model fabricated by 3D printing, and it detected the finger's movements and bending angles, showcasing its potential for robotic applications.

Bio-piezoelectric materials belong to organic piezoelectric materials and exhibit piezoelectric properties derived from biological origins or inspired by biological systems. They offer a unique combination of biocompatibility, biodegradability, and renewability, making them highly suitable for a wide range of applications. Lee *et al* developed a strategy

to synthesize large-scale aligned and unipolarized piezoelectric diphenylalanine nanotubes and designed a diphenylalanine peptide-based PENG (figure 7(d)) [151]. When subjected to mechanical stress, these nanotubes generated an electric charge due to their inherent piezoelectricity. These peptide-based energy converting materials could provide compatible energy harvesters or sensors for biomedical applications.

To enhance the output performance of PENGs, various advanced strategies can be employed, each targeting different aspects of the materials and device architecture. Chemical doping of piezoelectric materials is a widely used method, as it improves the intrinsic piezoelectric properties by introducing dopants that enhance polarization and energy conversion efficiency [152, 153]. Another effective approach is the preparation of aligned nanofibers, which allows for more efficient stress transfer and a higher degree of uniformity in the piezoelectric response, optimizing the mechanical-to-electrical energy conversion [154, 155]. Interfacial modifications, such as the introduction of conductive interlayers or surface treatments, are also crucial for enhancing charge transfer and improving the mechanical coupling between different layers in the device, thus reducing energy losses during operation [156, 157]. Furthermore, the development of nanocomposites [158, 159], where piezoelectric materials are combined with other nanostructured elements like conductive polymers, CNTs, or metallic nanoparticles, can introduce additional functional properties. These nanocomposites not only enhance mechanical durability and flexibility but also amplify electrical output by leveraging synergistic interactions between the composite components. Together, these strategies form a comprehensive approach to significantly boosting the efficiency and performance of PENGs, making them more viable for practical applications in areas like energy harvesting, wearable electronics, and self-powered systems.

Ye *et al* conducted a study on a composite material that utilizes piezoelectric properties for dual purposes: energy harvesting and radiation protection (figure 7(e)) [160]. In order to further enhance the performance of the flexible PENG, nanoimprint lithography was employed to facilitate the fabrication of longitudinal micropillars on the nanocomposite film. It was discovered that the PENG based on the microstructured P(VDF-TrFE)/BNNTs nanocomposite film exhibited an 11-fold enhancement in performance due to a synergistic effect of BNNTs and vertically well-aligned micropillar arrays. Liu *et al* developed an approach to significantly improve the piezoelectric properties and stability of piezopolymer composites (figure 7(f)) [161]. The GaIn nanodroplets (NDs) obtained via ultrasonication were embedded into the PVDF-TrFE matrix, forming GaIn NDs/PVDF-TrFE composites. It was revealed that this configuration of nanofillers could facilitate the formation of the polar β phase in PVDF-TrFE, and that the thickness of this dielectric oxide layer could affect the final contents of the β phase and then regulate the piezoelectric output. With this approach, it was possible to enhance by 10 times the output from PVDF-TrFE-based PENGs.

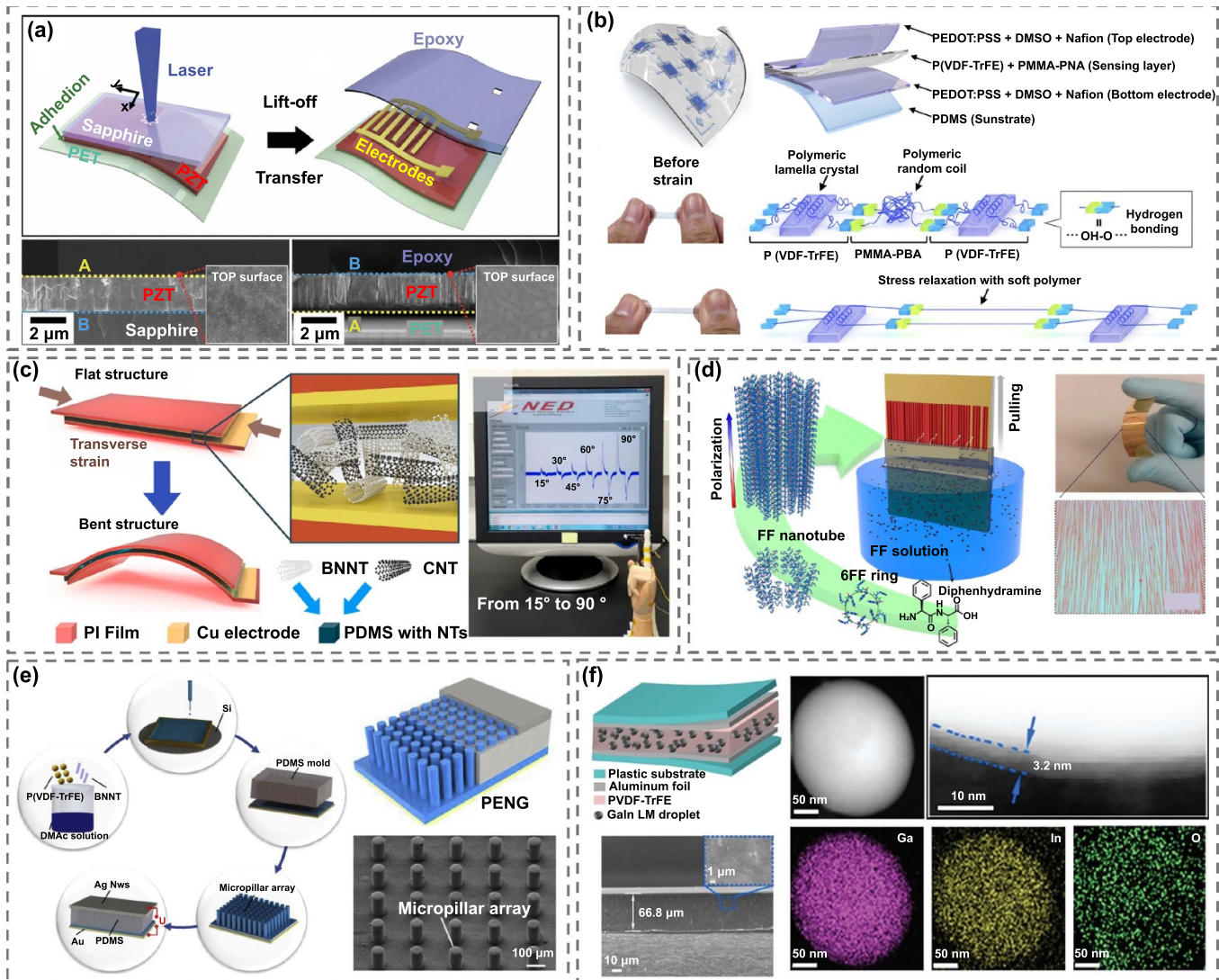


Figure 7. Design and strategies to enhance the output performance for PENGs. PENGs designed by (a) inorganic piezoelectric material. [148] John Wiley & Sons. © 2014 WILEY-VCH Verlag GmbH & Co. KGaA, Weinheim. Reprinted from [149], Copyright (2023), with permission from Elsevier. (c) Composite piezoelectric material. Reprinted with permission from [150]. Copyright (2020) American Chemical Society. (d) Bio-piezoelectric material. Reprinted with permission from [151]. Copyright (2018) American Chemical Society. (e) Strategy to enhance the output of PENGs by aligned nanofibers and nanocomposites. Reprinted from [160], Copyright (2019), with permission from Elsevier. (f) Strategy to enhance the output of PENGs by chemical doping and nanocomposites. Reproduced from [161]. CC BY 4.0.

3.3. Large-scale manufacturing techniques for nanogenerators

Large-scale manufacturing of nanogenerators represents a significant advancement towards realizing their potential in energy harvesting and self-powered sensing applications. Several factors must be carefully considered, including the use of materials with high triboelectric/piezoelectric properties, optimization of structural design, enhancement of energy conversion efficiency, standardization of fabrication processes, cost effectiveness, durability and longevity, as well as environmental sustainability. In this context, we present some techniques that show promising potential for the large-scale manufacturing of nanogenerators.

Lai *et al* introduced a triboelectric robotic skin made of flexible, stretchable materials, suitable for the dynamic shapes and movements of soft robots (figure 8(a)) [162]. Key materials included silicone elastomers and conductive polymers for their flexibility, durability, and triboelectric properties. The design used microstructures to enhance sensor sensitivity and extensibility, allowing accurate detection of proximity and pressure. The fabrication process involved creating a triangular microprism mold on an acrylic plate using a laser grinder. A silicone rubber solution was poured into the mold and cured to form a pressure-sensitive film. For the bottom layer, a silicone rubber solution was poured onto an acrylic plate pre-coated with silver sheets and cured. The film was then stripped off, embedding the silver matrix in the silicone rubber. A

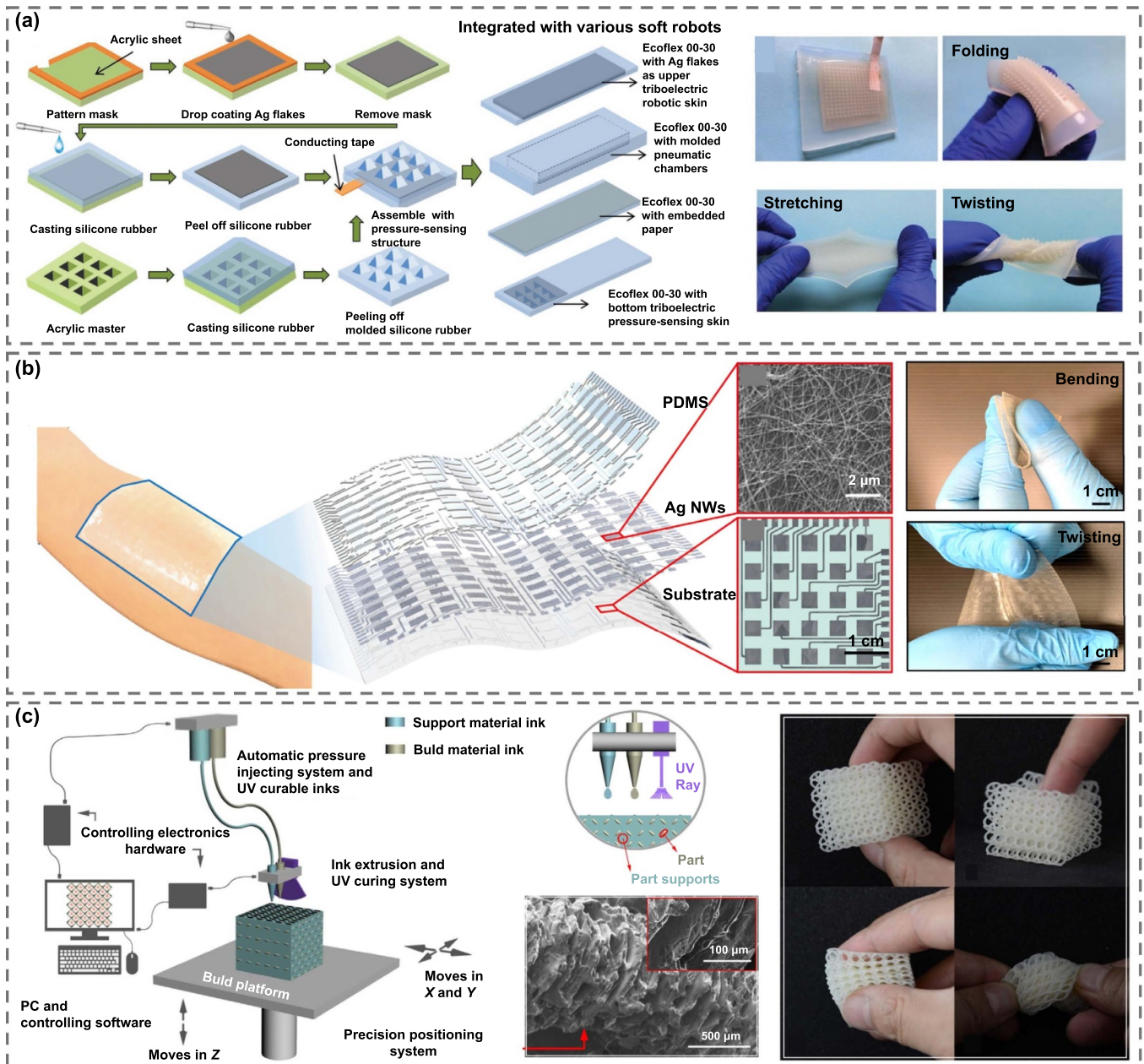


Figure 8. Potentially large-scale manufacturing technologies for TENGs. (a) Fabrication of the triboelectric robotic skin with high flexibility, stretchability and sensitivity. [162] John Wiley & Sons. © 2018 WILEY-VCH Verlag GmbH & Co. KGaA, Weinheim. (b) 3D printed flexible TENG sensor arrays with reducing crosstalk. Reproduced with permission from [88]. CC BY-NC-ND 2.0 OR CC BY-NC-ND 3.0 OR CC BY-NC-ND 4.0. (c) Three-dimensional-structure flexible TENG fabricated by the hybrid UV 3D printing technique. Reprinted from [165], Copyright (2018), with permission from Elsevier.

conductive copper strip was attached to the silver substrate. The final device was formed by adhering the bottom layer to the top pressure-sensitive film with silicone rubber solution, then curing. Potential applications include medical robots for safe human interaction, industrial robots for handling delicate objects, and wearable electronics.

3D printing is the process of creating three-dimensional objects from a digital file. This is achieved by laying down successive layers of material until the entire object is formed. It allows for high precision and customization, making it suitable for creating complex structures and intricate designs that

are difficult to achieve with traditional manufacturing methods [163, 164]. Incorporating 3D printing technology in the fabrication of TENGs offers several advantages. Firstly, 3D printing enables the creation of complex and precise geometries that can enhance the performance and efficiency of TENGs. Additionally, it allows for the customization of TENG designs to meet specific application requirements such as size, shape, and mechanical properties. Various materials can be used in 3D printing to fabricate TENGs including polymers, conductive materials, and composite materials. The typical process for 3D printing TENGs involves several steps: (1) design: a 3D

model of the TENG components is created using computer-aided design software. This model includes the triboelectric layers, electrodes, and any structural elements. (2) Material selection: appropriate materials are selected based on desired triboelectric properties and mechanical characteristics. (3) 3D printing: the selected materials are loaded into a 3D printer, and the TENG components are printed layer by layer according to the software design. (4) Assembly: the printed components are assembled to form the complete TENG device which may involve additional steps such as applying conductive coatings or integrating electrodes. Therefore, the use of 3D printing technology enhances both precision and customizability in TENG fabrication, making it an attractive option for creating complex structures and meeting specific application requirements while maintaining high performance standards.

Li *et al* developed advanced TENG sensor arrays to enhance tactile sensing by reducing crosstalk between sensors for better accuracy and reliability (figure 8(b)) [88]. The process used 3D printing to integrate TENGs into a soft, thin, flexible polyurethane acrylate substrate. The substrate was produced with a digital laser resin printer, treated with ethanol, and cured with UV light. UV-induced ozone treatment improved the bonding strength between Ag NWs electrodes and the substrate, reducing agglomeration. Ag NWs were spray-coated onto the substrate at a discharge rate of $1 \mu\text{L}\cdot\text{s}^{-1}$ using a steel mask to create electrode patterns. PDMS was then cast and smoothed over the substrate. The assembly was baked to cure the PDMS top layer and vacuum-pumped to remove bubbles. The resulting TENG sensor array, measuring $7.5 \text{ cm} \times 7.5 \text{ cm}$ with a thickness of 0.4 mm, comprised 100 sensing units. The combination of the soft substrate with ultra-thin Ag NWs and PDMS provided excellent flexibility, allowing the sensor array to endure bending, twisting, and rolling.

By using advanced hybrid UV 3D printing techniques, an approach was developed by Chen *et al* to fabricate complex three-dimensional structures that maximize the contact area and improve the energy conversion efficiency of the TENG (figure 8(c)) [165]. This technology allows for precise control over the geometry and dimensions of the TENG, enabling the creation of intricate and optimized structures that would be difficult to achieve with conventional manufacturing methods. The 3D printing process also allows for the integration of various materials with different properties, further enhancing the functionality of the TENG. In contrast to previous TENGs utilizing dielectric films as triboelectric materials, this ultra-flexible 3D-TENG utilized printed composite resin parts (with a high printing precision of $1 \mu\text{m}$) and ionic hydrogel as the electrification layer and electrode. The printing was performed using a UV curing 3D printer comprised of an automatic pressure injecting device, ink extrusion and UV curing system, precision positioning platform, PC, and hardware/software control system. The fabricated 3D TENG shows potential applications in wearable electronics.

R2R manufacturing is a high-throughput, continuous production process that fabricates devices on a flexible substrate by moving the material through various processing steps [166–168]. Widely used in the production of flexible electronics,

displays, and photovoltaic cells, R2R offers significant advantages for the scalable and cost-effective production of TENGs. This method allows for the continuous production of TENGs, significantly increasing the production rate and easily scaling up to accommodate large-area substrates for industrial-scale manufacturing. Its compatibility with flexible substrates makes it ideal for flexible electronic applications. The fabrication process involves preparing and loading the flexible substrate onto the R2R system, depositing triboelectric materials and electrodes using printing or coating techniques, laminating the deposited layers to create an integrated TENG structure, and undergoing curing or drying processes to enhance material properties and ensure long-term stability.

Fang *et al* reported a R2R processing approach to fabricate highly tribo-positive Nylon-11 films (figure 9(a)) [169]. This method involved melting and plasticizing Nylon-11 pellets using an extruder, then extruding the material to form a melt layer, which was rapidly cooled by chill rollers to achieve a film thickness of $25 \mu\text{m}$. The R2R process enhanced the surface functional groups and promoted the formation of a favorable pseudohexagonal crystal phase, significantly improving the transferred charge density and output performance of TENGs. Liu *et al* introduced a continuous fabrication approach for high-performance TENGs using R2R processing with ultrafast UV-induced polymerization (figure 9(b)) [170]. This method involved grafting a methacrylate-functional group onto PDMS to create methacrylate-functionalized PDMS (MAPDMS), which was polymerized under UV light in just 30 s. By introducing a fluorine-containing silane to enhance electronegativity, the resulting fluorine MAPDMS (MAPDMS-F) achieved a high surface charge density of $249 \mu\text{C}\cdot\text{m}^{-2}$, nearly double that of standard MAPDMS. This process was solvent-free, operated at room temperature, and could be employed on various conductive substrates. The R2R method allows for scalable, cost-effective, and efficient production of TENGs, advancing the development process. The fabricated TENGs demonstrate enhanced performance, making this approach highly promising for large-scale industrial applications.

Electrospinning is a technique used to produce fine fibers from a polymer solution or melt. This process involves the application of a high-voltage electric field to draw charged threads of polymer solution or melt, which then solidify to form nanofibers. Electrospinning is highly valued for its ability to create fibers with diameters ranging from nanometers to micrometers, offering a high surface area to volume ratio. It can be employed in the fabrication of TENGs to enhance their performance by creating nanostructured materials that maximize surface area and improve triboelectric interactions. Furthermore, electrospinning allows for the fabrication of composite fibers, incorporating various materials to tailor the triboelectric properties and mechanical strength of the TENG. The porous nature of electrospun fibers contributes to the flexibility and mechanical resilience of TENGs, making them suitable for wearable and flexible electronics. Various materials can be electrospun to create the triboelectric layers in TENGs, such as common polymers (PTFE,

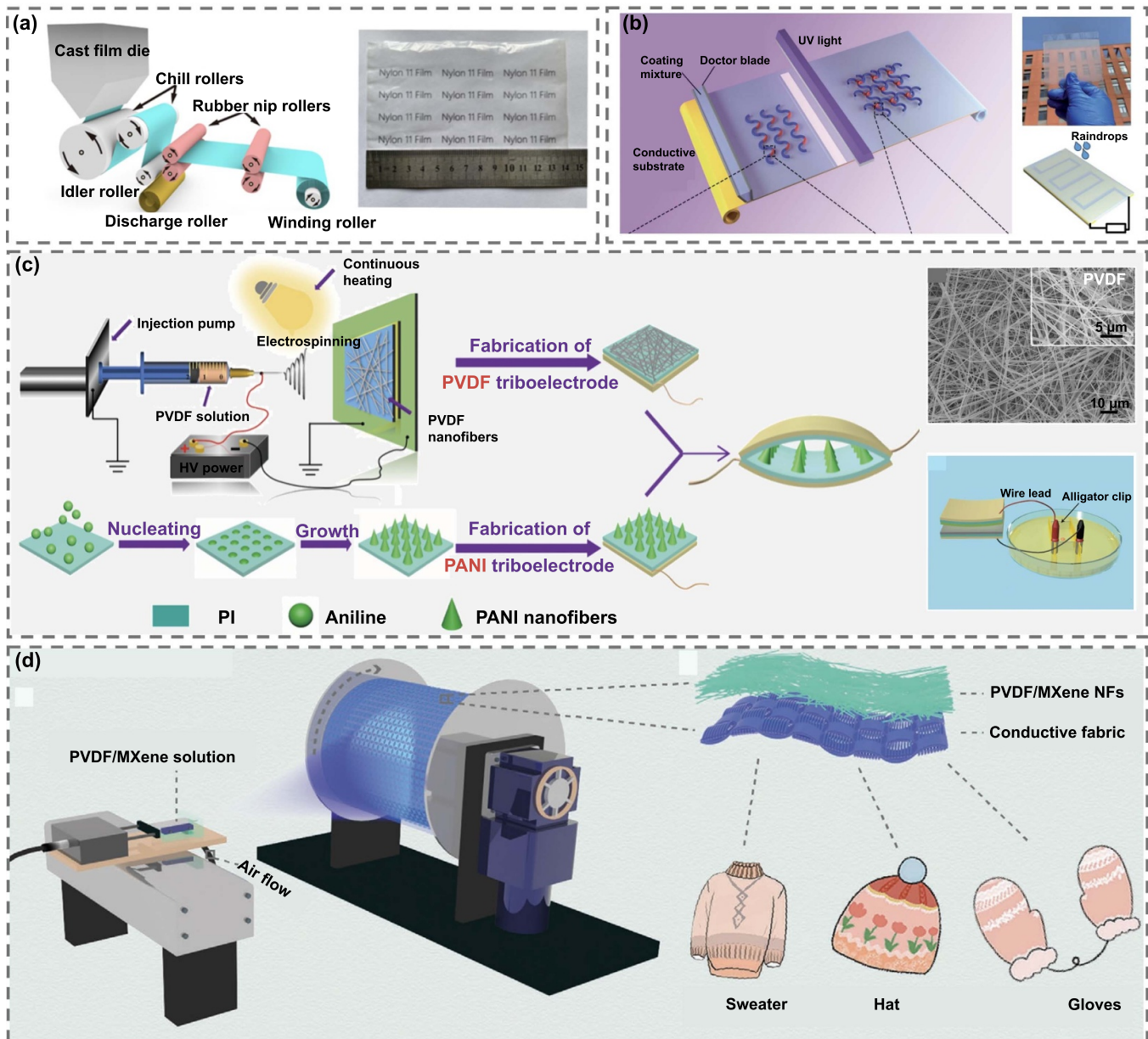


Figure 9. R2R and electrostatic spinning techniques for manufacturing TENGs. (a) R2R processing approach to fabricate highly tribo-positive Nylon-11 films. Reprinted with permission from [169]. Copyright (2024) American Chemical Society. (b) A continuous fabrication approach for high-performance TENGs using R2R processing with ultrafast UV-induced polymerization. Reproduced from [170] with permission from the Royal Society of Chemistry. (c) High-voltage pulse TENG with nano-structured tribo-charge layers. Reprinted from [171], Copyright (2021), with permission from Elsevier. (d) All-fibrous tailorble TENG with a large area based on one-step solution blow spinning technology. [172] John Wiley & Sons. © 2022 Wiley-VCH GmbH.

PVDF, nylon), composites (graphene, CNTs) and biodegradable materials (PLA). The typical process for incorporating electrospun fibers into TENGs involves several steps: (1) preparation of solutions: the polymer is dissolved in an appropriate solvent to create a solution with the desired viscosity and conductivity. (2) Electrospinning setup: the polymer solution is loaded into a syringe, and a high-voltage power supply is connected to the needle. The polymer solution is ejected and forms fibers under the influence of the electric field. (3)

Fiber collection: the nanofibers are collected on a grounded collector, often a rotating drum or a flat plate, forming a non-woven mat. (4) Integration into TENG: the electrospun mat is integrated into the TENG device as one of the triboelectric layers. Additional layers and electrodes are added to complete the device. Therefore, the flexibility in material choice and the ability to produce high surface area fibers make electrospinning a unique method for advancing the development of TENGs for various applications.

By employing electrospinning, Sun *et al* developed a high-voltage pulse TENG for manipulating water droplets in lubricating oil (figure 9(c)) [171]. The PANI NFs, which grow vertically on the PI substrate, exhibit a triangular cone structure due to a combined effect, forming the first tribo-charge layer. Additionally, the PVDF tribo-charge layer was prepared by electrospinning with nanostructure on its surface, resulting in a larger effective contact area with the PANI layer and thus generating more triboelectric charges during the CE process. This electrospinning was conducted under 14 kV and continuous heating. The PVDF solution was sprayed from the needle as filaments and adhered to the PI film to form PVDF nanowires. These nanowires were randomly and disorderly attached to the PI substrate, resembling human capillaries with diameters of about 0.5 μm . As a result of these fabrication techniques, the TENG had an open-circuit voltage of 1 502 V and short-circuit current of 50.61 μA , significantly larger than that from the TENG with a spin-coated smooth-structured PVDF layer (1015 V and 27.30 μA).

An all-fibrous tailororable TENG is presented by Xu *et al* using a one-step solution blow spinning technology (figure 9(d)) [172]. The TENG was composed of PVDF/MXene ($\text{Ti}_3\text{C}_2\text{Tx}$) nanofibers and conductive textile, with a large area of 20 cm \times 50 cm. It offered several advantages including good breathability, hydrophobicity, washability, easy operation, and high production efficiency. The fabrication process involved directly blowing PVDF/MXene nanofibers onto the conductive fabric using SBS technology. The prepared PVDF/MXene solution was drafted under high-speed airflow, and a roller covered with conductive textile received the fibers as the solution volatilized. By utilizing the SBS method, the LT-TENG could achieve area scalability with a well-designed receiving device. To enhance the output performance of LT-TENG, the 2D material MXene ($\text{Ti}_3\text{C}_2\text{Tx}$) was introduced. MXene containing the –F group had good electronegativity and superior electrical conductivity compared to commonly used polymers like PVDF and PTFE. This increased the surface charge density of the tribo-charge layer and improved the TENG's output. This TENG showed great potential prospects in wearable devices, intelligent robots, and human-machine interaction.

The manufacturing methods for PENGs encompass a wide range of techniques, from bulk processes to nanoscale methods, each offering distinct advantages for various applications in energy harvesting, sensing, and self-powered devices. Bulk manufacturing methods include sol–gel processing [173–175], which involves transitioning a solution into a solid gel phase to create ceramic and composite piezoelectric materials. This method allows for precise control over composition and homogeneity. Another bulk method is screen printing [176, 177], which uses a patterned screen to apply layers of piezoelectric materials onto substrates. This approach is cost-effective and scalable for large-area devices such as flexible electronics and sensors. Tape casting [178, 179] is also utilized in bulk manufacturing, involving the casting of a slurry of piezoelectric material onto a flat surface to produce thin ceramic tapes. This enables the production of thin, uniform films used in multilayered piezoelectric devices and capacitors.

Nanoscale manufacturing methods include chemical vapor deposition [180–182], which forms high-purity, uniform thin films with excellent crystallinity through gaseous reactants. Atomic layer deposition (ALD) [183–185] deposits thin films one atomic layer at a time, providing precise control over film thickness and composition for ultrathin piezoelectric layers and complex nanostructures. Hydrothermal synthesis [186, 187] produces high-quality piezoelectric nanocrystals from aqueous solutions at high temperatures and pressures, which are used for synthesizing nanoparticles and nanowires. Laser ablation [188–190] utilizes high-energy laser pulses to create micro- and nanostructures by removing material from a solid surface without damaging the substrate; it is employed in microelectromechanical systems and nanoscale piezoelectric devices.

The fabrication of PENGs involves several steps, starting with the preparation of piezoelectric materials, such as thin films, nanowires, or nanoparticles, using methods like ALD or hydrothermal synthesis. These materials are deposited on flexible or rigid substrates, such as PDMS or silicon, followed by the fabrication of top and bottom electrodes, typically made from metals like gold or silver, using sputtering or evaporation techniques. Patterning of the piezoelectric material and electrodes is often achieved through photolithography or nanoimprinting to optimize performance. The device is then encapsulated in a protective layer, such as PDMS, to safeguard it from environmental factors. The piezoelectric material undergoes a poling process, where a high-voltage electric field aligns the dipoles to enhance the piezoelectric effect. After the final assembly, the nanogenerator is tested and calibrated for its efficiency in converting mechanical energy into electrical output. Finally, the PENG can be integrated into various systems, such as wearable electronics, sensors, or energy-harvesting platforms.

In addition to the aforementioned methods, 3D printing [191, 192] and electrospinning [193, 194] are two advanced manufacturing techniques for PENGs. Similar to the applications for TENGs, 3D printing technology offers significant advantages in the fabrication of PENGs by enabling the creation of complex geometries, utilizing diverse materials, and allowing for high customization. It can be utilized for prototyping and producing intricate PENG designs. Zhou *et al* utilized 3D printing to create a fully integrated PENG with a unique kirigami-inspired design (figure 10(a)) [195]. The kirigami structure enhanced the stretchability and mechanical robustness of the device without compromising its electrical performance. The fabricating process involved several key steps: (1) initially, BaTiO_3 nanoparticle and P(VDF-TrFE) composite ink was 3D-printed onto ITO glass, which served as the bottom electrode during poling. Multiple layers were printed to achieve the desired thickness. (2) Subsequently, a conductive Ag flake/P(VDF-TrFE) ink was printed on top to form the top electrode, ensuring compatibility between the materials. (3) The printed structure, along with the ITO glass substrate, was then immersed in silicone oil and subjected to a high electric field at 100 °C for 2 h to align the ferroelectric dipoles within the P(VDF-TrFE) matrix and BaTiO_3 nanoparticles. (4) After poling, the silicone oil was removed, and

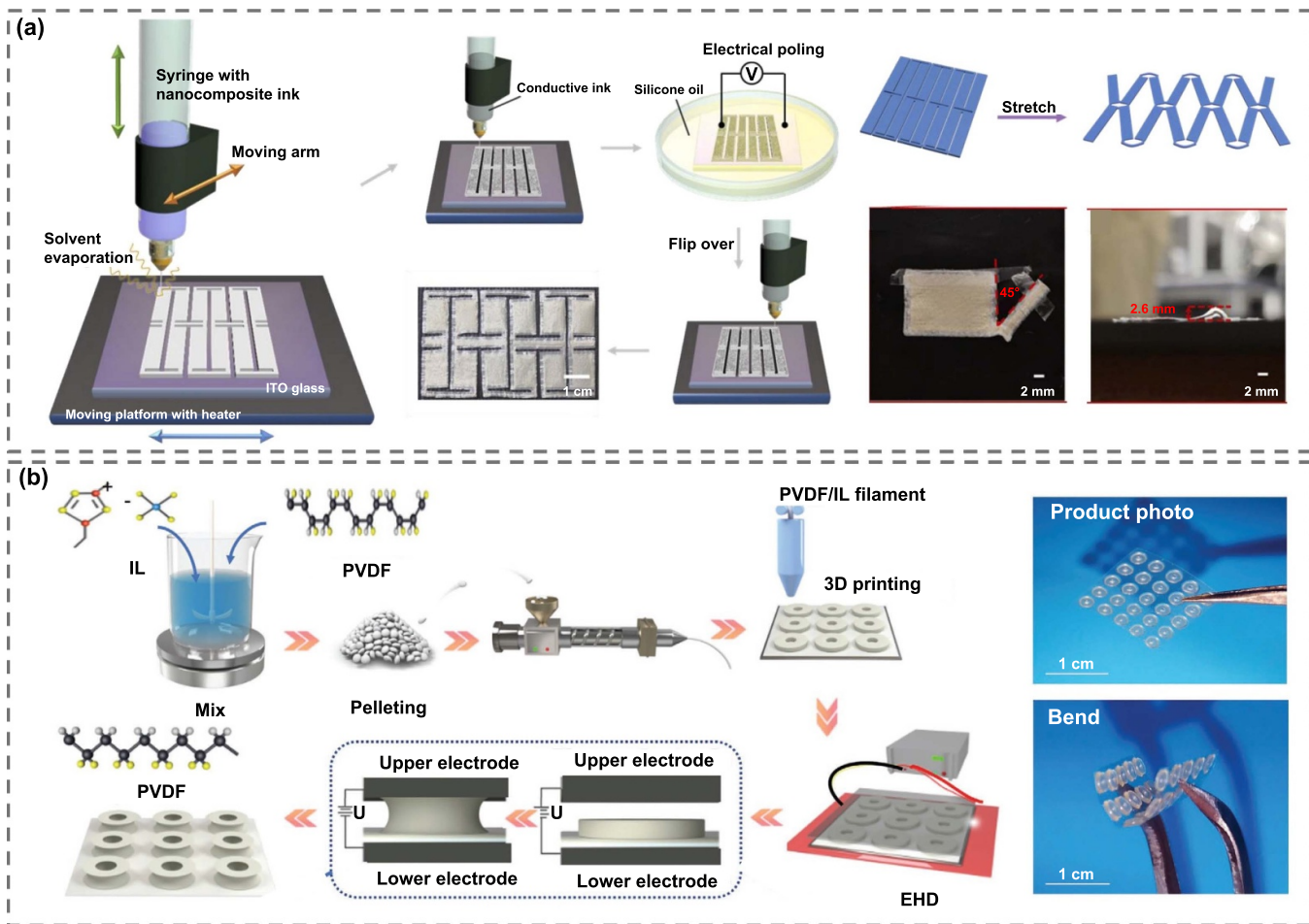


Figure 10. 3D printing techniques for manufacturing PENGs. (a) A fully integrated PENG with a unique kirigami-inspired design fabricated by 3D printing. Reprinted from [195], Copyright (2020), with permission from Elsevier. (b) 3D hyperboloidal β -PVDF sensor arrays based on electrohydrodynamic pulling and fused deposition modeling 3D printing technology. [196] John Wiley & Sons. © 2022 Wiley-VCH GmbH.

the sample is peeled from the substrate, flipped, and reattached for the bottom electrode printing. (5) The bottom electrode was printed using the same Ag flake/P(VDF-TrFE) conductive ink, completing the fabrication of the fully 3D-printed PENG. This meticulous process ensured a robust and efficient device suitable for flexible electronic applications.

By combining electrohydrodynamic pulling and fused deposition modeling 3D printing technology, He *et al* successfully developed 3D hyperboloidal self-polarized β -phase PVDF (β -PVDF) sensor arrays (figure 10(b)) [196]. This fabrication method improved the efficiency and functionality of the piezoelectric sensors (PESs) by ensuring optimal alignment and self-polarization of the β -PVDF structures. The process of fabricating the sensor array involved adding ionic liquid to PVDF filaments in order to induce β crystal formation. These filaments were then extruded via fused deposition modeling 3D printing onto conductive glass, forming annular pre-patterns that act as the lower electrode. A second conductive glass was placed above with an air gap, creating a capacitor-like device. Subsequently, the structure was heated to 220 °C while high voltage is applied, generating a Maxwell force that shaped the rings into hyperboloids connecting to the

upper electrode. This process effectively aligned the PVDF molecular dipoles. The array was then crystallized at 160 °C for 30 min to finalize the electroactive phase. This method achieved simultaneous structure formation and polarization, resulting in flexible arrays suitable for use in wearable devices.

Electrospinning is a highly effective technique for producing PENGs, allowing for the development of efficient and adaptable devices suited to a wide range of innovative applications. Guan *et al* introduced a method for creating hierarchically structured nanocomposite fiber mats by modifying BaTiO₃ nanoparticles with polydopamine (PDA) and incorporating them into a P(VDF-TrFE) matrix (figure 11(a)) [197]. This design significantly improved the piezoelectric properties and mechanical flexibility of the resulting nanocomposites. The modified BaTiO₃ nanoparticles enhanced compatibility and dispersion within the polymer matrix, leading to superior energy harvesting and sensing performance. The fabrication process of Pdop-BT@P(VDF-TrFE) nanocomposites involved first creating P(VDF-TrFE) membranes through electrospinning, followed by preparing Pdop-BT nanoparticles via dopamine (DA) self-polymerization in a Tris-HCl buffer containing dispersed BT nanoparticles. Subsequently, the

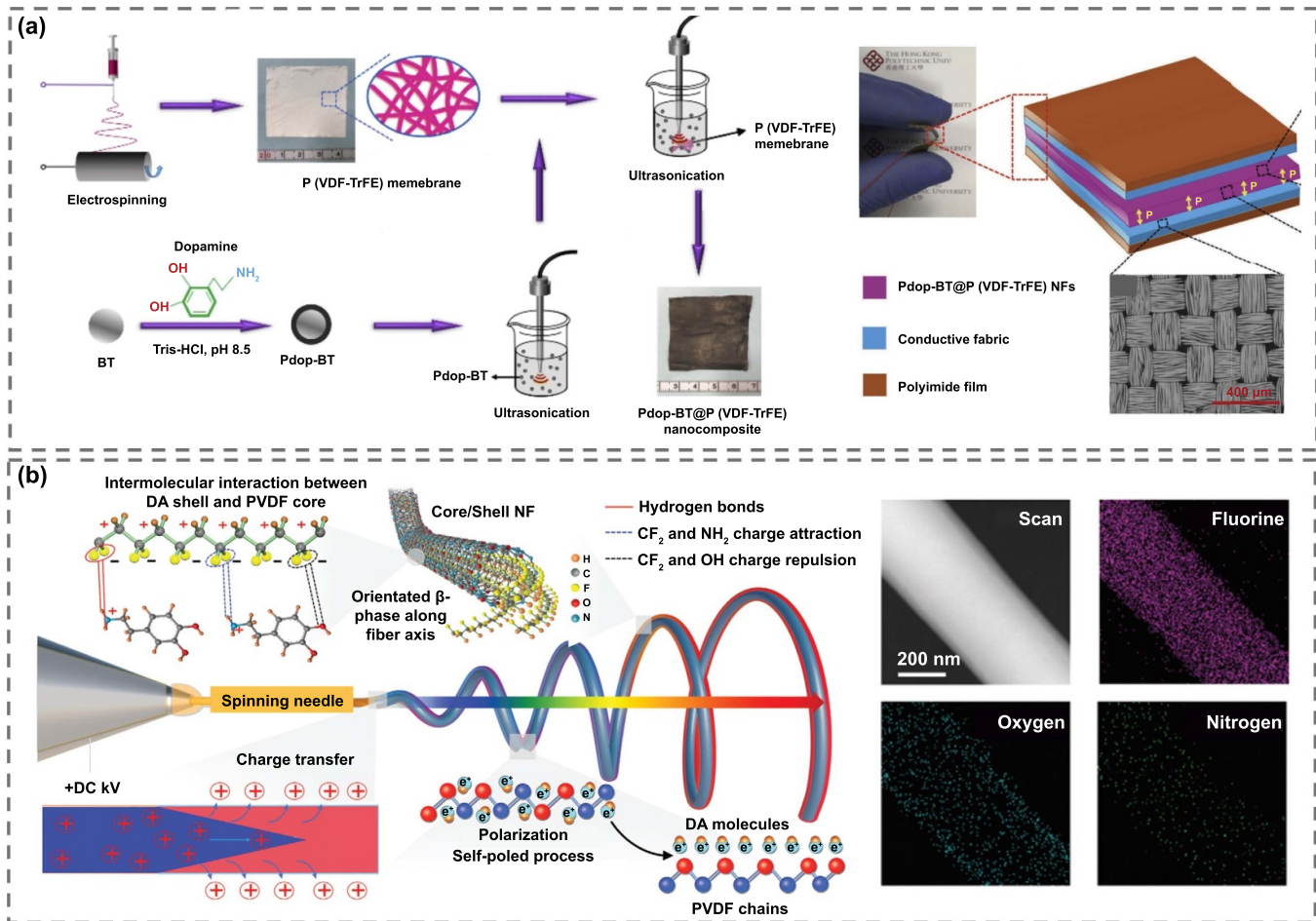


Figure 11. Electrostatic spinning techniques for manufacturing PENGs. (a) A method for creating hierarchically structured nanocomposite fiber mats. Reprinted from [197], Copyright (2020), with permission from Elsevier. (b) A straightforward one-step electrospinning method to fabricate core/shell PVDF/DA nanofibers. [198] John Wiley & Sons. © 2020 Wiley-VCH GmbH.

P(VDF-TrFE) membranes were immersed in the Pdop-BT suspension and ultrasonicated, causing the nanoparticles to attach to the nanofibers due to micro-jets and shock waves. PDA acts as a bridge, enhancing interaction between BT nanoparticles and P(VDF-TrFE) fibers through its $-\text{OH}$ and $-\text{NH}_2$ groups. The resulting PENG was successfully utilized as a self-powered sensor for efficiently detecting human body movements.

Li *et al* developed a straightforward one-step electrospinning method to fabricate core/shell PVDF/DA nanofibers (figure 11(b)) [198]. By introducing 1.0 wt% DA, the spontaneous formation and alignment of β -phase PVDF were significantly enhanced during electrospinning. This self-assembly process results from the formation of a continuous DA nanoshell around the PVDF core due to electrostatic repulsion among charged DA molecules. The strong intermolecular interaction between the $-\text{NH}_2$ groups on DA and the $-\text{CF}_2$ groups on PVDF is crucial for aligning PVDF chains and promoting β -phase nucleation. This continuous interfacial interaction also stabilizes the β -phase. The resulting PVDF/DA nanofibers exhibited excellent piezoelectric properties, stability, and biocompatibility. Flexible thin films made from randomly stacked PVDF/DA nanofibers were fabricated as PESs,

which can be conformally attached to various body surfaces (chest, neck, and wrist) to accurately measure weak mechanical stimulations from blood pulsations.

The manufacturing of TENGs and PENGs has advanced considerably, presenting promising prospects for diverse applications such as energy harvesting, self-powered sensing, wearable electronics, heart beating and position detection [199, 200]. Although challenges persist regarding scalability, cost, and durability, ongoing research and development endeavors are well-positioned to address these issues. The future of nanogenerators is promising, with the potential to revolutionize the way we harness and utilize energy from our environment.

4. Applications of nanogenerators for intelligent robotics

4.1. Nanogenerators enable intelligent sensing and human–robot interaction

Triboelectric and PESs are poised to revolutionize robotics by providing novel methods to harness and convert mechanical energy into electrical signals. Triboelectric sensors operate on

the principle of the triboelectric effect, where electrical signals generate when certain materials making contact and then separating from other materials. Meanwhile, PESs generate electrical signals in response to mechanical stress or pressure. By integrating both triboelectric and PESs, robots gain enhanced capabilities to interact with their environments and perform complex tasks more effectively. This integration improves the autonomy and versatility of robots, making them indispensable tools in a wide array of applications, from industrial automation to healthcare.

One of the primary applications of triboelectric and PESs in robotics is within the human–robot interface [201–203]. These sensors enable intuitive, safe, and secure control and feedback mechanisms between humans and robots, facilitating seamless collaboration. For instance, triboelectric and PESs can detect touch, pressure, and mechanical stress, allowing robots to respond to human gestures and commands in a natural and intuitive manner. This capability makes robots more user-friendly and easier to control, bridging the gap between human intentions and robotic actions. Additionally, by continuously monitoring force and pressure in real-time, these sensors ensure that interactions between humans and robots remain safe, preventing excessive force during physical contact and reducing the risk of injury in collaborative environments.

To address the critical issue of enhancing human–robot interaction, Pu *et al* designed a joint motion triboelectric quantization sensor for constructing a robotic hand synchronous control system (figure 12(a)) [204]. The TENG sensor consisted of an acrylic rectangular cavity, a copper electrode pattern, and a FEP thin film. By detecting flexion-extension degree and speed, it could accurately sense the rotation angles of finger joints with a minimum resolution angle of 3.8° . The sensor was worn on the index and middle human fingers, and the generated signals were used to control a commercial robotic hand for performing gestures like the victory v-sign and grasping objects in real-time, highlighting its precision and responsiveness. To further enhance the flexibility and wearability, Luo *et al* developed a simple-structured and high-resolution bending angle triboelectric sensor to construct a glove-based multi-dimensional HMI (figure 12(b)) [89]. This sensor was fabricated by PDMS, silicon rubber and with Cu mesh electrodes in these two materials for not influencing the flexibility. Equipped with this type of sensors, the smart glove system realized robotic hand control with different grabbing levels, speeds, and holding times, demonstrating the ability to handle objects delicately, such as grabbing a plastic block or an egg without causing damage. The integration of machine learning algorithms further enhanced the system's capabilities, achieving high accuracy in user identification and gesture recognition.

In order to expand the potential applications of soft robots and enhance their accessibility and ease of control for non-specialist users, Liu *et al* proposed a multimodal flexible sensory interface for interactive teaching of skilled locomotion to soft robots using only human hands (figure 12(c)) [205]. The sensor was composed of multiple flexible and stretchable layers, including a dielectric layer fabricated by casting

silicone rubber with micro-pyramid structures, an electrode layer made with patterned silver nanowire networks, a stimulation layer beneath the electrode layer, a liquid metal layer printed using a liquid metal printer, and a package layer ensuring the overall integrity of the sensor structure. Such fabricated sensor was capable of detecting both physical touch (tactile) and proximity (touchless) stimuli, enabling humans to interactively instruct soft robots equipped with the sensor in complex movements and tasks through bare hand-eye coordination, such as navigating mazes, taking throat swabs, and grasping objects.

Current sensors often lack omnidirectional perception in space and require further improvement in resolution for tactile perception. Taking inspiration from the platypus' beak, Mu *et al* proposed a bionic electro-mechanosensory finger (EM-Finger) that combined triboelectric and visuotactile sensing to provide touchless and tactile perception (figure 12(d)) [206]. Structurally, the EM-Finger featured a triboelectric sensor array created by spraying liquid-metal-polymer conductive ink on a transparent elastomer, encapsulated with a PDMS dielectric layer. Additionally, it included a visuotactile sensor that utilizes RGB LEDs for internal lighting and deformation measurement through marker detection. This integrated design allowed the EM-Finger to perform multiple functions, including omnidirectional touchless sensing, high-resolution tactile perception, amphibious communication, and accurate material identification. Equipped with the EM-Finger, a robotic arm could be wirelessly controlled by human hands to accurately identify, pick up, and move objects, demonstrating its potential for enhanced HRI.

For the application of PENGs on human–robot interaction, Deng *et al* introduced a flexible, self-powered PES utilizing cowpea-structured PVDF/ZnO nanofibers for remote gesture control in human–machine interfaces (figure 12(e)) [207]. The sensor's design combined ZnO nanospheres within a PVDF matrix, enhancing both flexibility and piezoelectric sensitivity, with MXene electrodes providing mechanical durability and conductivity. The sensor demonstrated high performance, with a bending sensitivity of $4.4 \text{ mV per degree}$, pressing sensitivity of $0.33 \text{ V}\cdot\text{kPa}^{-1}$, and fast response times of 76 ms for bending and 16 ms for pressing. It maintained stability through 5000 bending and pressing cycles, proving its mechanical robustness. The PES enabled gesture recognition and remote control of robotic hands, where it detected human finger motions and transmitted the data wirelessly to control a robotic hand in real time, accurately mimicking the user's gestures.

Triboelectric and PESs also play a crucial role in enhancing robotic exteroceptive sensing, which involves the robot's ability to perceive and understand the external environment [208, 209]. These sensors can determine contact force, texture, and other physical properties of objects, enabling robots to handle delicate items with precision and care. This capability is particularly important in applications such as fragile goods handling robots, where precise and gentle manipulation is essential. Furthermore, triboelectric and PESs can detect environmental stimuli such as vibrations and airflow, allowing robots to navigate complex and dynamic environments more effectively.

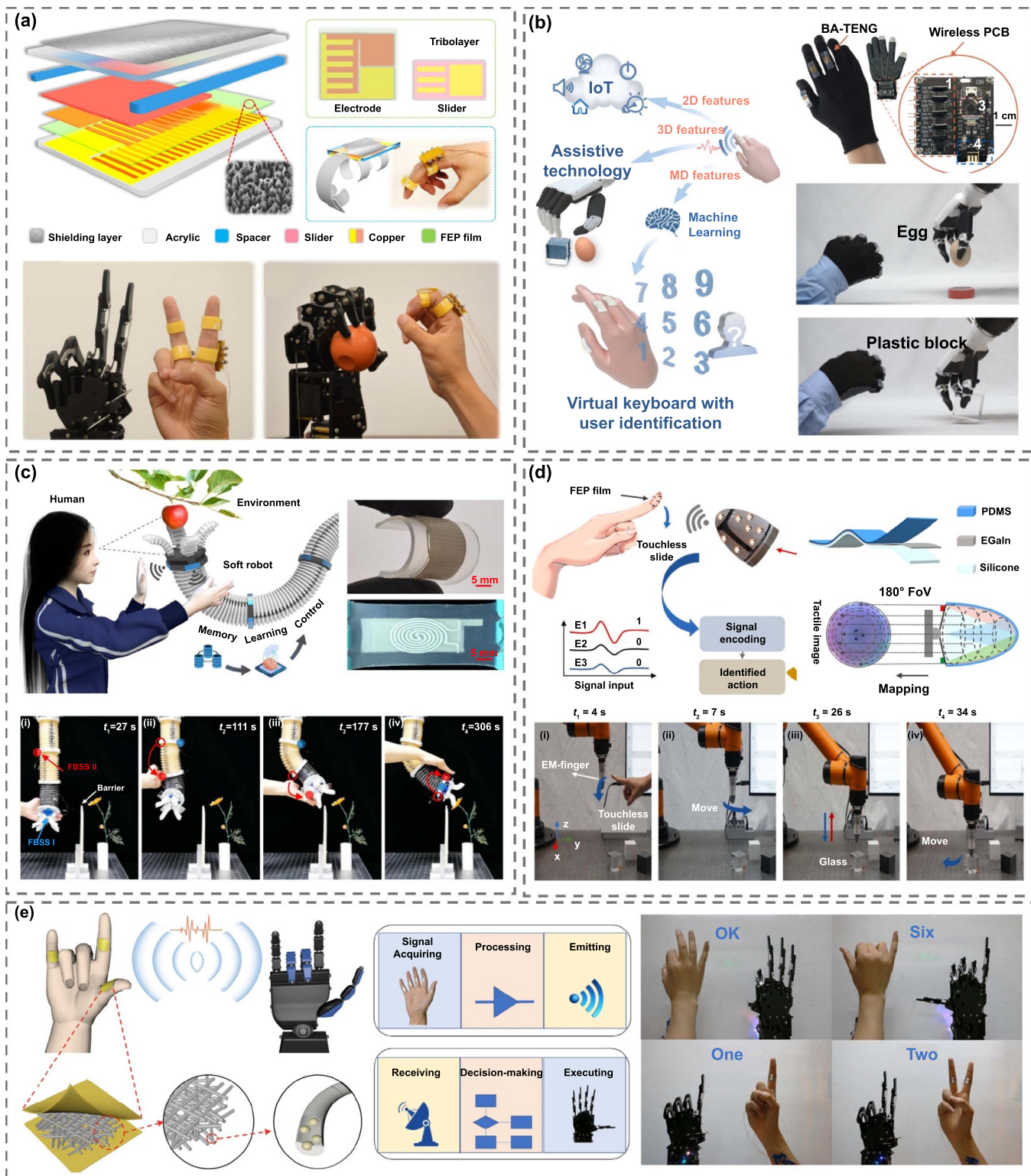


Figure 12. Applications of nanogenerators for human–robot interaction. (a) Joint motion triboelectric quantization sensor for constructing a robotic hand synchronous control system. Reprinted from [204], Copyright (2018), with permission from Elsevier. (b) Simple-structured and high-resolution bending angle triboelectric sensor to construct a glove-based multi-dimensional HMI. Reprinted from [89], Copyright (2021), with permission from Elsevier. (c) Multimodal flexible sensory interface for interactive teaching of skilled locomotion to soft robots using only human hands. Reproduced from [205]. CC BY 4.0. (d) Bionic electro-mechanosensory finger combining triboelectric and visuotactile sensing to provide both touchless and tactile perception. Reprinted from [206], Copyright (2023), with permission from Elsevier. (e) A flexible, self-powered piezoelectric sensor for remote gesture control in HMs. Reprinted from [207], Copyright (2019), with permission from Elsevier.

Inspired by the natural movements of caterpillars, Jin *et al* proposed a soft caterpillar robot that integrated two types of stretchable bionic sensors into a dual air-chamber pneumatic network structure (figure 13(a)) [210]. This design allows the robot to bend and move forward or backward by inflating and deflating the air chambers. The tactile sensing capabilities are provided by four triboelectric sensors, which are based on functional liquid metal and feature thorny-structured bionic whiskers. Additionally, two ultra-stretchable resistive sensors offer proprioceptive feedback on the robot's deformations. This combination enables the robot to perform complex adaptive behaviors by leveraging both external and internal sensory information, such as escaping from unexpected attacks, avoiding obstacles, and navigating through unknown tunnels.

In a similar vein, Zhu *et al* drew inspiration from insect antennae sensory mechanisms to propose a bionic antenna for micro-robotic tactile sensing (figure 13(b)) [211]. The antenna consists of three main components: the sensing section, nerve section, and muscle fibers. The sensing section is comprised of a triboelectric sensor fabricated from AgNW-coated Ecoflex Sponge that converts mechanical stimuli into electrical signals for material identification and contact force sensing. The nerve section utilizes a metal conductive wire to transmit these electrical signals from the sensor to the microprocessor. Meanwhile, muscle fibers composed of a two-stage actuator with shape memory alloy springs and PET film control the horizontal and vertical movements of the antenna. Leveraging this antenna design enables the micro-robot to perform both passive and active sensing tasks including navigation in complex terrains as well as obstacle avoidance and environmental recognition.

In recent years, significant progress has been made in the development of new sensing technologies that mimic the human sensory system through bionics. This advancement allows robots to possess the ability to touch, hear, smell, and taste like humans. Lu *et al* have developed a tactile sensor capable of converting tactile information into visible light signals without requiring an external power supply (figure 13(c)) [212]. They designed a high-output TENG to harvest mechanical energy from touch and convert it into electrical energy. The key structural components included chitosan and FEP as triboelectric materials, an X-shape TENG design for increased contact area, and the use of origami techniques to enhance flexibility and mechanical robustness. The generated electrical energy drove a light-emitting diode, providing real-time visual feedback on touch and pressure intensity. This sensor has improved the visual feedback of tactile perception and demonstrated applications in smart protective clothing, robotics, and rehabilitation training.

The auditory system serves as an efficient and straightforward communication strategy for connecting humans and robots. Guo *et al* developed a self-powered triboelectric auditory sensor to create an electronic auditory system and an architecture for external hearing aids in intelligent robotic applications (figure 13(d)) [213]. The sensor incorporated a FEP film with enhanced nanostructures to increase surface charge density as one of the triboelectric layers, while the Kapton film functioned as the vibration membrane, and an upper Au

electrode formed another triboelectric layer. A tunable gap spacer ensured proper membrane vibration. Additionally, the sensor's design included annular and sectorial inner boundary architectures, enabling frequency tuning and selective amplification. With a broad frequency response covering 100 Hz to 5000 Hz, it was suitable for capturing a wide range of acoustic signals, including human voice frequencies. Practical applications include controlling a desk lamp with sound, acting as an antitheft alarm, recording high-quality music, and recognizing voices. In hearing aid applications, the sensor successfully restored sound information in impaired frequency regions, demonstrating its potential as a new type of hearing aid.

Human taste perception in smart sensing devices is challenging to replicate due to the intricate processing abilities of gustatory organs. Traditional electronic taste systems often necessitate complex and costly analyses, as well as frequent battery replacements. To tackle this issue, Barman *et al* developed a self-powered triboelectric taste sensor integrated with a robotic platform for detecting mercury ions (Hg^{2+}), a highly toxic pollutant (figure 13(e)) [214]. The sensor used vertically aligned tellurium nanowires on a flexible aluminum substrate, serving as both the triboelectric material and sensing probe. Operating through solid–liquid CE, the nanowires formed mercury telluride nanowires upon contact with Hg^{2+} solutions, resulting in significant output voltage changes with increasing Hg^{2+} concentrations. The sensor successfully detected Hg^{2+} in real water and food samples with high sensitivity. Integration with the robotic hand enabled real-time, wireless detection and simultaneous detection of multiple analytes without interference.

Traditional electronic noses, commonly used in various industries for gas detection, are faced with several challenges. These include a reliance on batteries, high energy consumption, limited multidimensional information detection, and difficulties in real-time gas identification—particularly within the context of the Internet of Things. In response to these issues, Fu *et al* developed a self-powered wireless electronic nose system based on triboelectric discharge (figure 13(f)) [215]. This system incorporated a TENG to harness external mechanical energy and a tip-to-tip metal structure that is exposed to the tested gas. The TENG generates charges that initiate gas discharge, resulting in the production of electromagnetic waves for wireless sensing. These electromagnetic signals are then wirelessly transmitted to a computer for analysis and display. The system was trained using data from 60 different gas atmospheres, encompassing five different gases (Air, Ar, CO_2 , He, N_2) at 12 different pressures. Impressively, the deep learning model achieved an average recognition accuracy of 93.8%.

In the field of robotic proprioceptive sensing, which is analogous to self-awareness in humans, triboelectric and PESs play a crucial role in providing essential feedback on a robot's internal states, including position, orientation, and motion. These sensors are capable of measuring joint rotation angles and mechanical stress, thus offering precise feedback on the position and movement of robotic limbs. This capability enables robots to monitor their own movements and make real-time adjustments to enhance the accuracy and responsiveness

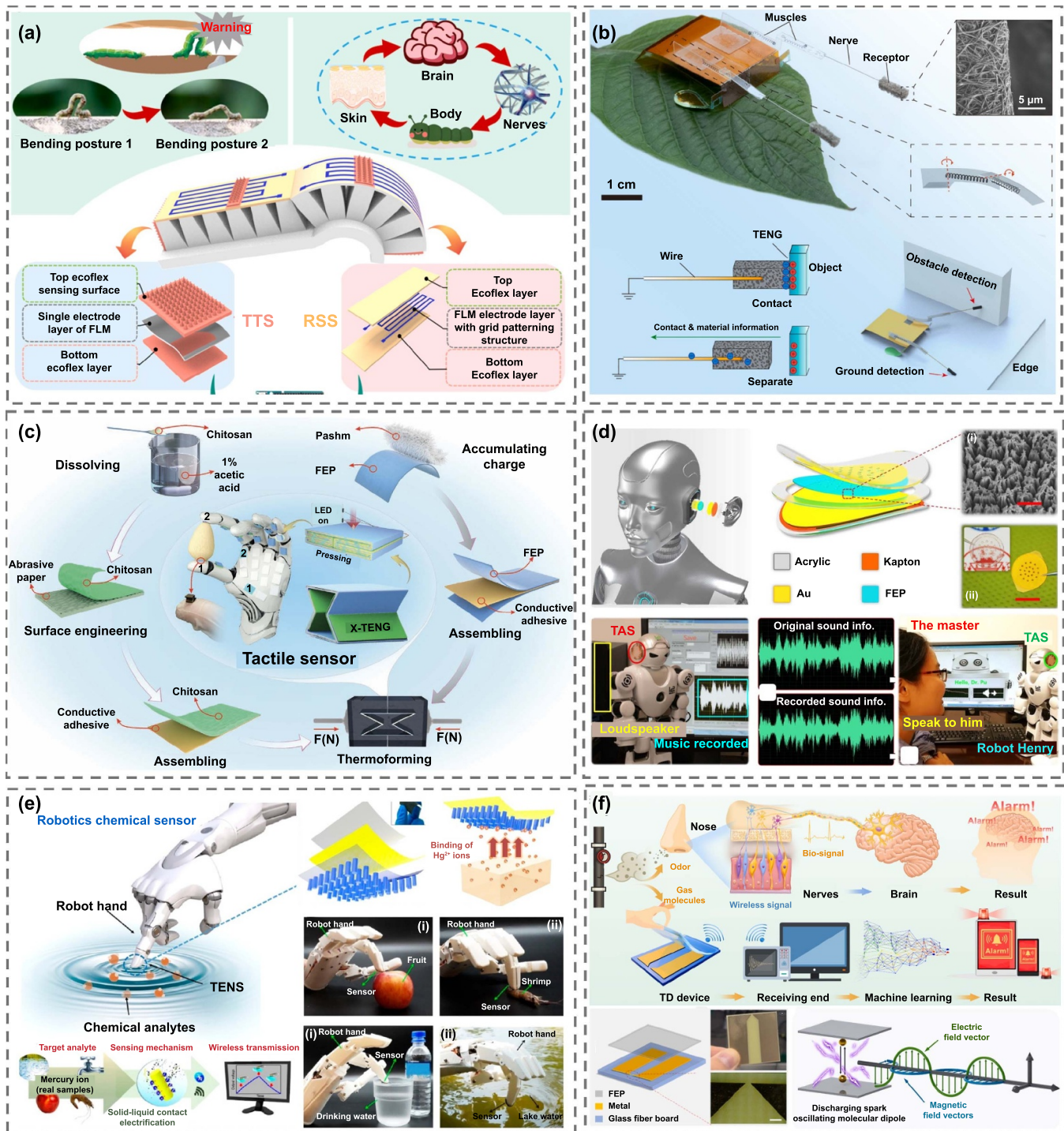


Figure 13. Applications of nanogenerators for robotic exteroceptive sensing. (a) Soft caterpillar robot that integrates two types of stretchable bionic sensors into a dual air-chamber pneumatic network structure. Reprinted from [210], Copyright (2021), with permission from Elsevier. (b) Bionic antenna for micro-robotic tactile sensing inspired by insect antennae sensory mechanisms. Reprinted from [211], Copyright (2023), with permission from Elsevier. (c) Tactile sensor capable of converting tactile information into visible light signals. [212] John Wiley & Sons. © 2022 Wiley-VCH GmbH. (d) Triboelectric auditory sensor to create an electronic auditory system and an architecture for external hearing aids in intelligent robotic applications. From [213]. Reprinted with permission from AAAS. (e) Droplet-tasting sensor system based on the dynamic morphological changes of droplets and liquid–solid contact electrification. Reprinted with permission from [214]. Copyright (2023) American Chemical Society. (f) Wireless electronic nose system based on triboelectric discharge. Reprinted from [215], Copyright (2024), with permission from Elsevier.

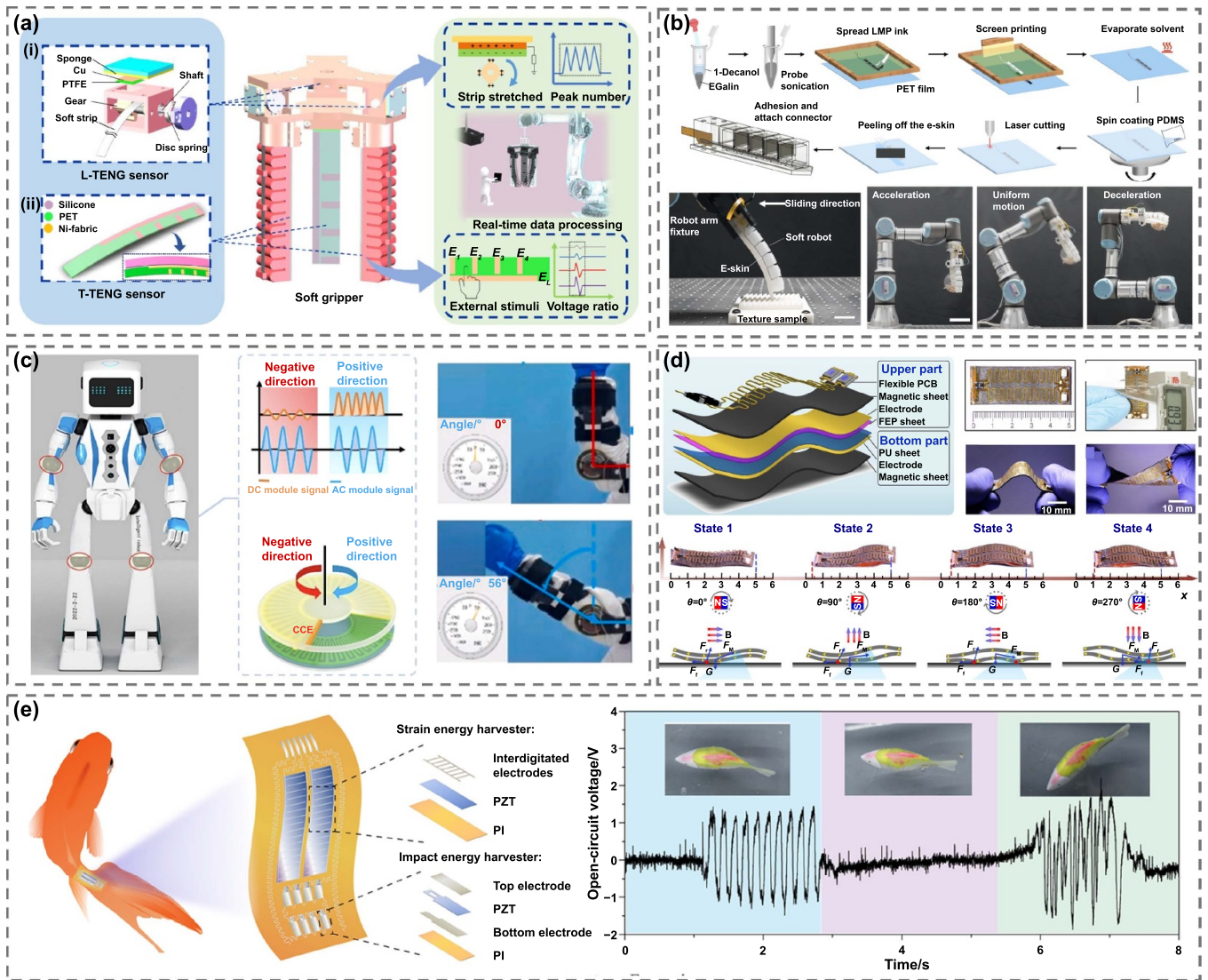


Figure 14. Applications of nanogenerators for robotic proprioceptive sensing. (a) Soft gripper integrated tactile TENG sensors and length TENG sensors to capture continuous motion and tactile information. Reproduced from [216]. CC BY 4.0. (b) Ultra-thin e-skin using a screen-printing technique with liquid metal particles and a kirigami design. © [2024] IEEE. Reprinted, with permission, from [66]. (c) Vector motion sensor based on a dual-mode TENG to monitor joint movements. Reprinted from [217], Copyright (2022), with permission from Elsevier. (d) Self-powered robot utilizing the slug's unique locomotion mechanics and integrated it with a TENG. Reprinted from [218], Copyright (2022), with permission from Elsevier. (e) A fish-wearable PENG for both energy harvesting and fish behavior monitoring. Reprinted with permission from [219]. Copyright (2023) American Chemical Society.

of robotic systems. Furthermore, these sensors can also measure strain or deformation in robotic components, ensuring that the robot operates within safe mechanical limits and preventing damage from excessive stress or overloading. As a result, they contribute to extending the operational lifespan of the robot.

Traditional sensors such as potentiometers and encoders are not suitable for soft robots due to their high nonlinear deformation and joint-less structure. While TENG sensors are compatible with soft materials and can generate self-powered outputs in response to strains and deformations, making them ideal for applications in soft robotics. Jin *et al* integrated tactile TENG sensors and length TENG sensors into a soft gripper to capture continuous motion and tactile information (figure 14(a))

[216]. The tactile sensor consisted of patterned Nickel-fabric electrodes on a PET substrate, coated with a layer of silicone rubber, allowing the detection of sliding, contact position, and contact mode. The length sensor featured a gear mechanism with Nickel-fabric and PTFE film, connected to a stretchable strip for continuous elongation detection. A disc spring ensured the strip's self-recovery, maintaining tension and preventing deviation. The integrated system demonstrated high accuracy and versatility in various applications including object identification, tactile sensing, length sensing, real-time control, and digital twin technology. Notably, the system successfully achieved real-time object identification and manipulation in virtual environments showcasing its potential for use in smart manufacturing and unmanned warehouses.

Vibration perception plays a crucial role in robotic applications, allowing robots to capture subtle motion profiles, interact intelligently with their environment, and maintain operational stability. However, current vibration sensors are either rigid or lack the necessary stretchability for use with soft robots. To address these challenges, Wang *et al* have developed an ultra-thin (0.1 mm) e-skin using a screen-printing technique with liquid metal particles and a kirigami design, ensuring seamless integration with the soft robot's body (figure 14(b)) [66]. The e-skin is composed of PDMS encapsulation with liquid metal particles (LMPs) and includes four parallel electrodes on the robot's air chamber intervals. The triboelectric mechanism generates electrical signals through contact-separation cycles between the PDMS and silicone layers, driven by the robot's vibrations. Fabrication involves creating LMPs ink, screen-printing the circuit pattern, and integrating the e-skin with a flexible printed circuit connector and platinum cure liquid silicone compounds. The e-skin enables vibration proprioception, texture recognition with 99% accuracy, and object property estimation (97.7% accuracy for type, 95.3% for weight) by analyzing vibration signals. This multifunctional e-skin expands the potential applications of dynamic proprioception in soft robotics.

In the age of AI and advanced automation, precise, reliable, and continuous motion sensing is crucial in fields such as smart robotics, personalized medical rehabilitation, and intelligent control systems. Traditional vector sensors that rely on external power supplies are burdened with high costs, complex maintenance, and performance instability. To tackle these challenges, Qiao *et al* have developed a self-powered vector motion sensor based on a dual-mode TENG (figure 14(c)) [217]. The TENG sensor comprises a high-output FEP film, a cross-electrode grid rail with induction electrodes, and a slider with a frictional and charge-collecting electrode. The device's precision, determined by the distance between cross-electrodes, reaches $1.7 \mu\text{m}$ in displacement and 0.05° in angle sensing. In smart robotics applications, it monitored joint movements and provided precise control feedback; while in personalized medical rehabilitation settings, it tracked joint movements during exercises to offer real-time health status feedback.

Bio-inspired robots mimic the adaptive capabilities of natural organisms, and the Grey Field Slug, known for its versatile navigation, serves as an ideal model. Peng *et al* utilized the slug's unique locomotion mechanics and integrated it with a TENG to develop a self-powered robot (figure 14(d)) [218]. The Slug-inspired TENG-Robot featured a compact, flexible structure consisting of a PCB, NdFeB-embedded magnetic sheets, and triboelectric layers made of FEP and PU film. These components were assembled in a sandwich-like configuration. The magnetic sheets were magnetized for remote actuation by an external rotating magnetic field, while the triboelectric layers generated electricity through contact and separation during movement. The robot was capable of self-detecting its own movement and environmental conditions. It could also sense high temperatures and respond accordingly, effectively mimicking the stimulus response behavior observed in animals. This robot demonstrated the ability to

crawl, climb, and steer on various terrains at speeds up to $200 \text{ mm}\cdot\text{s}^{-1}$ and navigate slopes up to 60° . Furthermore, it generated electricity to power onboard sensors and external devices, storing energy in capacitors and discharging it to power LEDs and other components. This showcased its multifunctionality and practicality in real-world applications.

To address the issue of power limitations in traditional fish bioelectric tags, which rely on cumbersome batteries that restrict the tags' lifespan, size, and functionality, Sheng *et al* developed a fish-wearable piezoelectric nanogenerator (FWPNG) that not only harvested energy from fish-tailing movements but also served as a self-powered sensing device for real-time fish behavior monitoring (figure 14(e)) [219]. The FWPNG integrated a strain energy harvester at the fish tail joint and an impact energy harvester at the tail tip, using piezoelectric $\text{Pb}(\text{Zr}_{0.6}\text{Ti}_{0.4})\text{O}_3$ (PZT) thin films on a flexible PI substrate. In experiments, the strain harvester generated 2.3 V and 11.7 nA at 1% strain, while the impact harvester produced 0.3 V and 150 nA under 82.6 kPa pressure. The device's ability to detect and respond to fish movements was demonstrated by mounting it on a robotic fish, where it successfully powered an acoustic transmitter, sending signals when tail movements surpassed a threshold. This dual-modal nanogenerator could function as a sensing mechanism, autonomously detecting changes in fish behavior without external power.

Triboelectric and PESs represent a significant advancement in robotics, offering enhanced capabilities for human–robot interaction, environmental perception, and self-awareness. Their ability to generate electrical signals from mechanical stimuli provides a self-powered, efficient, and versatile solution for various robotic sensing applications.

4.2. Nanogenerators based systems for computing and decision making

A nanogenerator-based system typically consists of triboelectric/PESs, signal acquisition devices, signal processing and control units, signal wireless transmission devices, and display interfaces. The integration of advanced systems and algorithms into robotic applications represents a significant milestone in the evolution of robotics, enhancing the precision, efficiency, and versatility of robotic systems. Machine learning and adaptive algorithms further enhance the capabilities of robotic systems by enabling them to learn from experience and adapt to new situations. This adaptability is crucial for robots operating in unstructured environments or performing complex tasks that require interaction with humans.

Song *et al* introduced the MTSensing system, a wireless and fully integrated tactile sensing solution designed for real-time and simultaneous material and texture recognition (figure 15(a)) [220]. The system utilized a grating-structured flexible TENG sensor attached to the fingertip of a robotic or human hand to convert touch into electrical signals. A key feature of the MTSensing system was its approach to signal decoupling and processing. By employing wavelet decomposition, the system separates these signals into macro

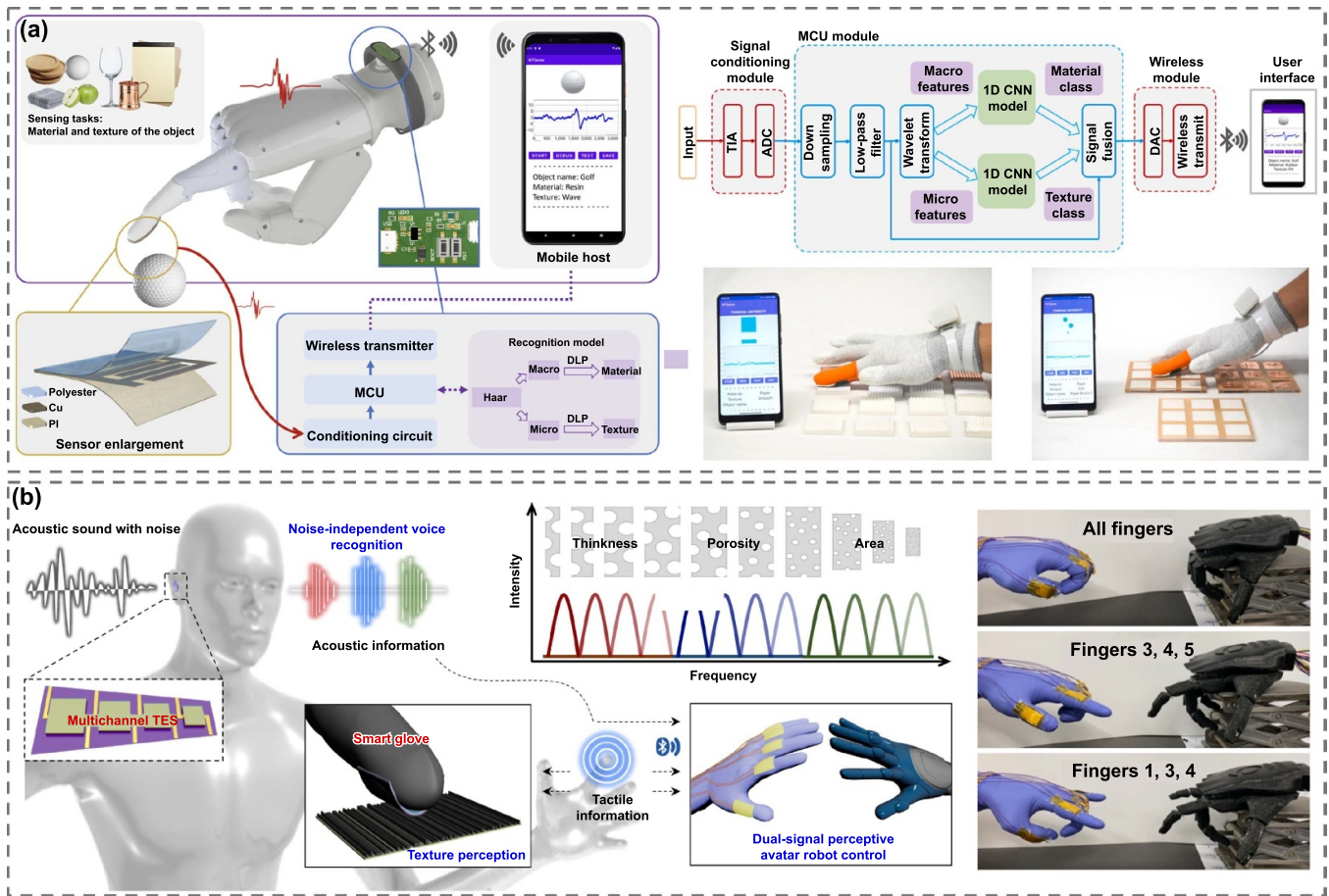


Figure 15. Nanogenerators based systems for computing and decision making. (a) A wireless and fully integrated tactile sensing system designed for real-time and simultaneous material and texture recognition. Reprinted from [220], Copyright (2022), with permission from Elsevier. (b) A TENG based system focusing on frequency-selective acoustic and haptic smart skin for dual-mode dynamic/static HMIs. Reproduced with permission from [221]. CC BY-NC 4.0.

features for material recognition, and micro features for texture recognition. These features were processed by two parallel 1D convolutional neural networks to achieve high prediction accuracy (99.07% and 99.32%). The MTSensing system includes a robust wireless data transmission mechanism. The sensor was connected to a wearable bracelet that amplifies, filters, and digitizes the signals. A microcontroller unit processes these digital signals and transmits the results wirelessly for real-time display. Notably, it can identify Braille characters made from different materials, aiding visually impaired individuals. Overall, the MTSensing system integrated flexible triboelectric sensors with advanced signal processing and machine learning, offering a versatile, scalable, and highly accurate solution for both robotic and human applications.

Another typical system is presented by Park *et al*, focusing on frequency-selective acoustic and haptic smart skin for dual-mode dynamic/static HMIs (figure 15(b)) [221]. The TENG sensors featured a hierarchical macrodome/micropore/nano-particle structure of ferroelectric composites, excelling in frequency selectivity to enable noise-independent voice recognition across various frequency noises (100–8000 Hz). With the assistance of an artificial neural network, the system achieved

over 95% voice recognition accuracy even in noisy environments. A multichannel acoustic sensor array with different resonance frequencies effectively canceled unexpected noise, ensuring high-accuracy voice recognition and texture perception. Integrated into a smart glove with sensors at the fingertips, the system could detect and differentiate between various surface textures, and control an avatar robot using both acoustic and mechanical signals. Equipped with a wireless platform, the smart glove enabled remote control of robotic hands and other devices, demonstrating capabilities in voice recognition, texture perception, and dynamic motion detection.

With the increasing demand for intelligent robots and autonomous systems capable of adaptive environmental interaction, traditional digital logic systems, while effective, rely heavily on external power and are not ideal for soft robotics and bio-inspired applications [222]. To overcome these limitations, there is a need for mechanical logic units that perform energy-efficient, programmable computations. Mechanical structures with reversible bistability offer a promising approach, functioning as mechanical bits for logic operations. Previous methods using mechanical actuators or shape memory materials have limitations in complexity and energy

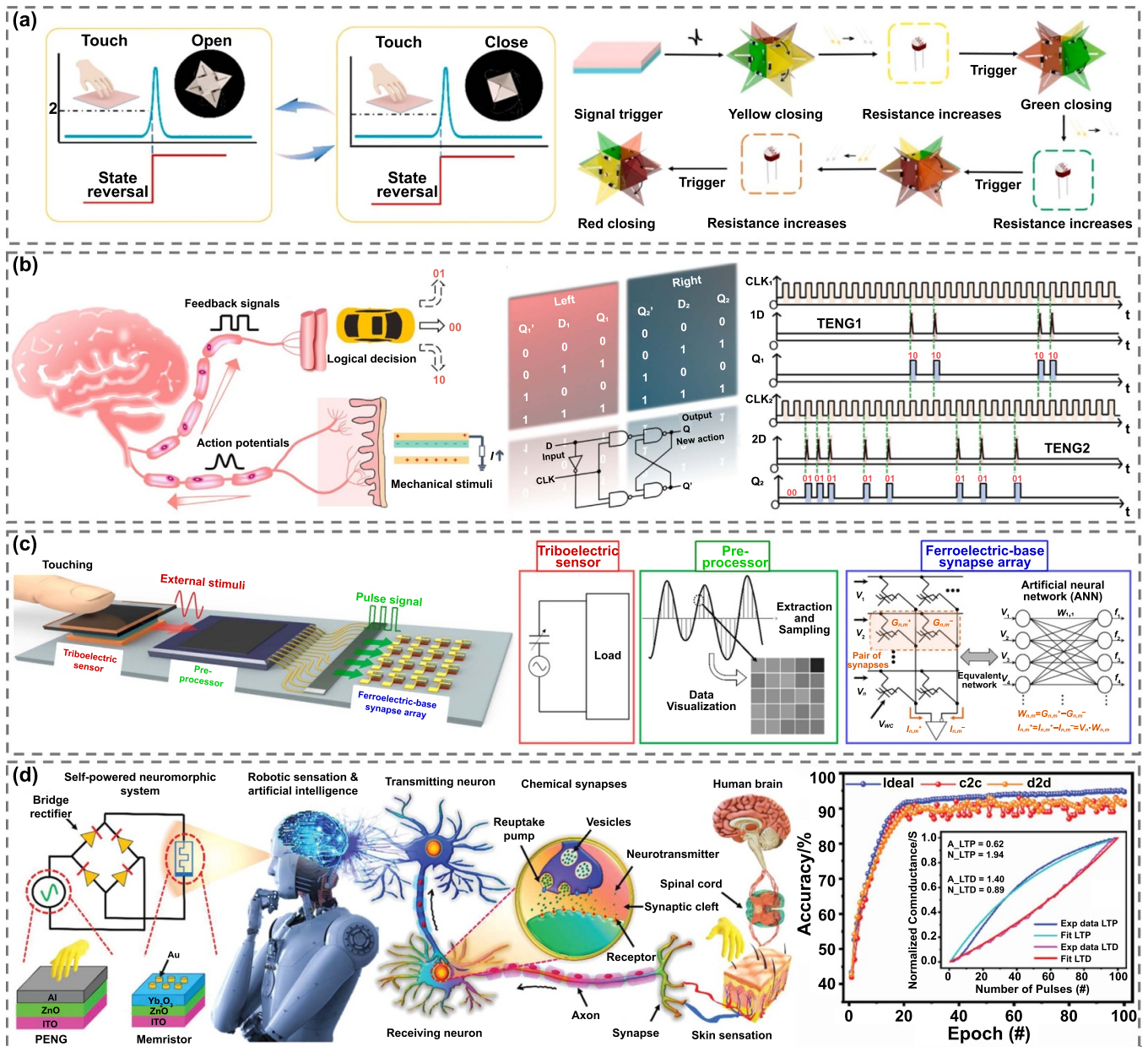


Figure 16. Nanogenerators based systems for computing and logic operations. (a) A kirigami interactive triboelectric mechanologic system that enables energy-efficient mechanical computation and logic operations. Reprinted from [224], Copyright (2022), with permission from Elsevier. (b) A self-powered prototype utilizing TENGs to implement sequential logic for low-power and adaptive mechanical logic computation. Reproduced from [90]. CC BY 4.0. (c) A tactile neuromorphic system aimed at replicating the signal processing capabilities of the human peripheral nervous system. Reprinted with permission from [225]. Copyright (2023) American Chemical Society. (d) A system that integrated a unidirectional neuromorphic resistive memory device with a PENG. [226] John Wiley & Sons. © 2023 The Authors. Advanced Functional Materials published by Wiley-VCH GmbH.

efficiency. In contrast, TENGs provide a self-powered, efficient way to harvest mechanical energy, enabling mechanical logic operations and sensing without external power [223].

Luo *et al* introduced a kirigami interactive triboelectric mechanologic system that enabled energy-efficient mechanical computation and logic operations, inspired by the human somatic reflex arc (figure 16(a)) [224]. The system integrated a self-powered TENG as a mechanoreceptor, a signal transmission/processing module, and adaptive bistable

kirigami structures to represent binary logic states (0 and 1). The TENG, composed of a silver electrode and PTFE triboelectric layer, generated triboelectric signals through contact–separation interactions, which were processed by a microcontroller to trigger the kirigami structures, allowing for operations like mechanical flip-flops, registers, and binary counting. In experiments, the TENG demonstrated a stable open-circuit voltage of 3.9 V, with a response time of 0.3 s, ensuring efficient logic switching. The kirigami structures

performed reliable bistable state transitions, enabling effective mechanical computation in registers and a four-bit asynchronous binary counter.

Xiong *et al* further developed a self-powered prototype utilizing TENGs to implement sequential logic for low-power and adaptive mechanical logic computation (figure 16(b)) [90]. Inspired by biological systems, the prototype mimicked sensory neurons and decision-making processes, converting external mechanical stimuli into spatiotemporal voltage spikes for dynamic processing through a TENG-based D flip-flop configuration. The TENG consisted of a top electrode, PTFE layer, and bottom electrode, generating electrical signals from mechanical inputs. Sequential logic was realized by capturing mechanical stimuli as inputs and utilizing clock cycles to transition between states, enabling the system to execute basic mechanical Boolean logic and more complex combinational logic, especially when dual TENG sensors were used. Experimental results demonstrated the prototype's ability to handle various mechanical logic states and navigate complex environments through an intelligent labyrinth-addressing process. Additionally, it successfully addressed mechanical race and hazard phenomena, ensuring robust operation in challenging conditions. This system is energy-efficient, consuming power only when stimuli are present. This study marked the first demonstration of TENGs with sequential logic, offering new potential for low-power, mechano-driven computation in real-time applications like human–machine interactions and neuromorphic computing.

Parallel computing technologies inspired by biological neural networks are revolutionizing computational efficiency, particularly in the processing of large volumes of unstructured data. These technologies replicate the intricate structure of biological neural networks, which manage complex information through interconnected neurons and synapses. In contrast to traditional serial computing that processes tasks sequentially, parallel computing distributes tasks across multiple processors or computing units, significantly enhancing speed and efficiency. The applications and advantages of these technologies are profound. They enable real-time processing of sensory data, making them ideal for robotics, autonomous systems, and advanced human–machine interfaces. Additionally, these systems are highly energy-efficient, consuming far less power than conventional computing systems—a crucial feature for battery-operated devices and large-scale implementations. Furthermore, the scalable nature of parallel computing allows these systems to handle increasingly complex tasks and larger datasets without a corresponding increase in power consumption or computational time.

Kim *et al* presented a tactile neuromorphic system designed to replicate the human peripheral nervous system's signal processing capabilities (figure 16(c)) [225]. By integrating a PDMS-based triboelectric sensor with a MoS₂/P(VDF-TrFE) ferroelectric synapse, they created a hardware platform that converts tactile stimuli into electrical signals, processing them similarly to biological synapses. The triboelectric sensor mimicked human tactile organs, using a PDMS layer and copper electrodes to detect mechanical stimuli and measure

the delay between press and release, producing corresponding electrical pulses. Complementing the sensor was the ferroelectric synapse, which used a MoS₂/P(VDF-TrFE) heterostructure to emulate synaptic functionality. This synapse exhibited long-term potentiation and depression characteristics, crucial for maintaining synaptic weights and supporting learning. The system excelled in real-time data processing and pattern recognition, achieving a 96.17% recognition rate for Morse code alphabets and 85.4% for MNIST handwritten digits, highlighting its practical application potential.

Implementing compact and highly parallel electronic systems presents notable challenges due to the absence of an electronic element capable of emulating the vast number of synapses in the human cerebral cortex. Khan *et al* introduced a novel system that integrated a unidirectional neuromorphic resistive memory device with a PENG to create a self-powered electronic system (figure 16(d)) [226]. The PENG converted mechanical stimuli into electrical signals, and the neuromorphic resistive memory device then processed these electrical signals, emulating neuronal functions. The changes in the conductance or resistance of the device in response to stimuli from the PENG represented synaptic weight changes, simulating signal transmission between neurons. This functionality enabled the system to efficiently analyze, process, and store external signals. Additionally, the study demonstrated the potential of this system for hardware implementations of neural networks. The weight changed in the memristor device, with a nonlinearity of potentiation and depression of 1.94 and 0.89, respectively, achieved an accuracy of 93%. This capability advanced the development of self-powered neuromorphic perception networks with correlated learning and trainable memory capabilities.

The significance of the nanogenerators based system with computing lies in its transformative potential for advanced robotics systems. They leverage the unique properties of TENGs and PENGs to convert mechanical stimuli into electrical signals, which are then processed by integrated computing units. From the MTsensing system's high-accuracy tactile recognition to the noise-resilient smart skin and the biologically inspired neuromorphic platforms, these advancements highlight the growing synergy between nanogenerators, sensory interfaces, and machine learning in developing sophisticated, adaptable robotic and human–machine interaction systems.

4.3. Nanogenerator based actuating system

Actuators are essential components in robotics, responsible for converting various forms of energy into mechanical motion [227–231]. This enables robots to perform tasks such as moving, grasping, and manipulating objects. Actuators play a pivotal role in defining the precision, speed, and efficiency of robotic systems. The development of TENGs has made a breakthrough in actuator technology. The high voltages generated by TENGs from low-frequency mechanical movements are particularly advantageous for actuators such as dielectric elastomer actuators (DEAs), which require high voltages for

operation. TENGs eliminate the need for bulky power supplies, enabling more compact, portable, and efficient actuator designs. The integration of TENGs with actuators facilitates the development of self-powered wireless robotic systems that can operate autonomously in remote or inaccessible locations. Similarly, PENGs have a profound impact on actuator technology. PENGs convert mechanical energy into electrical energy, providing a sustainable power source for low-energy devices and actuators. Meanwhile, PENGs can convert electrical energy into mechanical energy via inverse piezoelectric effect. Their compact and lightweight nature makes them ideal for miniaturized applications. The high sensitivity and precision of PENGs enhance actuation capabilities, making them suitable for applications requiring fine control and accurate responses.

Liu *et al* developed a triboelectric soft robot system that is powered by mechanical energy (figure 17(a)) [232]. This system consisted of a TENG, a soft-deformable body, triboelectric adhesion feet, a control module, and a real-time visual monitoring platform. The TENG efficiently converted mechanical energy into high voltage electricity to power the robot. The soft-deformable body was designed to mimic inchworm-like motions, enabling precise movement, while the triboelectric adhesion feet generated controllable adhesion forces for anchoring and movement. The control module effectively coordinated these components, and the onboard camera provided real-time images for inspection purposes. The robot demonstrated impressive capabilities as it could crawl on various surfaces such as wood and acrylic, and even climbed slopes up to 30°. Its crawling speed could be adjusted by varying the control signal frequency, with a maximum speed of 14.9 mm·s⁻¹. This made it ideal for inspecting and exploring narrow tunnels, pipes, and machinery interiors, capable of navigating complex terrains.

Soft robots have the capability to respond to various stimuli, including light, humidity, and temperature changes. This makes them suitable for use in artificial muscles, smart systems, and biomimetic devices. However, there are still challenges that need to be addressed in terms of adaptability, movement feedback, and environmental feedback. In a recent study by Jin *et al*, a bio-inspired soft actuator was introduced which leveraged the photothermal effect and TENG for high-performance actuation and real-time contact feedback (figure 17(b)) [233]. The actuator was composed of PET, carbon black ink, and PDMS, each material contributing unique properties to its functionality. The carbon black ink absorbed light and converts it to heat, causing the PDMS to expand and the actuator to bend. This mechanism allowed for large deformation angles, high response speeds, as well as shape memory capabilities. Furthermore, the actuator demonstrated the ability to revert back to its original shape under light exposure while also being able to withstand extreme conditions such as high temperatures and chemical solvents. Additionally, it could mimic the predation process of a frog tongue, and served as a mechanical gripper with real-time electrical feedback.

Aerial insects demonstrate remarkable agility in navigating cluttered environments and interacting with delicate objects such as flowers and leaves. In order to replicate this level of

agility, DEAs have been developed for use in sub-gram micro-aerial vehicles (MAVs). Despite their impressive performance, DEAs required high voltages (1–2 kV), which presented challenges for compact energy sources and boost electronics, thus limiting autonomous operation. Lee *et al* developed a soft-actuated MAV that powered by TENGs (figure 17(c)) [91]. The In-plane Charge Pump TENG significantly enhanced output voltage and energy generation by 280% and 920%, respectively, enabling the generation of high voltages up to 20 kV without the need for heavy electronics. DEAs served as the primary actuators, converting this high voltage into mechanical motion to drive the MAV's flapping wings. The system also included rectifying circuits to convert TENG's bipolar output into a unipolar signal, as well as energy storage circuits to release energy in controlled bursts. This integration allowed the MAV to operate autonomously in environments that were inaccessible to larger drones. With its lightweight design at only 160 mg and reliance on energy harvesting, this MAV was ideal for applications where size and weight were critical.

Another pertinent study conducted by Sun *et al* introduced a soft robot that addresses the limitations of conventional power supplies for DEAs (figure 17(d)) [234]. The robot incorporated a TENG operating in a freestanding mode, generating electrical charges without the constraints of dynamic tethering. This design provided a high-efficiency power supply directly to the soft robot, eliminating the necessity for complex control panels. The soft robot was equipped with a uni-directional DEA, a compliant arc-shaped body, and three one-way bearing wheels, aligning the actuation strain with its movement direction. This alignment maximized energy conversion efficiency, enabling the robot to achieve an impressive maximum crawling speed of 110 mm·s⁻¹ and carry a payload capacity of 40 g. The design ensured smooth strain transmission, thereby enhancing mechanical performance and reliability.

PENGs offer an effective means of converting electrical energy into mechanical energy across a wide frequency band. They presented several advantages, including rapid response, high-resolution, high-power density, and absence of electromagnetic interference, making them well-suited for miniaturized robots. An insect-scale soft robot was developed by Liang *et al* to improve agility and trajectory control (figure 17(e)) [235]. The main body of the robot featured a curved piezoelectric thin film driven at its resonant frequency, enabling swift and efficient forward movement. Additionally, two electrostatic footpads with a droplet shape maximized ground contact for enhanced frictional control. By adjusting the direct current bias voltages, the system could manipulate friction forces with precision. A tethered prototype successfully navigated a 120 cm maze in just 5.6 s, demonstrating its rapid and complex task performance capabilities. Inspired by arthropod metamorphism, Liu *et al* proposed a resonant piezoelectric millirobot with three segments functioning as legs (figure 17(f)) [236]. Each segment was equipped with eight PZT elements for horizontal and vertical bending vibrations. The robot achieved bidirectional linear motion, steering, and rotation using two AC voltages with a 90° phase shift. It reached speeds up to 516 mm·s⁻¹ and a resolution of 0.44 μm, carrying loads up

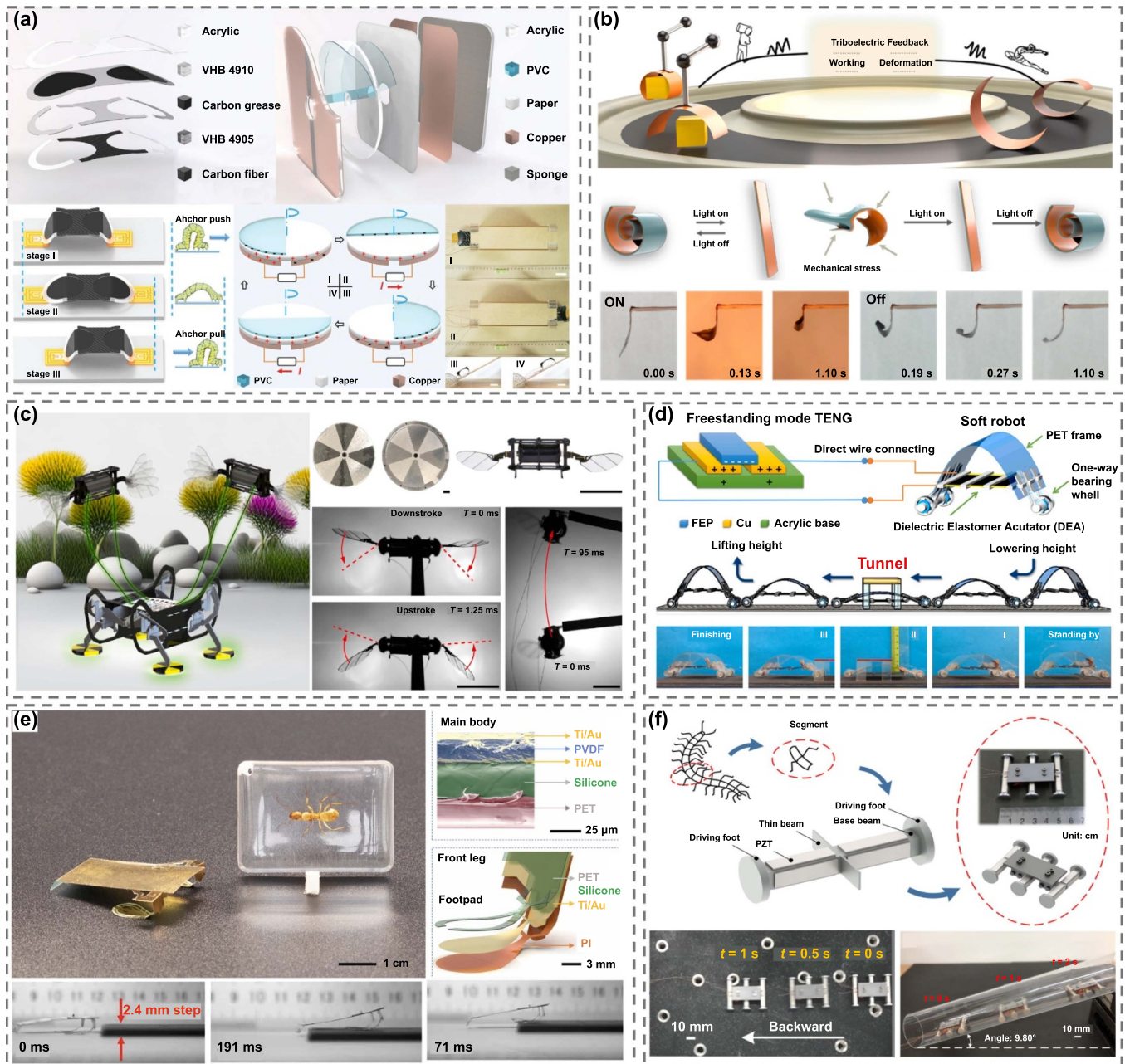


Figure 17. Applications of nanogenerators for robotic actuating. (a) Triboelectric soft robot system that is powered by mechanical energy. [232] John Wiley & Sons. © 2021 Wiley-VCH GmbH. (b) Bio-inspired soft leveraging the photothermal effect and TENG for high-performance actuation and real-time contact feedback. Reprinted from [233], Copyright (2022), with permission from Elsevier. (c) Self-actuated micro-aerial vehicle powered by TENGs. Reprinted from [91], Copyright (2024), with permission from Elsevier. (d) Unidirectional dielectric elastomer actuators driven soft robot. Reprinted from [234], Copyright (2021), with permission from Elsevier. (e) Insect-scale soft robot to improve agility and trajectory control. From [235]. Reprinted with permission from AAAS. (f) Resonant piezoelectric millirobot with three segments functioning as legs. Reproduced from [236]. CC BY 4.0.

to 4.7 times its weight and generating a dragged force of 61 mN. The compact design allowed it to navigate tight spaces effectively.

These studies highlight the significant advancements in nanogenerator-based actuator technology, showcasing their potential to revolutionize soft robotics and MAVs. By

leveraging the unique advantages of TENGs and PENGs and integrating them into robotic systems, researchers have developed innovative solutions that enhance autonomy, efficiency, and versatility. These advancements pave the way for more compact, lightweight, and self-sufficient robots capable of performing complex tasks in diverse environments.

5. Conclusion and perspectives

This review provides a comprehensive summary and analysis of TENGs and PENGs for intelligent robotics, covering the fundamental theories, design and manufacturing approaches, as well as applications. The basic theory of TENGs can be categorized into two main aspects. In terms of CE, the underlying cause of charge transfer lies in the ability of electrons to move from the metal electrode to the dielectric material when their energy exceeds the interface barrier. The metal donor is characterized by having a Fermi level greater than the internal barrier, while the receptor (e.g. PTFE) possesses electron-deficient structures at C atoms. LUMO acts as a receptor for electrons, with F atoms playing an indirect but significant role in electron acquisition. Furthermore, nuclei of C atoms provide the driving force for charge transfer. External mechanical force has dual effects: it induces surface deficiency and brings atoms from two materials close enough for their electron clouds to overlap. Therefore, differences between materials in gaining or losing electrons, contact pressure, and contact area are key parameters influencing charge transfer during CE.

Since the distribution of charge is a fundamental requirement for solving the electric field and charge transfer process in TENG, theoretical modeling begins with an analysis of the initial charge distribution. This includes considering pre-charging charges on the dielectric material, compensation charges on the base electrode, and triboelectric charges on both the dielectric material and independent electrode simultaneously. By applying electrostatic theory with charge conservation, zero electric fields inside the electrodes, and equal potential between two connected electrodes, equations can be derived to solve for the entire charge distribution of TENG. Furthermore, this approach allows for determining the relationship between infinitesimal charge transfer (dQ) and infinitesimal internal distance (dz). The transferred charge can then be determined by integrating dQ , while current is obtained through differentiation of transferred charge with respect to time.

Piezoelectric materials exhibit the piezoelectric and inverse piezoelectric effects. External forces deform these crystals, displacing charge centers and generating polarization proportional to the force. Conversely, an electric field induces deformation. Piezoelectric crystals can be non-spontaneously or spontaneously polarized, with properties influenced by external forces. Their electrical output is analyzed using constitutive equations that incorporate mechanical and electrical parameters.

Significant charge transfer occurs between materials with different tribo-charge abilities, guided by the triboelectric series. Designing TENGs involves considering weight, flexibility, transparency, stretchability, waterproofness, and biocompatibility. Materials like bioinspired textiles and stretchable sensors show potential in robotics. Surface modifications, such as micro/nano structuring and chemical treatments, enhance TENG performance. Piezoelectric materials—categorized as inorganic, organic, and composite—each have unique applications. Improving PENG performance involves strategies like chemical doping, aligning nanofibers, and

developing nanocomposites. Large-scale nanogenerator manufacturing is vital for energy harvesting and self-powered sensing. Techniques like 3D printing and electrospinning are promising. 3D printing allows precise, customized, complex designs by layering materials. Electrospinning creates nanofibers with high surface area to volume ratios, enhancing TENG performance through improved triboelectric interactions.

Nanogenerators in robotics play a crucial role in sensing, computing, and actuating. Sensing is categorized into human–robot interaction, exteroceptive sensing, and proprioceptive sensing. Triboelectric/PESs are capable of detecting touch, pressure, and mechanical stress, enabling robots to respond intuitively to human gestures and enhancing user-friendliness. These sensors also improve exteroceptive sensing by allowing robots to have touch, hearing, smell and taste capabilities. In terms of proprioceptive sensing, they provide feedback on a robot's internal states such as position and motion to ensure safe operation and prevent damage. A nanogenerator-based system consists of triboelectric/PESs, signal acquisition units, processing units, wireless transmission components, and display interfaces. Integration of advanced systems and algorithms such as machine learning enhances robotic precision, efficiency, and versatility, enabling robots to learn and adapt to new situations which is crucial for operating in unstructured environments or performing complex human-interactive tasks. Actuators convert energy into mechanical motion, enabling robots to move or manipulate objects. TENGs generate high voltages from mechanical energy, making them ideal for DEAs that allow compact and efficient designs without bulky power supplies. Piezoelectric actuators are compact and lightweight, suitable for miniaturized applications requiring fine control and precision.

Nanogenerators have demonstrated significant potential for applications in robotics, but there are still some issues that need to be addressed, and future development trends (figure 18) may be analyzed from the following aspects:

5.1. Issues to be solved for fundamentals

- For sensing:

The theoretical framework of nanogenerators remains incomplete and requires further development. A deeper understanding of the fundamental mechanisms of charge generation and transfer is necessary, including the influence of material properties, surface states, and environmental conditions. Advances in quantum mechanics and sophisticated instrumentation may facilitate the investigation and verification of these mechanisms [237]. More accurate theoretical models for various types of nanogenerator sensors need to be developed. These models and their derived governing equations should be comprehensive enough to match actual phenomena and provide practical guidance for researchers to conduct experiments [85]. Numerical simulations should be based on rigorous and clear mechanisms to improve accuracy, in order to enable convenient use by more researchers.

Future development of nanogenerators for intelligent robotics			
	Fundamentals	Design	Manufacturing
Sensing	<ul style="list-style-type: none"> • Complete theoretical frameworks. • Deepen the understanding of charge generation. • Develop accurate theoretical models to predict sensors output. • Improve accuracy of sensors simulations. 	<ul style="list-style-type: none"> • Develop new materials with high tribo/piezoelectric properties. • Optimize structure design. • Develop high-density sensor arrays minimizing crosstalk. • Develop biosensors like electroreceptor, eardrum, compound eyes. 	<ul style="list-style-type: none"> • Develop scalable synthesis methods to ensure consistency. • Implement automated assembly lines for production. • Develop robust encapsulation methods for protection. • Optimize manufacturing processes to reduce cost.
Computing	<ul style="list-style-type: none"> • Advanced noise filtering techniques. • Adaptive models for varying conditions/inputs. • Optimize AI algorithms for low power operation. 	<ul style="list-style-type: none"> • Fully self-powered system. • Integrate nanogenerators with neuromorphic computing architectures. • Edge computing solutions for local data processing. 	<ul style="list-style-type: none"> • Incorporate energy storage solutions. • Integrate low-power microcontrollers and processors. • Complete embodied artificial intelligence.
Actuating	<ul style="list-style-type: none"> • Optimize energy conversion efficiency. • Theories for maximum force and displacement. • Understand deformation behavior of nanogenerators. 	<ul style="list-style-type: none"> • Develop actuators with high output force and displacement. • Design flexible actuators for complex shapes and movements. • Develop artificial muscle, catheter robot, implantable robot. 	<ul style="list-style-type: none"> • Utilize advanced techniques to create complex actuator geometries. • Use wear-resistant materials to ensure durability. • Incorporate self-healing materials.



Figure 18. Future development of nanogenerators for intelligent robotics.

• For computing:

Advanced noise filtering techniques for clean signal processing involve the development and implementation of sophisticated algorithms to eliminate unwanted background noise, ensuring that the signal remains clear and accurate for further analysis. Simultaneously, adaptive models for varying conditions and inputs are designed to dynamically adjust and learn from changing environmental factors, allowing the system to maintain high performance and reliability across different scenarios. Additionally, optimizing AI algorithms for low-power operation focuses on reducing the computational load and energy consumption of AI processors, making them more efficient and suitable for deployment in power-constrained environments such as mobile and embedded systems [238].

• For actuating:

Optimizing energy conversion efficiency for actuation involves refining the mechanisms that convert input energy into mechanical motion, ensuring minimal energy loss and maximum output. Concurrently, theories on designing geometries for maximum force and displacement focus on creating structural designs that enhance the performance of actuators, allowing them to exert greater force and achieve larger movements. Additionally, understanding the deformation behavior of nanogenerator-based actuators requires studying how these materials change shape under various conditions, which is crucial for improving their reliability and effectiveness in practical applications.

5.2. Development trends of design

• For sensing:

To optimize the design of nanogenerator sensors, it is essential to develop new materials with high triboelectric and piezoelectric charge densities as well as excellent mechanical properties. Composite materials that combine the advantages of

different materials should be designed to achieve higher efficiency and durability. Meanwhile, enhancing the output performance of flexible and stretchable designs to meet practical requirements is crucial. This involves optimizing the contact-separation mechanism to maximize contact area and energy conversion efficiency, and developing adaptive designs that can adjust to varying environmental conditions and mechanical inputs. Additionally, it is important to develop high-density highly sensitive sensor arrays that minimize crosstalk to ensure accurate and reliable signal detection. Furthermore, there is significant potential in developing specialized biosensors, such as electroreceptors [206, 239], eardrum analogs [240, 241], and compound eye-inspired sensors [242, 243], which can provide advanced sensing capabilities for a wide range of applications.

• For computing:

Achieving fully self-powered sensing with nanogenerators is an important goal. While these sensors can convert mechanical agitation into electrical signals without an external power source, their signal acquisition modules still often require external power. Developing nanogenerators with higher energy conversion efficiency is expected to address this issue in the future. Furthermore, implementing edge computing solutions for local data processing will further enhance the functionality and autonomy of these sensors by allowing them to process data on-site, reducing latency and dependence on centralized computing resources [244].

• For actuating:

To enhance output force and displacement, future actuators may be designed with multiple layers, leveraging composite structures to generate greater power and achieve substantial movements through the synergy of each layer's mechanical properties. Flexible materials will enable these actuators to adapt seamlessly to complex shapes and dynamic

environments, paving the way for advanced applications in areas such as robotic hands and wearable devices. The development of artificial muscles [245, 246], catheter robots [247, 248], and implantable robots [249, 250] will revolutionize medical technology, providing advanced solutions for minimally invasive surgeries, precise drug delivery, and enhancing human physical capabilities with biomimetic performance and functionality.

5.3. Development of manufacturing

- For sensing:

To advance the manufacturing of nanogenerators, it is crucial to develop scalable synthesis methods for high-performance triboelectric materials, ensuring consistency and quality. Innovative fabrication techniques for composite materials should be employed to enhance triboelectric properties while maintaining mechanical robustness. Implementing automated assembly lines will increase production efficiency and reduce labor costs, while precision alignment techniques will ensure the accurate and consistent placement of device components. Furthermore, robust encapsulation methods should be developed to protect TENGs from environmental factors such as moisture, dust, and mechanical wear, and flexible packaging solutions should be designed for wearable and flexible TENG applications. Additionally, optimizing manufacturing processes to reduce waste and energy consumption will help lower production costs.

- For computing:

Energy storage solutions such as thin-film batteries or supercapacitors should be incorporated to store harvested energy and provide a stable power supply for computing tasks. At the same time, low-power microcontrollers and processors optimized for energy efficiency could be integrated to be powered by TENG and PENG modules. Embodied intelligence highlights the role of the physical body in enabling intelligent behavior, especially in robotics, where intelligence arises from the interaction between robots and their environment. Flexible triboelectric/PESs connect the physical and digital realms, allowing robots to sense pressure, touch, motion, and material properties. These low-cost, adaptable sensors address challenges in acquiring multimodal data for advanced robotic interaction. Future efforts should focus on standardizing these technologies to enhance integration, user-friendliness, and compatibility with existing systems. Standardization will streamline development, simplify implementation, and support future updates, making these sensors easier to incorporate into robotic systems and accelerating innovation in embodied intelligence. This will help overcome adoption barriers and create an ecosystem where nanogenerator technology is accessible and adaptable to evolving robotic needs.

- For actuating:

Advanced manufacturing techniques should be employed for creating complex actuator geometries and integrating multiple functionalities into a single device, allowing for the production of sophisticated and highly capable actuators that perform various tasks with greater efficiency and precision.

Wear-resistant and fatigue-resistant materials should be used to ensure the long-term durability of actuators, providing the resilience needed to endure repeated use and harsh operational conditions without significant degradation. Self-healing materials could also be incorporated to extend the lifespan and reliability of actuators, enabling them to autonomously repair minor damages and maintain performance over an extended period, thus reducing maintenance costs and enhancing overall system reliability.

The objective of the development of nanogenerators is to achieve industrialization and commercialization. As technology advances and new applications are developed, key issues are expected to be resolved. The future of nanogenerators is poised for significant growth and impact. Their potential to provide sustainable and versatile energy/sensing solutions makes them a promising technology for various applications, contributing to a more energy-efficient and intelligent world.

Acknowledgment

This work was supported by the National Natural Science Foundation of China (Grants Nos. 62104125 and 62311530102), Shenzhen Science and Technology Program (Grant Nos. JCYJ20220530143013030 and JCYJ20240813111910014), Guangdong Innovative and Entrepreneurial Research Team Program (Grant No. 2021ZT09L197), and Tsinghua Shenzhen International Graduate School-Shenzhen Pengrui Young Faculty Program of Shenzhen Pengrui Foundation (Grant No. SZPR2023005).

ORCID iD

Wenbo Ding  <https://orcid.org/0000-0002-0597-4512>

References

- [1] Billard A and Kragic D 2019 Trends and challenges in robot manipulation *Science* **364** eaat8414
- [2] Wang T Y, Pierce C, Kojouharov V, Chong B X, Diaz K, Lu H and Goldman D I 2023 Mechanical intelligence simplifies control in terrestrial limbless locomotion *Sci. Robot.* **8** eadi2243
- [3] Pan M, Yuan C G, Liang X R, Zou J, Zhang Y and Bowen C 2020 Triboelectric and piezoelectric nanogenerators for future soft robots and machines *iScience* **23** 101682
- [4] Qu X C, Yang Z, Cheng J, Li Z and Ji L H 2023 Development and application of nanogenerators in humanoid robotics *Nano Trends* **3** 100013
- [5] Shih B, Shah D, Li J X, Thuruthel T G, Park Y L, Iida F, Bao Z N, Kramer-Bottiglio R and Tolley M T 2020 Electronic skins and machine learning for intelligent soft robots *Sci. Robot.* **5** eaaz9239
- [6] Long Y H, Wei W, Huang T, Wang Y H and Dou Q 2023 Human-in-the-loop embodied intelligence with interactive simulation environment for surgical robot learning *IEEE Robot. Autom. Lett.* **8** 4441–8
- [7] Zador A *et al* 2023 Catalyzing next-generation artificial intelligence through NeuroAI *Nat. Commun.* **14** 1597
- [8] Zhang S, Zhang B S, Zhao D, Gao Q, Wang Z L and Cheng T H 2022 Nondestructive dimension sorting by soft

- robotic grippers integrated with triboelectric sensor *ACS Nano* **16** 3008–16
- [9] Zhang C, Liu S Y, Huang X, Guo W, Li Y Y and Wu H 2019 A stretchable dual-mode sensor array for multifunctional robotic electronic skin *Nano Energy* **62** 164–70
- [10] Chen T, Shi Q F, Zhu M L, He T Y Y, Sun L N, Yang L and Lee C 2018 Triboelectric self-powered wearable flexible patch as 3D motion control interface for robotic manipulator *ACS Nano* **12** 11561–71
- [11] Zhou Y K, Shen M L, Cui X, Shao Y C, Li L J and Zhang Y 2021 Triboelectric nanogenerator based self-powered sensor for artificial intelligence *Nano Energy* **84** 105887
- [12] Ma S C *et al* 2022 Neuromorphic computing chip with spatiotemporal elasticity for multi-intelligent-tasking robots *Sci. Robot.* **7** eabk2948
- [13] Wen F, Sun Z D, He T Y Y, Shi Q F, Zhu M L, Zhang Z X, Li L H, Zhang T and Lee C 2020 Machine learning glove using self-powered conductive superhydrophobic triboelectric textile for gesture recognition in VR/AR applications *Adv. Sci.* **7** 2000261
- [14] Liu Y Z, Yue S Z, Tian Z Y, Zhu Z J, Li Y J, Chen X Y, Wang Z L, Yu Z Z and Yang D 2024 Self-powered and self-healable extraocular-muscle-like actuator based on dielectric elastomer actuator and triboelectric nanogenerator *Adv. Mater.* **36** 2309893
- [15] Luo Y L, Sun J F, Zeng Q X, Zhang X F, Tan L M, Chen A, Guo H Y and Wang X 2023 Programmable tactile feedback system for blindness assistance based on triboelectric nanogenerator and self-excited electrostatic actuator *Nano Energy* **111** 108425
- [16] Zheng Z P, Wang B Q, Yin H, Chen Y J, Bao Y and Guo Y P 2023 Self-powered piezoelectric actuation systems based on triboelectric nanogenerator *Adv. Funct. Mater.* **33** 2302648
- [17] Kim S R, Lee S and Park J W 2022 A skin-inspired, self-powered tactile sensor *Nano Energy* **101** 107608
- [18] Chun S, Son W, Kim H, Lim S K, Pang C and Choi C 2019 Self-powered pressure- and vibration-sensitive tactile sensors for learning technique-based neural finger skin *Nano Lett.* **19** 3305–12
- [19] Hajra S, Sahu M, Padhan A M, Swain J, Panigrahi B K, Kim H G, Bang S W, Park S, Sahu R and Kim H J 2021 A new insight into the ZIF-67 based triboelectric nanogenerator for self-powered robot object recognition *J. Mater. Chem. C* **9** 17319–30
- [20] Lin Y C, Duan S S, Zhu D, Li Y H, Wang B H and Wu J 2023 Self-powered and interface-independent tactile sensors based on bilayer single-electrode triboelectric nanogenerators for robotic electronic skin *Adv. Intell. Syst.* **5** 2100120
- [21] Shi Q F and Lee C 2019 Self-powered bio-inspired spider-net-coding interface using single-electrode triboelectric nanogenerator *Adv. Sci.* **6** 1900617
- [22] Han J H *et al* 2018 Machine learning-based self-powered acoustic sensor for speaker recognition *Nano Energy* **53** 658–65
- [23] Yun S Y, Han J K, Lee S W, Yu J M, Jeon S B and Choi Y K 2023 Self-aware artificial auditory neuron with a triboelectric sensor for spike-based neuromorphic hardware *Nano Energy* **109** 108322
- [24] Liu Y D, Zhu Y X, Liu J Y, Zhang Y, Liu J and Zhai J Y 2018 Design of bionic cochlear basilar membrane acoustic sensor for frequency selectivity based on film triboelectric nanogenerator *Nanoscale Res. Lett.* **13** 191
- [25] Zhu J X, Sun Z D, Xu J K, Walczak R D, Dziuban J A and Lee C 2021 Volatile organic compounds sensing based on Bennet doubler-inspired triboelectric nanogenerator and machine learning-assisted ion mobility analysis *Sci. Bull.* **66** 1176–85
- [26] He H X, Dong C Y, Fu Y M, Han W X, Zhao T M, Xing L L and Xue X Y 2018 Self-powered smelling electronic-skin based on the piezo-gas-sensor matrix for real-time monitoring the mining environment *Sens. Actuators B* **267** 392–402
- [27] Kim C, Kang M S, Raja I S, Oh J W, Joung Y K and Han D W 2024 Current issues and perspectives in nanosensors-based artificial olfactory systems for breath diagnostics and environmental exposure monitoring *Trends Analyt. Chem.* **174** 117656
- [28] Wei X L, Wang B C, Cao X L, Zhou H L, Wu Z Y and Wang Z L 2023 Dual-sensory fusion self-powered triboelectric taste-sensing system towards effective and low-cost liquid identification *Nat. Food* **4** 721–32
- [29] Kim J H, Chun J, Kim J W, Choi W J and Baik J M 2015 Self-powered, room-temperature electronic nose based on triboelectrification and heterogeneous catalytic reaction *Adv. Funct. Mater.* **25** 7049–55
- [30] Wang Z M, An J, Nie J H, Luo J J, Shao J J, Jiang T, Chen B D, Tang W and Wang Z L 2020 A self-powered angle sensor at nanoradian-resolution for robotic arms and personalized medicare *Adv. Mater.* **32** 2001466
- [31] Zhu M Z, Xie M Y, Lu X M, Okada S and Kawamura S 2020 A soft robotic finger with self-powered triboelectric curvature sensor based on multi-material 3D printing *Nano Energy* **73** 104772
- [32] Hou X Y, Zhu M L, Sun L N, Ding T X, Huang Z Y, Shi Y T, Su Y L, Li L, Chen T and Lee C 2022 Scalable self-attaching/assembling robotic cluster (S2A2RC) system enabled by triboelectric sensors for in-orbit spacecraft application *Nano Energy* **93** 106894
- [33] Wang Z H, Zhang F D, Yao T, Li N, Li X and Shang J F 2020 Self-powered non-contact triboelectric rotation sensor with interdigitated film *Sensors* **20** 4947
- [34] Chen S E, Pang Y K, Yuan H Y, Tan X B and Cao C Y 2020 Smart soft actuators and grippers enabled by self-powered tribo-skins *Adv. Mater. Technol.* **5** 1901075
- [35] Wen F, Zhang Z X, He T Y Y and Lee C 2021 AI enabled sign language recognition and VR space bidirectional communication using triboelectric smart glove *Nat. Commun.* **12** 5378
- [36] Zhu M L, Sun Z D, Zhang Z X, Shi Q F, He T Y Y, Liu H C, Chen T and Lee C 2020 Haptic-feedback smart glove as a creative human-machine interface (HMI) for virtual/augmented reality applications *Sci. Adv.* **6** eaaz8693
- [37] Dfaz Ledezma F and Haddadin S 2023 Machine learning-driven self-discovery of the robot body morphology *Sci. Robot.* **8** eadh0972
- [38] Zhang H, Zhang D Z, Wang Z H, Xi G S, Mao R Y, Ma Y H, Wang D Y, Tang M C, Xu Z Y and Luan H X 2023 Ultrastretchable, self-healing conductive hydrogel-based triboelectric nanogenerators for human-computer interaction *ACS Appl. Mater. Interfaces* **15** 5128–38
- [39] Gao L X *et al* 2022 A high performance triboelectric nanogenerator based on ordered doping technique for human-machine interaction sensing *Nano Energy* **95** 107025
- [40] Doganay D, Cicek M O, Durukan M B, Altuntas B, Agbahce E, Coskun S and Unalan H E 2021 Fabric based wearable triboelectric nanogenerators for human machine interface *Nano Energy* **89** 106412
- [41] Sun Q Z *et al* 2021 Fully sustainable and high-performance fish gelatin-based triboelectric nanogenerator for wearable movement sensing and human-machine interaction *Nano Energy* **89** 106329
- [42] Hajra S, Panda S, Khanberh H, Vivekananthan V, Chamanehpour E, Mishra Y K and Kim H J 2023

- Revolutionizing self-powered robotic systems with triboelectric nanogenerators *Nano Energy* **115** 108729
- [43] Ye G M, Wan Y F, Wu J M, Zhuang W B, Zhou Z Q, Jin T S, Zi J Y, Zhang D D, Geng X M and Yang P 2022 Multifunctional device integrating dual-temperature regulator for outdoor personal thermal comfort and triboelectric nanogenerator for self-powered human-machine interaction *Nano Energy* **97** 107148
- [44] Jiao P C 2021 Emerging artificial intelligence in piezoelectric and triboelectric nanogenerators *Nano Energy* **88** 106227
- [45] Han Z C, Jiao P C and Zhu Z Y 2021 Combination of piezoelectric and triboelectric devices for robotic self-powered sensors *Micromachines* **12** 813
- [46] Wang Z L 2020 Triboelectric nanogenerator (TENG)—sparking an energy and sensor revolution *Adv. Energy Mater.* **10** 2000137
- [47] Luo J J, Gao W C and Wang Z L 2021 The triboelectric nanogenerator as an innovative technology toward intelligent sports *Adv. Mater.* **33** 2004178
- [48] Zhao H F *et al* 2022 A highly sensitive triboelectric vibration sensor for machinery condition monitoring (*Adv. Energy Mater.* 37/2022) *Adv. Energy Mater.* **12** 2270154
- [49] Gu L, Liu J M, Cui N Y, Xu Q, Du T, Zhang L, Wang Z, Long C B and Qin Y 2020 Enhancing the current density of a piezoelectric nanogenerator using a three-dimensional intercalation electrode *Nat. Commun.* **11** 1030
- [50] Cao X L, Xiong Y, Sun J, Zhu X X, Sun Q J and Wang Z L 2021 Piezoelectric nanogenerators derived self-powered sensors for multifunctional applications and artificial intelligence *Adv. Funct. Mater.* **31** 2102983
- [51] Liu H Z, Zhang G H, Zheng X, Chen F J and Duan H G 2020 Emerging miniaturized energy storage devices for microsystem applications: from design to integration *Int. J. Extrem. Manuf.* **2** 042001
- [52] Persano L, Dagdeviren C, Su Y W, Zhang Y H, Girardo S, Pisignano D, Huang Y G and Rogers J A 2013 High performance piezoelectric devices based on aligned arrays of nanofibers of poly(vinylidene fluoride-co-trifluoroethylene) *Nat. Commun.* **4** 1633
- [53] Shanbedi M, Ardebili H and Karim A 2023 Polymer-based triboelectric nanogenerators: materials, characterization, and applications *Prog. Polym. Sci.* **144** 101723
- [54] Huang L B, Xu W, Tian W, Han J C, Zhao C H, Wu H L and Hao J H 2020 Ultrasonic-assisted ultrafast fabrication of polymer nanowires for high performance triboelectric nanogenerators *Nano Energy* **71** 104593
- [55] Niu X S *et al* 2019 High-performance PZT-based stretchable piezoelectric nanogenerator *ACS Sustain. Chem. Eng.* **7** 979–85
- [56] Abbasipour M, Khajavi R and Akbarzadeh A H 2022 A comprehensive review on piezoelectric polymeric and ceramic nanogenerators *Adv. Eng. Mater.* **24** 2101312
- [57] Zhang P, Zhang W K, Deng L and Zhang H H 2021 A triboelectric nanogenerator based on temperature-stable high dielectric BaTiO₃-based ceramic powder for energy harvesting *Nano Energy* **87** 106176
- [58] Hwang G T *et al* 2014 Self-powered cardiac pacemaker enabled by flexible single crystalline PMN-PT piezoelectric energy harvester *Adv. Mater.* **26** 4880–7
- [59] Yang Y Q *et al* 2018 Liquid-metal-based super-stretchable and structure-designable triboelectric nanogenerator for wearable electronics *ACS Nano* **12** 2027–34
- [60] Zhang Z, Jiang D D, Zhao J Q, Liu G X, Bu T Z, Zhang C and Wang Z L 2020 Tribovoltaic effect on metal-semiconductor interface for direct-current low-impedance triboelectric nanogenerators *Adv. Energy Mater.* **10** 1903713
- [61] Ghosh S K and Mandal D 2016 Efficient natural piezoelectric nanogenerator: electricity generation from fish swim bladder *Nano Energy* **28** 356–65
- [62] Kaur J, Sawhney R S, Singh H, Singh M and Godara S K 2021 Scavenging mechanical energy from human motions using novel-biomaterial-based triboelectric nanogenerator *Phys. Status Solidi a* **218** 2100161
- [63] Huang J J, Jiang T, Zhang Z F, Zhang W Q, Wang S L, Chen Z M, Wan J J, Li P, Li H L and Gui C M 2023 Fabrication of biomaterial-based triboelectric nanogenerators: study of the relationship between output performance and strain in dielectric materials *ACS Sustain. Chem. Eng.* **11** 9540–52
- [64] Habib M, Lantgos I and Hornbostel K 2022 A review of ceramic, polymer and composite piezoelectric materials *J. Appl. Phys.* **55** 423002
- [65] Sun R X, Gao L X, Shou M J, Li B, Chen X, Wang F Y, Mu X J, Xie L and Liao C R 2020 Tribo-material based on a magnetic polymeric composite for enhancing the performance of triboelectric nanogenerator *Nano Energy* **78** 105402
- [66] Wang Z H, Lei K C, Tang H Z, Luo Y, Zhao H F, He P S, Ding W B and Lin L W 2024 Stretchable liquid metal e-skin for soft robot proprioceptive vibration sensing *IEEE Sens. J.* **24** 18327–35
- [67] Zhao H F, Xiao X, Xu P, Zhao T C, Song L G, Pan X X, Mi J C, Xu M Y and Wang Z L 2019 Dual-tube Helmholtz resonator-based triboelectric nanogenerator for highly efficient harvesting of acoustic energy *Adv. Energy Mater.* **9** 1902824
- [68] Wan H C, Cao Y Q, Lo L W, Xu Z H, Sepúlveda N and Wang C 2019 Screen-printed soft triboelectric nanogenerator with porous PDMS and stretchable PEDOT: PSS electrode *J. Semicond.* **40** 112601
- [69] Gu G Q, Han C B, Lu C X, He C, Jiang T, Gao Z L, Li C J and Wang Z L 2017 Triboelectric nanogenerator enhanced nanofiber air filters for efficient particulate matter removal *ACS Nano* **11** 6211–7
- [70] Gao Y Y, Li Z H, Xu B G, Li M Q, Jiang C H Z, Guan X Y and Yang Y J 2022 Scalable core-spun coating yarn-based triboelectric nanogenerators with hierarchical structure for wearable energy harvesting and sensing via continuous manufacturing *Nano Energy* **91** 106672
- [71] Pyo S, Kim M O, Kwon D S, Kim W, Yang J H, Cho H S, Lee J H and Kim J 2020 All-textile wearable triboelectric nanogenerator using pile-embroidered fibers for enhancing output power *Smart Mater. Struct.* **29** 055026
- [72] Li T, Feng Z Q, Qu M H, Yan K, Yuan T, Gao B B, Wang T, Dong W and Zheng J 2019 Core/shell piezoelectric nanofibers with spatial self-orientated β -phase nanocrystals for real-time micropressure monitoring of cardiovascular walls *ACS Nano* **13** 10062–73
- [73] Chen H Y, Zhou L L, Fang Z, Wang S Z, Yang T, Zhu L P, Hou X M, Wang H L and Wang Z L 2021 Piezoelectric nanogenerator based on *in situ* growth all-inorganic CsPbBr₃ perovskite nanocrystals in PVDF fibers with long-term stability *Adv. Funct. Mater.* **31** 2011073
- [74] Zhang H C *et al* 2023 Recent advances in nanofiber-based flexible transparent electrodes *Int. J. Extrem. Manuf.* **5** 032005
- [75] Chen B D, Tang W and Wang Z L 2021 Advanced 3D printing-based triboelectric nanogenerator for mechanical energy harvesting and self-powered sensing *Mater. Today* **50** 224–38
- [76] Chen S *et al* 2018 A single integrated 3D-printing process customizes elastic and sustainable triboelectric nanogenerators for wearable electronics *Adv. Funct. Mater.* **28** 1805108

- [77] Tong Y X, Feng Z A, Kim J, Robertson J L, Jia X T and Johnson B N 2020 3D printed stretchable triboelectric nanogenerator fibers and devices *Nano Energy* **75** 104973
- [78] Zhou L Y, Fu J Z and He Y 2020 A review of 3D printing technologies for soft polymer materials *Adv. Funct. Mater.* **30** 2000187
- [79] Shepelin N A, Sherrell P C, Goudeli E, Skountzos E N, Lussini V C, Dicinoski G W, Shapter J G and Ellis A V 2020 Printed recyclable and self-poled polymer piezoelectric generators through single-walled carbon nanotube templating *Energy Environ. Sci.* **13** 868–83
- [80] Yuan X T, Gao X Y, Yang J K, Shen X Y, Li Z M, You S J, Wang Z H and Dong S X 2020 The large piezoelectricity and high power density of a 3D-printed multilayer copolymer in a rugby ball-structured mechanical energy harvester *Energy Environ. Sci.* **13** 152–61
- [81] Ji S, Shin J, Yoon J, Lim K H, Sim G D, Lee Y S, Kim D H, Cho H and Park J 2022 Three-dimensional skin-type triboelectric nanogenerator for detection of two-axis robotic-arm collision *Nano Energy* **97** 107225
- [82] Goh Q L, Chee P S, Lim E H and Ng D W K 2022 An AI-assisted and self-powered smart robotic gripper based on Eco-EGaIn nanocomposite for pick-and-place operation *Nanomaterials* **12** 1317
- [83] Liang F, Zhao X J, Li H Y, Fan Y J, Cao J W, Wang Z L and Zhu G 2020 Stretchable shape-adaptive liquid-solid interface nanogenerator enabled by *in-situ* charged nanocomposite membrane *Nano Energy* **69** 104414
- [84] Wang Z L and Wang A C 2019 On the origin of contact-electrification *Mater. Today* **30** 34–51
- [85] Zhao H F, Wang H, Yu H Y, Xu Q H, Li X S, Guo J, Shao J J, Wang Z L, Xu M Y and Ding W B 2024 Theoretical modeling of contact-separation mode triboelectric nanogenerators from initial charge distribution *Energy Environ. Sci.* **17** 2228–47
- [86] Fan F R, Tang W and Wang Z L 2016 Flexible nanogenerators for energy harvesting and self-powered electronics *Adv. Mater.* **28** 4283–305
- [87] Pang Y K, Xu X C, Chen S E, Fang Y H, Shi X D, Deng Y M, Wang Z L and Cao C Y 2022 Skin-inspired textile-based tactile sensors enable multifunctional sensing of wearables and soft robots *Nano Energy* **96** 107137
- [88] Li J *et al* 2023 Thin, soft, 3D printing enabled crosstalk minimized triboelectric nanogenerator arrays for tactile sensing *Fundam. Res.* **3** 111–7
- [89] Luo Y, Wang Z H, Wang J Y, Xiao X, Li Q, Ding W B and Fu H Y 2021 Triboelectric bending sensor based smart glove towards intuitive multi-dimensional human-machine interfaces *Nano Energy* **89** 106330
- [90] Xiong Y, Wang Y F, Zhang J T, Zheng L, Liu Y, Jiao H S, Yang J H, Wang Z L and Sun Q J 2024 Endowing TENGs with sequential logic *Device* **2** 100472
- [91] Lee Y, Ren Z J, Hsiao Y H, Kim S, Song W J, Lee C and Chen Y F 2024 Liftoff of a soft-actuated micro-aerial-robot powered by triboelectric nanogenerators *Nano Energy* **126** 109602
- [92] Wang Z L 2017 On Maxwell's displacement current for energy and sensors: the origin of nanogenerators *Mater. Today* **20** 74–82
- [93] Sun J F, Zhang L J, Gong S Q, Chen J and Guo H Y 2024 Device physics and application prospect of the emerging high-voltage supply technology arising from triboelectric nanogenerator *Nano Energy* **119** 109010
- [94] Xu C *et al* 2018 On the electron-transfer mechanism in the contact-electrification effect *Adv. Mater.* **30** 1706790
- [95] Choi D, Kim D W, Yoo D, Cha K J, La M and Kim D S 2017 Spontaneous occurrence of liquid-solid contact electrification in nature: toward a robust triboelectric nanogenerator inspired by the natural lotus leaf *Nano Energy* **36** 250–9
- [96] Xu C *et al* 2018 Raising the working temperature of a triboelectric nanogenerator by quenching down electron thermionic emission in contact-electrification *Adv. Mater.* **30** 1803968
- [97] Bai P, Zhu G, Zhou Y S, Wang S H, Ma J S, Zhang G and Wang Z L 2014 Dipole-moment-induced effect on contact electrification for triboelectric nanogenerators *Nano Res.* **7** 990–7
- [98] Zhang H, Quan L W, Chen J K, Xu C K, Zhang C H, Dong S R, Lü C F and Luo J K 2019 A general optimization approach for contact-separation triboelectric nanogenerator *Nano Energy* **56** 700–7
- [99] Shao J J, Willatzen M and Wang Z L 2020 Theoretical modeling of triboelectric nanogenerators (TENGs) *J. Appl. Phys.* **128** 111101
- [100] Dharmasena R D I G, Jayawardena K D G I, Mills C A, Deane J H B, Anguita J V, Dorey R A and Silva S R P 2017 Triboelectric nanogenerators: providing a fundamental framework *Energy Environ. Sci.* **10** 1801–11
- [101] Wu J, Wang X L, Li H Q, Wang F, Yang W X and Hu Y Q 2018 Insights into the mechanism of metal-polymer contact electrification for triboelectric nanogenerator via first-principles investigations *Nano Energy* **48** 607–16
- [102] Zhou Y S, Wang S H, Yang Y, Zhu G, Niu S M, Lin Z-H, Liu Y and Wang Z L 2014 Manipulating nanoscale contact electrification by an applied electric field *Nano Lett.* **14** 1567–72
- [103] Wang S H, Xie Y N, Niu S M, Lin L, Liu C, Zhou Y S and Wang Z L 2014 Maximum surface charge density for triboelectric nanogenerators achieved by ionized-air injection: methodology and theoretical understanding *Adv. Mater.* **26** 6720–8
- [104] Zhao H F *et al* 2022 Underwater wireless communication via TENG-generated Maxwell's displacement current *Nat. Commun.* **13** 3325
- [105] Zi Y L, Niu S M, Wang J, Wen Z, Tang W and Wang Z L 2015 Standards and figure-of-merits for quantifying the performance of triboelectric nanogenerators *Nat. Commun.* **6** 8376
- [106] Zi Y L, Guo H Y, Wen Z, Yeh M H, Hu C G and Wang Z L 2016 Harvesting low-frequency (<5 Hz) irregular mechanical energy: a possible killer application of triboelectric nanogenerator *ACS Nano* **10** 4797–805
- [107] Tang L R, Hui X D, Chen J, Guo H Y and Wu F 2023 Self-powered, anti-detectable wireless near-field communication strategy based on mechano-driven Maxwell's displacement current *Nano Energy* **118** 109001
- [108] Gao Z Y, Zhou J, Gu Y D, Fei P, Hao Y, Bao G and Wang Z L 2009 Effects of piezoelectric potential on the transport characteristics of metal-ZnO nanowire-metal field effect transistor *J. Appl. Phys.* **105** 113707
- [109] Wang Z L and Song J H 2006 Piezoelectric nanogenerators based on zinc oxide nanowire arrays *Science* **312** 242–6
- [110] Seol M, Kim S, Cho Y, Byun K E, Kim H, Kim J, Kim S K, Kim S W, Shin H J and Park S 2018 Triboelectric series of 2D layered materials *Adv. Mater.* **30** 1801210
- [111] Yoo D, Jang S, Cho S, Choi D and Kim D S 2023 A liquid triboelectric series *Adv. Mater.* **35** 2300699
- [112] Khandelwal G, Maria Joseph Raj N P and Kim S J 2021 Materials beyond conventional triboelectric series for fabrication and applications of triboelectric nanogenerators *Adv. Energy Mater.* **11** 2101170
- [113] Qu X C, Liu Z, Tan P C, Wang C, Liu Y, Feng H Q, Luo D, Li Z and Wang Z L 2022 Artificial tactile perception smart finger for material identification based on triboelectric sensing *Sci. Adv.* **8** eabq2521

- [114] Yao G, Xu L, Cheng X W, Li Y Y, Huang X, Guo W, Liu S Y, Wang Z L and Wu H 2019 Bioinspired triboelectric nanogenerators as self-powered electronic skin for robotic tactile sensing *Adv. Funct. Mater.* **30** 1907312
- [115] Bu T Z *et al* 2018 Stretchable triboelectric–photonic smart skin for tactile and gesture sensing *Adv. Mater.* **30** 1800066
- [116] He J H, Xie Z Q, Yao K M, Li D F, Liu Y M, Gao Z, Lu W, Chang L Q and Yu X G 2021 Trampoline inspired stretchable triboelectric nanogenerators as tactile sensors for epidermal electronics *Nano Energy* **81** 105590
- [117] Zhou Y H, Deng W L, Xu J and Chen J 2020 Engineering materials at the nanoscale for triboelectric nanogenerators *Cell Rep. Phys. Sci.* **1** 100142
- [118] Cui X, Nie J H and Zhang Y 2024 Recent advances in high charge density triboelectric nanogenerators *Int. J. Extrem. Manuf.* **6** 042001
- [119] Moradi F, Karimzadeh F and Kharaziha M 2023 Rational micro/nano-structuring for high-performance triboelectric nanogenerator *J. Alloys Compd.* **960** 170693
- [120] Huang J, Fu X P, Liu G X, Xu S H, Li X W, Zhang C and Jiang L 2019 Micro/nano-structures-enhanced triboelectric nanogenerators by femtosecond laser direct writing *Nano Energy* **62** 638–44
- [121] Yang W X, Wang X L, Li H Q, Wu J, Hu Y Q, Li Z H and Liu H 2019 Fundamental research on the effective contact area of micro-/nano-textured surface in triboelectric nanogenerator *Nano Energy* **57** 41–47
- [122] Li S Y, Fan Y, Chen H Q, Nie J H, Liang Y X, Tao X L, Zhang J, Chen X Y, Fu E G and Wang Z L 2020 Manipulating the triboelectric surface charge density of polymers by low-energy helium ion irradiation/implantation *Energy Environ. Sci.* **13** 896–907
- [123] Shin S H, Bae Y E, Moon H K, Kim J, Choi S H, Kim Y, Yoon H J, Lee M H and Nah J 2017 Formation of triboelectric series via atomic-level surface functionalization for triboelectric energy harvesting *ACS Nano* **11** 6131–8
- [124] Jie Y, Wang N, Cao X, Xu Y, Li T, Zhang X J and Wang Z L 2015 Self-powered triboelectric nanosensor with poly(tetrafluoroethylene) nanoparticle arrays for dopamine detection *ACS Nano* **9** 8376–83
- [125] Zhang Y J, Zhou Z T, Sun L, Liu Z, Xia X X and Tao T H 2018 “Genetically engineered” biofunctional triboelectric nanogenerators using recombinant spider silk *Adv. Mater.* **30** 1805722
- [126] Busolo T, Szewczyk P K, Nair M, Stachewicz U and Kar-Narayan S 2021 Triboelectric yarns with electrospun functional polymer coatings for highly durable and washable smart textile applications *ACS Appl. Mater. Interfaces* **13** 16876–86
- [127] Sun W X, Luo N, Liu Y B, Li H and Wang D A 2022 A new self-healing triboelectric nanogenerator based on polyurethane coating and its application for self-powered cathodic protection *ACS Appl. Mater. Interfaces* **14** 10498–507
- [128] Chen H M, Bai L, Li T, Zhao C, Zhang J S, Zhang N, Song G F, Gan Q Q and Xu Y 2018 Wearable and robust triboelectric nanogenerator based on crumpled gold films *Nano Energy* **46** 73–80
- [129] Liang Y *et al* 2024 Advances of strategies to increase the surface charge density of triboelectric nanogenerators: a review *Small* **20** 2308469
- [130] Wu C X, Kim T W and Choi H Y 2017 Reduced graphene-oxide acting as electron-trapping sites in the friction layer for giant triboelectric enhancement *Nano Energy* **32** 542–50
- [131] Li Z K, Yu A F, Zhang Q and Zhai J Y 2024 Recent advances in fabricating high-performance triboelectric nanogenerators via modulating surface charge density *Int. J. Extrem. Manuf.* **6** 052003
- [132] Kang X F, Pan C X, Chen Y H and Pu X 2020 Boosting performances of triboelectric nanogenerators by optimizing dielectric properties and thickness of electrification layer *RSC Adv.* **10** 17752–9
- [133] Seung W *et al* 2017 Boosting power-generating performance of triboelectric nanogenerators via artificial control of ferroelectric polarization and dielectric properties *Adv. Energy Mater.* **7** 1600988
- [134] Fan F R, Lin L, Zhu G, Wu W Z, Zhang R and Wang Z L 2012 Transparent triboelectric nanogenerators and self-powered pressure sensors based on micropatterned plastic films *Nano Lett.* **12** 3109–14
- [135] Park I W *et al* 2019 Vertically aligned cyclo-phenylalanine peptide nanowire-based high-performance triboelectric energy generator *Nano Energy* **57** 737–45
- [136] Liu Y H, Fu Q, Mo J L, Lu Y X, Cai C C, Luo B and Nie S X 2021 Chemically tailored molecular surface modification of cellulose nanofibrils for manipulating the charge density of triboelectric nanogenerators *Nano Energy* **89** 106369
- [137] Sun J G, Guo H Y, Ribera J, Wu C S, Tu K K, Binelli M, Panzarasa G, Schwarze F W M R, Wang Z L and Burgert I 2020 Sustainable and biodegradable wood sponge piezoelectric nanogenerator for sensing and energy harvesting applications *ACS Nano* **14** 14665–74
- [138] Jin L, Ma S Y, Deng W L, Yan C, Yang T, Chu X, Tian G, Xiong D, Lu J and Yang W Q 2018 Polarization-free high-crystallization β -PVDF piezoelectric nanogenerator toward self-powered 3D acceleration sensor *Nano Energy* **50** 632–8
- [139] Huang X M *et al* 2021 Piezoelectric nanogenerator for highly sensitive and synchronous multi-stimuli sensing *ACS Nano* **15** 19783–92
- [140] Lin X D, Feng Z Y, Xiong Y, Sun W W, Yao W C, Wei Y C, Wang Z L and Sun Q J 2024 Piezotronic neuromorphic devices: principle, manufacture, and applications *Int. J. Extrem. Manuf.* **6** 032011
- [141] Liu Y Z, Hao Z W, Yu J X, Zhou X R, Lee P S, Sun Y, Mu Z C and Zeng F L 2019 A high-performance soft actuator based on a poly (vinylidene fluoride) piezoelectric bimorph *Smart Mater. Struct.* **28** 055011
- [142] Wang S P, Rong W B, Wang L F, Xie H, Sun L N and Mills J K 2019 A survey of piezoelectric actuators with long working stroke in recent years: classifications, principles, connections and distinctions *Mech. Syst. Signal Process.* **123** 591–605
- [143] Sezer N and Koç M 2021 A comprehensive review on the state-of-the-art of piezoelectric energy harvesting *Nano Energy* **80** 105567
- [144] Yan J, Liu M, Jeong Y G, Kang W M, Li L, Zhao Y X, Deng N P, Cheng B W and Yang G 2019 Performance enhancements in poly (vinylidene fluoride)-based piezoelectric nanogenerators for efficient energy harvesting *Nano Energy* **56** 662–92
- [145] Hanani Z *et al* 2021 Lead-free nanocomposite piezoelectric nanogenerator film for biomechanical energy harvesting *Nano Energy* **81** 105661
- [146] Zhu Q L, Wu T and Wang N 2023 From piezoelectric nanogenerator to non-invasive medical sensor: a review *Biosensors* **13** 113
- [147] Zaszczyńska A, Gradyś A and Sajkiewicz P 2020 Progress in the applications of smart piezoelectric materials for medical devices *Polymers* **12** 2754
- [148] Park K I *et al* 2014 Highly-efficient, flexible piezoelectric PZT thin film nanogenerator on plastic substrates *Adv. Mater.* **26** 2514–20
- [149] Sekine T *et al* 2023 Robotic e-skin for high performance stretchable acceleration sensor via combinations of novel

- soft and functional polymers *Appl. Mater. Today* **33** 101877
- [150] Kim I, Roh H, Yu J, Jayababu N and Kim D 2020 Boron nitride nanotube-based contact electrification-assisted piezoelectric nanogenerator as a kinematic sensor for detecting the flexion–extension motion of a robot finger *ACS Energy Lett.* **5** 1577–85
- [151] Lee J H, Heo K, Schulz-Schönhagen K, Lee J H, Desai M S, Jin H E and Lee S W 2018 Diphenylalanine peptide nanotube energy harvesters *ACS Nano* **12** 8138–44
- [152] Wei H G *et al* 2018 An overview of lead-free piezoelectric materials and devices *J. Mater. Chem. C* **6** 12446–67
- [153] Chen Y, Zhang D L, Peng Z, Yuan M D and Ji X R 2021 Review of research on the rare-earth doped piezoelectric materials *Front. Mater.* **8** 679167
- [154] Zhai L D, Kim H C, Kim J W and Kim J 2020 Alignment effect on the piezoelectric properties of ultrathin cellulose nanofiber films *ACS Appl. Bio Mater.* **3** 4329–34
- [155] Jiang Y G, Gong L L, Hu X H, Zhao Y, Chen H W, Feng L and Zhang D Y 2018 Aligned P(VDF-TrFE) nanofibers for enhanced piezoelectric directional strain sensing *Polymers* **10** 364
- [156] Su Y J *et al* 2021 Piezoelectric fiber composites with polydopamine interfacial layer for self-powered wearable biomonitoring *Nano Energy* **89** 106321
- [157] Chen X L, Shao J Y, Tian H M, Li X M, Tian Y Z and Wang C 2018 Flexible three-axial tactile sensors with microstructure-enhanced piezoelectric effect and specially-arranged piezoelectric arrays *Smart Mater. Struct.* **27** 025018
- [158] Bairagi S and Ali S W 2020 Flexible lead-free PVDF/SM-KNN electrospun nanocomposite based piezoelectric materials: significant enhancement of energy harvesting efficiency of the nanogenerator *Energy* **198** 117385
- [159] Lv F, Hong Z J, Ahmad Z, Li H Y, Wu Y J and Huang Y H 2023 Design of flexible piezoelectric nanocomposite for energy harvesters: a review *Energy Mater. Adv.* **4** 0043
- [160] Ye S B *et al* 2019 High-performance piezoelectric nanogenerator based on microstructured P(VDF-TrFE)/BNNTs composite for energy harvesting and radiation protection in space *Nano Energy* **60** 701–14
- [161] Liu J Y, Zeng S, Zhang M R, Xiong J, Gu H S, Wang Z, Hu Y M, Zhang X H, Du Y and Ren L 2023 Giant piezoelectric output and stability enhancement in piezopolymer composites with liquid metal nanofillers *Adv. Sci.* **10** 2304096
- [162] Lai Y C, Deng J N, Liu R Y, Hsiao Y C, Zhang S L, Peng W B, Wu H M, Wang X F and Wang Z L 2018 Actively perceiving and responsive soft robots enabled by self-powered, highly extensible, and highly sensitive triboelectric proximity-and pressure-sensing skins *Adv. Mater.* **30** 1801114
- [163] Gao Z Q, Wu S K, Wei Y H, Ibrahim M, Abdelhamid H N, Jiang G Y, Cao J, Sun X H and Wen Z 2024 Holistic and localized preparation methods for triboelectric sensors: principles, applications and perspectives *Int. J. Extrem. Manuf.* **6** 052002
- [164] Wu L X, Meng L, Wang Y Y, Lv M, Ouyang T Y, Wang Y L and Zeng X Y 2023 Fabrication of polyetheretherketone (PEEK)-based 3D electronics with fine resolution by a hydrophobic treatment assisted hybrid additive manufacturing method *Int. J. Extrem. Manuf.* **5** 035003
- [165] Chen B D *et al* 2018 Three-dimensional ultraflexible triboelectric nanogenerator made by 3D printing *Nano Energy* **45** 380–9
- [166] Huang T, Zhang Y J, He P, Wang G, Xia X X, Ding G Q and Tao T H 2020 “Self-matched” tribo/piezoelectric nanogenerators using vapor-induced phase-separated poly(vinylidene fluoride) and recombinant spider silk *Adv. Mater.* **32** 1907336
- [167] Liang X W, Lu J B, Zhao T, Yu X C, Jiang Q S, Hu Y G, Zhu P L, Sun R and Wong C P 2019 Facile and efficient welding of silver nanowires based on UVA-induced nanoscale photothermal process for roll-to-roll manufacturing of high-performance transparent conducting films *Adv. Mater. Interfaces* **6** 1801635
- [168] Yildirim A *et al* 2020 Roll-to-roll production of novel large-area piezoelectric films for transparent, flexible, and wearable fabric loudspeakers *Adv. Mater. Technol.* **5** 2000296
- [169] Fang C, Zhong H F, Liu M J, Zhang S H, Huang Z X and Qu J P 2024 Highly tribo-positive Nylon-11 film fabricated by multiscale structural regulation through a roll-to-roll processing *ACS Appl. Mater. Interfaces* **16** 29257–66
- [170] Liu Y B *et al* 2022 The continuous fabrication of a high-performance triboelectric nanogenerator by a roll-to-roll process *J. Mater. Chem. A* **10** 16547–54
- [171] Sun X, Feng Y G, Wang B Q, Liu Y, Wu Z S, Yang D, Zheng Y B, Peng J L, Feng M and Wang D A 2021 A new method for the electrostatic manipulation of droplet movement by triboelectric nanogenerator *Nano Energy* **86** 106115
- [172] Xu H Y, Tao J, Liu Y, Mo Y P, Bao R R and Pan C F 2022 Fully fibrous large-area tailororable triboelectric nanogenerator based on solution blow spinning technology for energy harvesting and self-powered sensing *Small* **18** 2202477
- [173] Shin S H, Choi S Y, Lee M H and Nah J 2017 High-performance piezoelectric nanogenerators via imprinted sol–gel BaTiO₃ nanopillar array *ACS Appl. Mater. Interfaces* **9** 41099–103
- [174] Ganesh R S, Sharma S K, Abinnas N, Durgadevi E, Raji P, Ponnusamy S, Muthamizhchelvan C, Hayakawa Y and Kim D Y 2017 Fabrication of the flexible nanogenerator from BTO nanopowders on graphene coated PMMA substrates by sol–gel method *Mater. Chem. Phys.* **192** 274–81
- [175] Liu S Y, Zou D, Yu X G, Wang Z K and Yang Z B 2020 Transfer-free PZT thin films for flexible nanogenerators derived from a single-step modified sol–gel process on 2D mica *ACS Appl. Mater. Interfaces* **12** 54991–9
- [176] Li H and Lim S 2022 Screen printing of surface-modified barium titanate/polyvinylidene fluoride nanocomposites for high-performance flexible piezoelectric nanogenerators *Nanomaterials* **12** 2910
- [177] Emamian S, Narakathu B B, Chlaihawi A A, Bazuin B J and Atashbar M Z 2017 Screen printing of flexible piezoelectric based device on polyethylene terephthalate (PET) and paper for touch and force sensing applications *Sens. Actuators A* **263** 639–47
- [178] Lu L J, Ding W Q, Liu J Q and Yang B 2020 Flexible PVDF based piezoelectric nanogenerators *Nano Energy* **78** 105251
- [179] Hu D W, Yao M G, Fan Y, Ma C R, Fan M J and Liu M 2019 Strategies to achieve high performance piezoelectric nanogenerators *Nano Energy* **55** 288–304
- [180] Yin B, Qiu Y, Zhang H Q, Ji J Y, Lei J X, Luo Y M, Zhao Y and Hu L Z 2015 Piezoelectric nanogenerator with 3D-ZnO micro-thornyballs prepared by chemical vapour deposition *J. Mater. Sci., Mater. Electron.* **26** 742–6
- [181] Kim S K, Bhatia R, Kim T H, Seol D, Kim J H, Kim H, Seung W, Kim Y, Lee Y H and Kim S W 2016 Directional dependent piezoelectric effect in CVD grown monolayer MoS₂ for flexible piezoelectric nanogenerators *Nano Energy* **22** 483–9

- [182] Al-Rugeishi M S, Mohiuddin T, Al-Habsi B, Al-Rugeishi F, Al-Fahdi A and Al-Khusaibi A 2019 Piezoelectric nanogenerator based on ZnO nanorods *Arab. J. Chem.* **12** 5173–9
- [183] Cao V A, Kim M, Hu W G, Lee S, Youn S, Chang J, Chang H S and Nah J 2021 Enhanced piezoelectric output performance of the SnS₂/SnS heterostructure thin-film piezoelectric nanogenerator realized by atomic layer deposition *ACS Nano* **15** 10428–36
- [184] Zhu L Y, Yang J G, Yuan K, Chen H Y, Wang T, Ma H P, Huang W, Lu H L and Zhang D W 2018 Enhanced piezoelectric performance of the ZnO/AlN stacked nanofilm nanogenerator grown by atomic layer deposition *APL Mater.* **6** 121109
- [185] Li Y, Goei R, Ong A J, Zou Y M, Dayan A S, Rahmany S, Etgar L and Tok A I Y 2024 Atomic layer deposition of piezoelectric materials: a timely review *Mater. Today Energy* **39** 101457
- [186] Zhang Z, Chen Y and Guo J S 2019 ZnO nanorods patterned-textile using a novel hydrothermal method for sandwich structured-piezoelectric nanogenerator for human energy harvesting *Physica E* **105** 212–8
- [187] Ou C L, Sanchez-Jimenez P E, Datta A, Boughey F L, Whiter R A, Sahonta S L and Kar-Narayan S 2016 Template-assisted hydrothermal growth of aligned zinc oxide nanowires for piezoelectric energy harvesting applications *ACS Appl. Mater. Interfaces* **8** 13678–83
- [188] Li W, Cao Y Q and Sepúlveda N 2022 Thin film piezoelectric nanogenerator based on (100)-oriented nanocrystalline AlN grown by pulsed laser deposition at room temperature *Micromachines* **14** 99
- [189] Cho H, Jo S, Kim I and Kim D 2021 Film-sponge-coupled triboelectric nanogenerator with enhanced contact area based on direct ultraviolet laser ablation *ACS Appl. Mater. Interfaces* **13** 48281–91
- [190] Vakulov Z, Geldash A, Khakhulin D, Il'ina M V, Il'in O I, Klimin V S, Dzhuplin V N, Konoplev B G, He Z B and Ageev O A 2020 Piezoelectric energy harvester based on LiNbO₃ thin films *Materials* **13** 3984
- [191] Yao D S *et al* 2019 Achieving the upper bound of piezoelectric response in tunable, wearable 3D printed nanocomposites *Adv. Funct. Mater.* **29** 1903866
- [192] Zhang J *et al* 2020 3D printed piezoelectric BNNTs nanocomposites with tunable interface and microarchitectures for self-powered conformal sensors *Nano Energy* **77** 105300
- [193] Su Y J *et al* 2022 High-performance piezoelectric composites via β phase programming *Nat. Commun.* **13** 4867
- [194] Wang S, Shao H Q, Liu Y, Tang C Y, Zhao X, Ke K, Bao R Y, Yang M B and Yang W 2021 Boosting piezoelectric response of PVDF-TrFE via MXene for self-powered linear pressure sensor *Compos. Sci. Technol.* **202** 108600
- [195] Zhou X R, Parida K, Halevi O, Liu Y Z, Xiong J Q, Magdassi S and Lee P S 2020 All 3D-printed stretchable piezoelectric nanogenerator with non-protruding kirigami structure *Nano Energy* **72** 104676
- [196] He L R, Lu J, Han C, Liu X G, Liu J F and Zhang C H 2022 Electrohydrodynamic pulling consolidated high-efficiency 3D printing to architect unusual self-polarized β -PVDF arrays for advanced piezoelectric sensing *Small* **18** 2200114
- [197] Guan X Y, Xu B G and Gong J L 2020 Hierarchically architected polydopamine modified BaTiO₃@P(VDF-TrFE) nanocomposite fiber mats for flexible piezoelectric nanogenerators and self-powered sensors *Nano Energy* **70** 104516
- [198] Li T *et al* 2021 High-performance poly(vinylidene difluoride)/dopamine core/shell piezoelectric nanofiber and its application for biomedical sensors *Adv. Mater.* **33** 2006093
- [199] Hui X D, Tang L R, Zhang D W, Yan S L, Li D X, Chen J, Wu F, Wang Z L and Guo H Y 2024 Acoustically enhanced triboelectric stethoscope for ultrasensitive cardiac sounds sensing and disease diagnosis *Adv. Mater.* **36** 2401508
- [200] Hu Z H, Hui X D, Li S M, Tang L R, Sun J F, Zeng H J, Chen J and Guo H Y 2023 A self-powered, high-precision and minimum-channel touch panel coupling triboelectrification and uniform resistance film *Nano Energy* **114** 108676
- [201] Ding W B, Wang A C, Wu C S, Guo H Y and Wang Z L 2019 Human-machine interfacing enabled by triboelectric nanogenerators and tribotronics *Adv. Mater. Technol.* **4** 1800487
- [202] Xu Z Y, Zhou F H, Yan H Z, Gao G R, Li H J, Li R and Chen T 2021 Anti-freezing organohydrogel triboelectric nanogenerator toward highly efficient and flexible human-machine interaction at -30°C *Nano Energy* **90** 106614
- [203] Zhu P C, Zhang B S, Wang H Y, Wu Y H, Cao H J, He L B, Li C Y, Luo X P, Li X and Mao Y C 2022 3D printed triboelectric nanogenerator as self-powered human-machine interactive sensor for breathing-based language expression *Nano Res.* **15** 7460–7
- [204] Pu X J, Guo H Y, Tang Q, Chen J, Feng L, Liu G L, Wang X, Xi Y, Hu C G and Wang Z L 2018 Rotation sensing and gesture control of a robot joint via triboelectric quantization sensor *Nano Energy* **54** 453–60
- [205] Liu W B *et al* 2022 Touchless interactive teaching of soft robots through flexible bimodal sensory interfaces *Nat. Commun.* **13** 5030
- [206] Mu S L *et al* 2023 A platypus-inspired electro-mechanosensory finger for remote control and tactile sensing *Nano Energy* **116** 108790
- [207] Deng W L *et al* 2019 Cowpea-structured PVDF/ZnO nanofibers based flexible self-powered piezoelectric bending motion sensor towards remote control of gestures *Nano Energy* **55** 516–25
- [208] Ahmed A, Zhang S L, Hassan I, Saadatnia Z, Zi Y L, Zu J and Wang Z L 2017 A washable, stretchable, and self-powered human-machine interfacing triboelectric nanogenerator for wireless communications and soft robotics pressure sensor arrays *Extrem. Mech. Lett.* **13** 25–35
- [209] Lee H S *et al* 2014 Flexible inorganic piezoelectric acoustic nanosensors for biomimetic artificial hair cells *Adv. Funct. Mater.* **24** 6914–21
- [210] Jin G Q, Sun Y Y, Geng J J, Yuan X, Chen T, Liu H C, Wang F X and Sun L N 2021 Bioinspired soft caterpillar robot with ultra-stretchable bionic sensors based on functional liquid metal *Nano Energy* **84** 105896
- [211] Zhu D K, Lu J F, Zheng M J, Wang D K, Wang J Y, Liu Y X, Wang X H and Zhang M 2023 Self-powered bionic antenna based on triboelectric nanogenerator for micro-robotic tactile sensing *Nano Energy* **114** 108644
- [212] Lu D J *et al* 2023 Wearable triboelectric visual sensors for tactile perception *Adv. Mater.* **35** 2209117
- [213] Guo H Y *et al* 2018 A highly sensitive, self-powered triboelectric auditory sensor for social robotics and hearing aids *Sci. Robot.* **3** eaat2516
- [214] Roy Barman S, Lin Y J, Lee K M, Pal A, Tiwari N, Lee S and Lin Z H 2023 Triboelectric nanosensor integrated with robotic platform for self-powered detection of chemical analytes *ACS Nano* **17** 2689–701
- [215] Fu J J, Song Z W, Wang H Y, Xu G Q, Li X Y, Ding W B and Zi Y L 2024 Deep-learning assisted biomimetic

- self-powered wireless electronic noses system enabled by triboelectric discharge *Nano Energy* **121** 109156
- [216] Jin T *et al* 2020 Triboelectric nanogenerator sensors for soft robotics aiming at digital twin applications *Nat. Commun.* **11** 5381
- [217] Qiao W Y *et al* 2022 A self-powered vector motion sensor for smart robotics and personalized medical rehabilitation *Nano Energy* **104** 107936
- [218] Peng L L, Zhang Y X, Wang J, Wang Q Y, Zheng G Z, Li Y Y, Chen Z P, Chen Y, Jiang L L and Wong C P 2022 Slug-inspired magnetic soft millirobot fully integrated with triboelectric nanogenerator for on-board sensing and self-powered charging *Nano Energy* **99** 107367
- [219] Sheng T Y, He Q P, Cao Y D, Dong Z H, Gai Y S, Zhang W Q, Zhang D Y, Chen H W and Jiang Y G 2023 Fish-wearable piezoelectric nanogenerator for dual-modal energy scavenging from fish-tailing *ACS Appl. Mater. Interfaces* **15** 39570–7
- [220] Song Z W *et al* 2022 A flexible triboelectric tactile sensor for simultaneous material and texture recognition *Nano Energy* **93** 106798
- [221] Park J *et al* 2022 Frequency-selective acoustic and haptic smart skin for dual-mode dynamic/static human-machine interface *Sci. Adv.* **8** eabj9220
- [222] Cao X L, Xiong Y, Sun J, Xie X Y, Sun Q J and Wang Z L 2023 Multidiscipline applications of triboelectric nanogenerators for the intelligent era of Internet of Things *Nano-Micro Lett.* **15** 14
- [223] Wang Y F, Sun Q J, Yu J R, Xu N, Wei Y C, Cho J H and Wang Z L 2023 Boolean logic computing based on neuromorphic transistor *Adv. Funct. Mater.* **33** 2305791
- [224] Luo L *et al* 2022 Kirigami interactive triboelectric mechanologic *Nano Energy* **99** 107345
- [225] Kim H, Oh S, Choo H, Kang D H and Park J H 2023 Tactile neuromorphic system: convergence of triboelectric polymer sensor and ferroelectric polymer synapse *ACS Nano* **17** 17332–41
- [226] Khan M U, Abbas Y, Rezeq M D, Alazzam A and Mohammad B 2024 Unidirectional neuromorphic resistive memory integrated with piezoelectric nanogenerator for self-power electronics *Adv. Funct. Mater.* **34** 2305869
- [227] Gao X Y, Yang J K, Wu J G, Xin X D, Li Z M, Yuan X T, Shen X Y and Dong S X 2020 Piezoelectric actuators and motors: materials, designs, and applications *Adv. Mater. Technol.* **5** 1900716
- [228] Xavier M S *et al* 2022 Soft pneumatic actuators: a review of design, fabrication, modeling, sensing, control and applications *IEEE Access* **10** 59442–85
- [229] Suzumori K and Faudzi A A 2018 Trends in hydraulic actuators and components in legged and tough robots: a review *Adv. Robot.* **32** 458–76
- [230] Wu S, Baker G L, Yin J and Zhu Y 2022 Fast thermal actuators for soft robotics *Soft Robot.* **9** 1031–9
- [231] Yang Z X and Zhang L 2020 Magnetic actuation systems for miniature robots: a review *Adv. Intell. Syst.* **2** 2000082
- [232] Liu Y, Chen B D, Li W, Zu L L, Tang W and Wang Z L 2021 Bioinspired triboelectric soft robot driven by mechanical energy *Adv. Funct. Mater.* **31** 2104770
- [233] Jin X, Shi Y P, Yuan Z H, Huo X Q, Wu Z Y and Wang Z L 2022 Bio-inspired soft actuator with contact feedback based on photothermal effect and triboelectric nanogenerator *Nano Energy* **99** 107366
- [234] Sun W J, Li B, Zhang F, Fang C L, Lu Y J, Gao X, Cao C J, Chen G M, Zhang C and Wang Z L 2021 TENG-Bot: triboelectric nanogenerator powered soft robot made of uni-directional dielectric elastomer *Nano Energy* **85** 106012
- [235] Liang J M *et al* 2021 Electrostatic footpads enable agile insect-scale soft robots with trajectory control *Sci. Robot.* **6** eabe7906
- [236] Liu Y X, Li J, Deng J, Zhang S J, Chen W S, Xie H and Zhao J 2021 Arthropod-metamerism-inspired resonant piezoelectric millirobot *Adv. Intell. Syst.* **3** 2100015
- [237] Wang Z L 2021 From contact electrification to triboelectric nanogenerators *Rep Prog. Phys.* **84** 096502
- [238] Xia H S, Zhang Y C, Rajabi N, Taleb F, Yang Q T, Krug D and Li Z J 2024 Shaping high-performance wearable robots for human motor and sensory reconstruction and enhancement *Nat. Commun.* **15** 1760
- [239] Guo Z H, Wang H L, Shao J J, Shao Y S, Jia L Y, Li L W, Pu X and Wang Z L 2022 Bioinspired soft electroreceptors for artificial precontact somatosensation *Sci. Adv.* **8** eabo5201
- [240] Gou G Y *et al* 2022 Two-stage amplification of an ultrasensitive MXene-based intelligent artificial eardrum *Sci. Adv.* **8** eabn2156
- [241] Jiang Y, Zhang Y F, Ning C, Ji Q Q, Peng X, Dong K and Wang Z L 2022 Ultrathin eardrum-inspired self-powered acoustic sensor for vocal synchronization recognition with the assistance of machine learning *Small* **18** 2106960
- [242] Hu Z Y, Zhang Y L, Pan C, Dou J Y, Li Z Z, Tian Z N, Mao J W, Chen Q D and Sun H B 2022 Miniature optoelectronic compound eye camera *Nat. Commun.* **13** 5634
- [243] Zhang Y Z, Chen X, Wang M Y and Yu H Y 2022 Multidimensional tactile sensor with a thin compound eye-inspired imaging system *Soft Robot.* **9** 861–70
- [244] Chen J S and Ran X K 2019 Deep learning with edge computing: a review *Proc. IEEE* **107** 1655–74
- [245] Guo Y X, Qin Q C, Han Z Q, Plamthottam R, Possinger M and Pei Q B 2023 Dielectric elastomer artificial muscle materials advancement and soft robotic applications *SmartMat* **4** e1203
- [246] Zhao L M, Tian H M, Liu H R, Zhang W T, Zhao F B, Song X W and Shao J Y 2023 Bio-inspired soft-rigid hybrid smart artificial muscle based on liquid crystal elastomer and helical metal wire *Small* **19** 2206342
- [247] Nguyen C C *et al* 2023 Development of a soft robotic catheter for vascular intervention surgery *Sens. Actuators A* **357** 114380
- [248] Baburova P I, Kladko D V, Lokteva A, Pozhitkova A, Rumyantseva V, Rumyantseva V, Pankov I V, Taskaev S and Vinogradov V V 2023 Magnetic soft robot for minimally invasive urethral catheter biofilm eradication *ACS Nano* **17** 20925–38
- [249] Hu L, Bonnemain J, Saeed M Y, Singh M, Quevedo Moreno D, Vasilyev N V and Roche E T 2023 An implantable soft robotic ventilator augments inspiration in a pig model of respiratory insufficiency *Nat. Biomed. Eng.* **7** 110–23
- [250] Desai T and Grattoni A 2023 Robotic self-modulation enhances implantable long-acting drug delivery devices *Sci. Robot.* **8** eadj8292